Modelling The Time Dependent Behaviour of Anisotropic Soft Clay Using Non-Stationary Flow Surface Theory

Dinh Hung, Nguyen

M.Sc., B.Eng.

Thesis submitted to the University of Nottingham for the degree of Doctor of Philosophy

August 2021

Declaration

I hereby declare that except where specific reference is made to the work of others, the contents of this dissertation are original and have not been submitted in whole or in part for consideration for any other degree or qualification in this, or any other university. This dissertation is my own work and contains nothing which is the outcome of work done in collaboration with others, except as specified in the text and Acknowledgements. This dissertation contains 36,949 words including appendices, references, tables and figures.

Dinh Hung Nguyen

August 2021

Abstract

Prediction of the long-term deformation of a soft clay under different loading conditions has been a challenging task for geotechnical engineering since the time dependency of soft clay is a complex matter. This topic has attracted the attention of researchers for many decades. An insight into a scenario related to the time dependency of soft clay is a significant pathway to provide the best solution in geotechnical design for geo-structures constructed on soft ground. This thesis is made an attempt to study the time dependent behaviour of soft clay and proposed an advanced time dependent constitutive model, namely NSFS-SCLAY1S model which can capture the significant advanced features of soft clay regarding fabric anisotropy, destructuration of inter-particle bonding and time dependency. The model was developed based on the non-stationary flow surface theory (NSFS) which was proposed by Perzyna in 1964. The NSFS theory is a further development of inviscid elasto-plastic theory, in which a time variable parameter is introduced in the yield surface equation to obtain the simultaneous description of strain hardening and the effect of time. This means that the yield surface can change at any moment. The inherent framework from the classical elasto-plastic theory is used in determining the viscoplastic strain, leading to the simplification of the numerical solution. The preference of NSFS theory in this research is due to the limitation of overstress-based consititutive models of describing properly the creep behaviour of soft clay. The proposed NSFS-SCALY1S model, in contrast, is capable of capturing the strain rate effects and creep response of soft clay. In particular, it is able to simulate tertiary creep response, which is an important phase of creep behaviour which leads to creep failure of soft soil deposits.

Before development of an advanced time dependent constitutive model , namely NSFS-SCLAY1S which is capable of describing all significant features of soft clay such as fabric anisotropy, destructuration and time dependency, a preliminary time-dependent constitutive model using non-stationary flow surface (NSFS) in combination with a well-known Modified Cam Clay (MCC) model was developed first, called NSFS-MCC model. This model was focused on evaluation of the capacity the NSFS theory on prediction of the time dependency of soft clay so soft soil is assumed as an isotropic material. Both NSFS-SCLAY1S and NSFS-MCC models were verified qualitatively and quantitatively. Some elementary tests such as undrained triaxial compression & extension tests, oedometer tests and undrained

triaxial creep tests were employed to verify the models. NSFS-SCLAY1S model reproduced very well the laboratory test results, proving its capacity to provide an optimum prediction of a practical geotechnical challenge. The detail of determination model parameters was presented and discussed.

Acknowledgement

This thesis would not have been completed without the support from many people and resources. I am very pleased to express my gratitude to all of them.

Firstly, I would like to express my profound gratitude and sincere appreciation to my principal supervisor, Dr. Mohammad Rezania, for his valuable guidance, and tireless support during my PhD study. My motivation and mood were sometimes low but with his help and encouragement, I could overcome the difficulties that I encountered during my PhD. All his advice and suggestions enabled me to focus on the essential points of my research topic and gain more skills that I had not touched before such as coding or finite element analysis. His feedback and working style opened my horizon in research experience. He has not only given me the valuable advice in academic but also in my social life during my low mood and depressed time. It lifted me up and continue my research journey to the end. Although he moved to another University at the beginning of my third year, he has still spent his time to support me until the end. I am also deeply indebted to my other supervisors, Dr. Savvas Triantafyllou, Dr. Panos Psimoulis for their help and great support during my writing period.

The work of this thesis was funded by the International Cooperation Deparment of Vietnamese Ministry of Education and Training and the Faculty of Engineering of The University of Nottingham. Therefore, I would like to express my gratitude to The Vietnamese Government which gave me the great opportunity to carry out this PhD course in the UK. I also would like to thank my research colleagues at The University of Nottingham: Hossein, Meghdad, Hussein, Alec, Maha, Long Huynh, Tung Nguyen and others, who have enriched my research through many discussions.

Last but not least, I am sincerely grateful to my family for their constant support, love, kindness and sincere care. In particular, I would like to express my greatest gratitude to my wife who is always at my side and gave me the tireless support and encouragement during the most difficult period. Her care and unconditional love enabled me to go ahead and keep constant belief that I could get my research done. I am also inspired by SuSu, my little daughter and Tim, my little son, who were always beside me and gave me much love over this research journey.

Content

List of Figures

List of Tables

List of Notations

The main notations used in this thesis are given in this section. The notations are described in the relevant section too.

a	absolute effectiveness of destructuration
b	relative effectiveness of plastic deviatoric strains on destructuration
c'	soil effective cohesion
e_0	initial void ratio
e	void ratio
$[D^e]$	elastic stress constitutive matrix
$[D^{ep}]$	elasto-plastic stress constitutive matrix
E	Young modulus
F	Flow function
f_y	yield function
G	shear modulus
K	elastic bulk modulus
K'_w	bulk modulus of water
K_0	coefficient of earth pressure at rest
K_0^{nc}	coefficient of earth pressure at rest for normally consolidated soil
k_x	permeability in x-direction
k_y	permeability in y-direction
M	slope of critical state line
M_c	value of M in triaxial compression
M_e	value of M in triaxial extension
p'	mean effective stress
p'_m	size of yield curve in p:q-space
p'_{m0i}	size of intrinsic yield curve in p:q-space
$p'_{m,0}$	initial size of yield curve in p:q-space
p_y	plastic potential function
q	deviatoric stress
t	time
t_0	initial time
Δt	change of time
u	pore water pressure
v	specific volume
$\dot{v}_0$	initial volumetric strain rate

α	scalar rotation of yield function
α_0	initial α value
α_{xx}	x-component of deviatoric fabric tensor
α_{yy}	y-component of deviatoric fabric tensor
α_{zz}	zz- component of deviatoric fabric tensor
α_{xy}	xy- component of deviatoric fabric tensor
α_{yz}	yz- component of deviatoric fabric tensor
α_{zx}	zx- component of deviatoric fabric tensor
α_d	deviatoric fabric tensor
ω	relative effectiveness of plastic deviatoric strains on rotational hardening
C_α	coefficient of secondary consolidation
$\Delta\Lambda$	plastic multiplier
ϵ^e	elastic strain vector
ϵ^p	plastic strain vector
ϵ_v^p	plastic volumetric strain
ϵ_v^{vp}	visco-plastic volumetric strain
$\Delta\epsilon_q^e$	triaxial elastic deviatoric strain increment
$\Delta\epsilon_v^e$	triaxial elastic volumetric strain increment
$\Delta\epsilon_q^p$	triaxial plastic deviatoric strain increment
$\Delta\epsilon_v^p$	triaxial plastic volumetric strain increment
γ'	effective unit weight of soil
κ	slope of the swelling line
λ	slope of the normal compression line
λ_i	slope of the normal intrinsic compression line
$\bar{\sigma}'$	effective stress vector
$\Delta\bar{\sigma}'$	effective stress increment vector
σ'	effective stress state
v'	Poisson's ratio
η	stress ratio
ηc	stress ratio at normally consolidated state
ηK0	stress ratio at K0 state
η0	initial stress ratio
x	degree of bonding
x0	initial degree of bonding

CC	Cam-clay model
CSL	critical state line
MCC	modified Cam-clay model
OCR	over consolidation ratio
POP	pre-overburden pressure
UDSM	user defined soil model

CHAPTER 1 :

INTRODUCTION

1.1 Problem statements

Since ancient times, urbanisation has developed on river valleys and coastal plains due to transportation and agricultural activities. The resulting density of population of these areas requires more building and infrastructural projects. However, the soil of such areas are extensively composed of soft clay, which has high compressibility, low bearing capacity and rheological characteristics and therefore the ground under the application of external loading – such as embankments, bridges, or high-rise buildings – experienced a large amount of deformation over many years ([1]–[4]). This time-dependent behaviour holds potential to cause damage, not only to the superstructure system but also to users. Hence, the time effect is considered a compulsory factor in the current geotechnical design process. However, calculation of creep deformation remains a significant challenge for geotechnical engineers because the phenomenon is a complex response to different applied factors.

It has been noted that the long-term behaviour of soil is difficult to estimate and control in advance. A well-known example of long-term (creep) deformation is the uneven settlement of the Tower of Pisa, Italy. The inclination is currently estimated at about 5.5^0 and the mean settlement due to creep is evaluated to be about 1.5m. A further illustration, in this case of geohazard, can be seen in the failure of the Vayont reservoir in Italy, where in 1963 there was sliding of the reservoir's side due to gravitational creep, which caused the loss of 3000 lives [5]. These examples indicate that studying the time-dependent behaviour of soil, in particular soft clay soil, is important for a safe and economic environment by delivering a better prediction of the in-situ behaviour of soil.

In general, there are two types of time-dependent behaviour discussed in soil mechanics. One is associated with the hydrodynamic process, known as the dissipation of excess pore pressure during the primary consolidation process, and the other is related to the viscous or creep dependence of the nature of soil. In this thesis, the term 'time-dependency' or 'time-dependent behaviour' will hereafter refer to the second type of time-dependent behaviour of soil.

Time-dependency has attracted attention since the 1930s when Buisman [6], considered the earliest person to carry out an investigation of long term settlement tests, first proposed the creep law. However, the research which has stemmed from this has been limited to a specific condition; the proposed models were based on empirical relationship until the 1960s, when more theories about description of time-dependent behaviour were proposed, for example Isotache concept [7], overstress theory [8], nonstationary flow surface (NSFS) theory [9], [10] and critical state concept [11].

In recent years, standard elastoplastic models, such as the Modified Cam Clay (MCC) model, have not been employed to analyse practical boundary problems because it only concerned the basic features such as isotropic assumption, or volumetric change. Some other advanced models, e.g. SCLAY1 [12], SCAY-1S [13] or SANICLAY [14] models were developed to describe some advanced features of soft soil regarding fabric anisotropy and destructuration; however, their limitation is that they are incapable of describing the time dependent behaviour of soil. There are a significant number of studies that have been carried out to develop a constitutive model to reflect the time-dependent behaviour of soft clay (e.g. [15]–[22]). However, these models mostly describe the rate-dependency of soft clay, rather than the creep behaviour of soil, and they have not fully described some of the advanced features of natural clay regarding fabric anisotropy and destructuration as discussed by Burland [23], Leroueil and Vaughan [24] and Taiebat [14]. Otherwise, the models are highly complicated, leading to the incapability of application in practical geotechnical engineering. Therefore, it is necessary to develop a simple model, with capacity of anticipating the tertiary creep behaviour (creep rupture), describing the advanced features of soft clay and determining of model parameters – which is possible from standard laboratory tests.

This thesis attempts to address the abovementioned aspects of modelling the time-dependent behaviour soft clay. It simplifies the formulation of model and model parameter for practical application.

1.2 Aims and Objectives

The aim of this research is to develop a generalized time-dependent constitutive model using the Non-stationary Flow Surface Theory in addition to verifying the prediction ability of this model against the laboratory tests and against

the in-field boundary level. The proposed time-dependent constitutive model concerns the natural characteristic of soft clay regarding fabric anisotropy and destructuration.

The following objectives underpin the aims of this research, which seeks to:

- review the literature on the nature of soft clay, the time-related phenomenon and approaches to modelling the time-dependent behaviour, to establish the place of this thesis within the wider literature.
- explore a numerical solution for implementing an advanced constitutive model of soft clay in programming software Matlab and Fortran.
- develop a time-dependent constitutive model capable of fully anticipating the creep behaviour of normally consolidated soft clay, in particular creep rupture, with the inclusion of the fabric anisotropy and destructuration of soft clay.
- verify the proposed model at element test levels with natural soil data.

1.3 Layout of the thesis

The thesis includes six chapters; of which the first and the last chapter refer to the introduction and conclusion of the thesis respectively. The other four chapters focus on the literature review and work done over the period of research. A brief overview of each chapter is presented as follows:

Chapter 1 has provided an overview of the current problems related to the research topic; the time-dependent behaviour of soft clay and the necessity of an adequate solution for this issue. Following this, the aims, objectives of this thesis have been stated.

Chapter 2 reviews the literature, to provide insight into a scenario related to the research topic so that a gap in modelling time dependent behaviour of soft clay is highlighted and the approach to filling this gap set out. This chapter has three key sections. The first reviews some advanced features of soft clay that few constitutive models have fully described. The next section focus on time-related phenomena such as creep, stress relaxation and rate effect to provide insight into the mechanism of those phenomena and the importance of accounting for these behaviours. The last section is focused on two well-known theories regarding overstress and non-stationary flow surface theory, on which many time/rate dependent constitutive models are based. The advantages and limitations of each theory are discussed to finally offer a superior choice for a time dependent constitutive model as set out in the following chapters.

Chapter 3 proposes a preliminary time-dependent constitutive model using non -stationary flow surface (NSFS) in combination with a well-known Modified Cam Clay (MCC) model. The model is named as NSFS-MCC. It can describe creep behaviour of soft clay appropriately; however, it cannot cover some advanced features of soft clay regarding fabric anisotropy and destructuration. This chapter also presents determination of NSFS-MCC model's parameters and a numerical solution. Some qualitative verifications for the model are also addressed.

Chapter 4 is a further development of the isotropic time-dependent constitutive model NSFS-MCC to describe some advanced features of soft clay regarding fabric anisotropy and destructuration. This advanced model is named as NSFS-SCLAY1S. The name indicates that the model uses NSFS theory in combination with an advanced inviscous model, namely SCLAY1S. The model parameters and implementation are discussed in this chapter.

Chapter 5 concludes the thesis. As well as a summary, the chapter highlights the contribution that this research makes to the field of the time-dependent behaviour of soft clay. Some recommendations for further research are also set out.

CHAPTER 2 :

LITERATURE REVIEW

This chapter provides an overview of the existing knowledge relevant to the research topic: modelling time-dependent behaviour of soft clay. Summaries, and critical evaluations of the field are presented, providing an overview of sources that have informed this research on the time-dependent behaviour; moreover, the chapter places this research in the context of the larger field, to reveal the gap in knowledge that needs to focus. Finally, possible approaches for developing a model capable of describing the time-dependent behaviour of soft clay are also reviewed and evaluated to explore their advantages and drawbacks, before opting for an approach to develop a time-dependent model.

This chapter will focus on three key areas regarding the advanced features of soft clay, followed by its time-dependent behaviour and possible approaches to modelling this behaviour. A summary will then clarify the importance of understanding firstly the structure of natural soft clay, secondly its responses under the effect of time and thirdly the approach for modelling time dependent behaviour. Moreover, the gap in the existing research relevant to modelling time-dependent behaviour of soft clay is also ascertained, to highlight the extent to which the proposed model provides a significant contribution to knowledge with regards to the prediction of the complicated behaviour of soft clay under the effect of time.

2.1 Advanced features of soft clay

Studying the advanced features of soft clay to understand the possible mechanism of soft clay under the effect of time by an application of the external loading is a significant knowledge base for developing a time dependent constitutive model. The section attempts to firstly review the nature of soft soil which roots the establishment of some advanced features of soft clay regarding fabric anisotropy and destructuration which are presented in the sequel.

2.1.1 The nature of soft clay

Soft clay soil is characterised by its low shearing strength, low bearing capacity, high moisture content and high compressibility. It is identified specifically by low undrained shear strength (C_u<40 kPa) and high value of compression index C_c from 0.19 to 0.44 [25]. Soft clay soils typically have been found at high natural moisture content ranging from 40% to 60% while their plasticity index is located between 45% and 65% [26]. It is noticed that normally consolidated soft clay may be compressed ten times more than normally consolidated sand [27]. With these characteristics, soft clay may bring significant damage to construction projects built on it, such as road embankments, buildings or bridges. Prediction of long-term settlement and stability of soft clay is always a contentious issue in geotechnical engineering due to its complicated behaviour, associated with various factors such as structure, clay mineralogy, fabric anisotropy, inter-particle bonding and time effect [28].

The term ‘structure’ mentioned above refers to the combination of ‘fabric’ (the arrangement of particles) and ‘bonding’ (the inter-particle forces) of natural soft clay [29]. The properties of fabric include: inhomogeneities; layering; distribution of the soil particles and fissures, which are normally anisotropic, so-called fabric anisotropy [30]. Bonding is the combination of forces acting to connect the particles. Leroueil and Vaughan [31] emphasize that the structure can be key to determining the engineering behaviour of soil.

Natural clay is composed of small mineral particles, which are formed by the chemical weathering process, resulting in the formation of a group of crystalline particles of colloidal size (<0.002 mm) [32]. Natural clay can be formed in-place (residual soil) or transported from another places via streams or rivers and then deposited. The depositing period may range from months to thousands of years. During the deposition period, natural clay experiences various geological processes

and environmental effects, which confer a ‘structure’ that combines various aspects of soil behaviour regarding yielding, strength and stiffness.

Therefore, studying the structure of natural clay – regarding its mineralogy, fabric anisotropy and bonding – enables a better interpretation of the behaviour of natural clay under different loading conditions.

2.1.1.1 *Clay mineralogy*

Clay mineralogy is a significant factor determining the size, shape and properties of clay and is a key constituent that determines the viscous characteristic of soft clay. Therefore, prior knowledge of what the minerals are in natural soft clay provides important insight into its possible behaviour. However, chemical composition, alone or in conjunction with size distribution, is not adequate to determine clay behaviour, since the mechanical behaviour of natural clay depends directly on the gas phase and applied potentials regarding temperature, stress hydraulic head or electrical potential. Nonetheless, the structure of natural clay does provide a significant prediction of its potential interaction with adjacent phases.

Clay minerals are normally the hydrated aluminium, iron or magnesium silicate, combined in a manner to produce sheet-like structures which are built from two basic structural units: the tetrahedral unit of silica, forming Silica sheet structure and octahedral unit of the hydroxide of aluminium, iron, or magnesium forming octahedral sheet (aluminium octahedral sheet is termed a gibbsite sheet and magnesium octahedral sheet is referred to the brucite sheet), as shown in Figure 2.1 [29]. It is notable that a high number of electric charges remain unbalanced in these sheets (normally negative charge) leading to the attraction of water dipoles and cations, which enables clay to possess properties such as cohesion, low permeability, matrix suction and swelling-shrinkage behaviour. The combination of two sheets of silica and gibbsite in different arrangement and condition encourages the formation of dissimilar clay minerals. The most abundant clay minerals in the deposits can be categorized into three principled groups, namely Kaolin, Illite and Smectite, in which the representative minerals for each group are respectively Kaolinite, Illite and Montmorillonite [33], [34], which will be discussed in turn. A schematic diagram of the structures of these three minerals is presented in Figure 2.2.

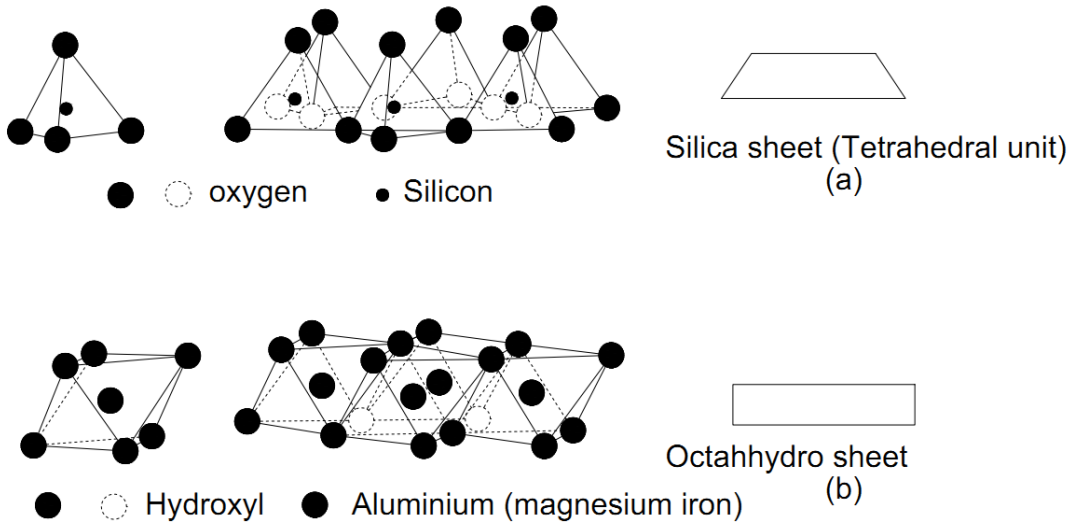

Figure 2.1: Two basic structural units of clay: Tetrahedral unit and Octahedral sheet (Adapted from [29]).

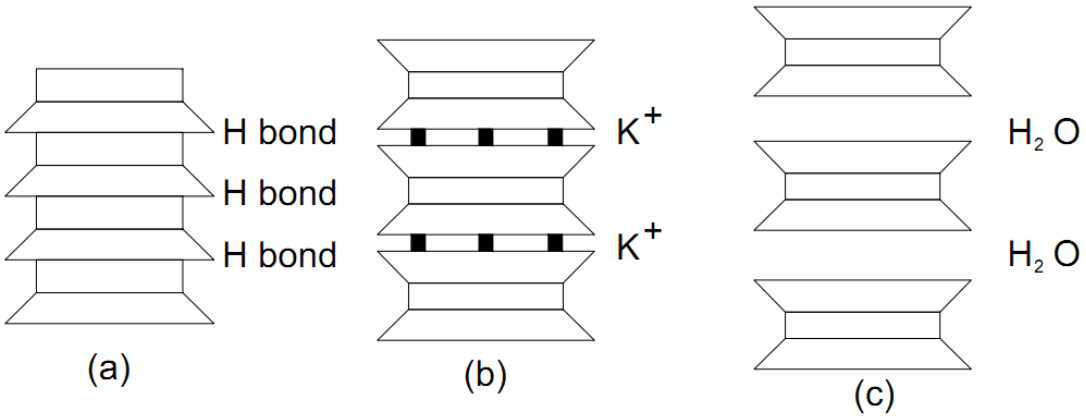

Figure 2.2: Structure of main clay minerals: (a) Kaolinite, (b) Illite, (c) Montmorillonite (Adapted from [32])

Kaolinite

Kaolinite is the most common mineral of residual clay deposit and the main constituent (occupies 85% to 95%) of well-known clay, namely Kaolin which is referred to as China clay. The name Kaolin originated from the Chinese term "Kau-Ling", the name of a hill close to Jauchau in China, where the substance was excavated many centuries ago and used in ceramic manufacturing [35], [36]. Kaolinite is classified as a two-layer clay (1:1 structure), in which a single sheet of silica is stacked on a single sheet of octahedral. These successive layers are held together, relatively strongly, by both Van der Waals forces and hydrogen bonds (Figure 2.2a). The

Kaolinite mineral is therefore stable – water hardly enters between the sheets. Therefore, kaolinite has low shrinkage and swelling responses to water content variation. The electron micrograph of Kaoline (Figure 2.4) shows that it has a moderately sharp crystalline morphology, which presents a pseudo-hexagonal shape.

The isomorphous substitution in Kaolinite is very limited so the charge on the layer is minimal and the capacity of cation exchange is low. A Kaolinite particle may have over 100 stacks [32]. The structural formula is $(OH)_8Si_4Al_4O_{10}$ [29]. Kaolinite is white or near white in colour, related to its chemical composition.

It can be seen from the structure of Kaolinite (Figure 2.3), in the plane of the atom to both sheets, two thirds are oxygen atoms and are shared by the cations of the silicon and octahedral sheets. The remaining atoms are hydroxyls (OH). The distance between one oxygen and another oxygen is typically different in tetrahedral and octahedral layers, which causes the distortion of the ideal tetrahedral network. As a result, kaolinite is considered triclinic instead of monoclinic.

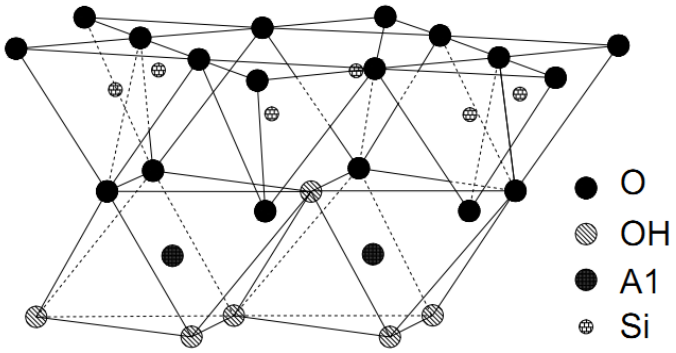

Figure 2.3: A sketch of the structure of kaolinite (Adapted from [29])

Figure 2.4: A scanning electron microscope (SEM) of well crystallized kaolinite from sandstone [37]

Illite

The term Illite was derived from the State of Illinois following the proposal of Grim et al. [38]. It not only refers to a clay mineral but also names the clay mineral constituent of argillaceous sediments associated to the mica group. It was confirmed that the term Illite is valid for the 10 Å nonexpanding clay mineral in argillaceous sediments [39]. Its general formula is expressed as $(OH)_4K_y(Al_4.Fe_4.Mg_4.Mg_6)(Si_{8-y} . Al_y) O_{20}$.

Illite comprises a 2:1 layer mineral structure, in which a basic layer consisting of a gibbsite sheet is sandwiched between two inward-pointing silica sheets (Figure 2.2b). There is partial substitution of silicon by aluminium in silica sheets and the resultant charge deficiency is balanced by non-exchangeable potassium ions (K^+) [40]. Potassium ions (K^+) occur between unit layers, creating K^+ bonding, which is weaker than hydrogen bonding (Figure 2.5). Therefore, Illite tends to absorb more water than Kaolinite and has higher swelling and shrinkage properties.

Some Illite minerals may contain magnesium, iron or aluminium in the octahedral sheet, as shown in Figure 2.5. Iron-rich Illite is referred to as glauconite, usually recognisable as earthy green pellets. A scanning electron microscope of Illite is shown in Figure 2.6.

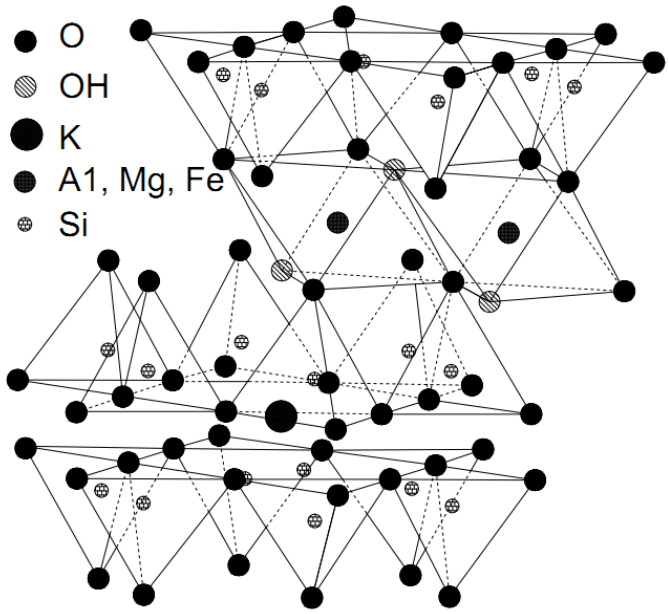

Figure 2.5: A sketch of the structure of Illite (Adapted from [29])

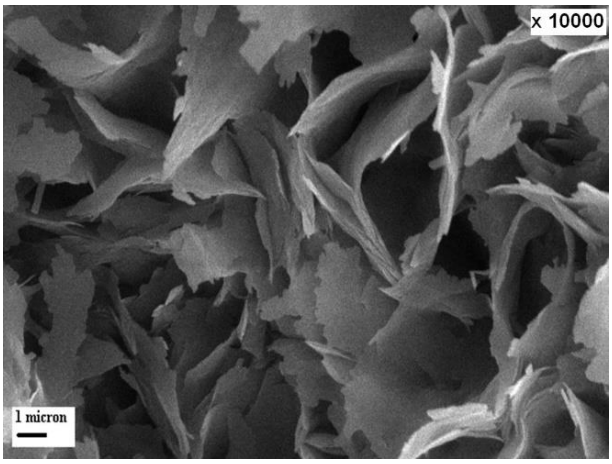

Figure 2.6: A SEM of Illite sample [41]

Montmorillonite

Montmorillonite is a member of the smectite group. The name Montmorillonite originated from the town of Montmorillon in France, where the first sample was obtained and studied [42]. The composition of all members of this group can be represented by a common formula $(OH)_4Al_4Si_8O_{20}.nH_20$. The basic structural unit of Montmorillonite is similar to Illite. It has a 2:1 layer mineral structure, in which two inward-pointing silica sheets are attached to a central gibbsite sheet but in the gibbsite sheet aluminium is partially substituted by magnesium or iron, as shown in Figure 2.2 and Figure 2.7. The oxygen forming the tip of the silica sheet is shared with the gibbsite sheet. The successive layers are bonded together by Van de Waals forces and by cations that balance charge deficiency in the structure. The space between layers is occupied by a water molecule and exchangeable cations other than potassium (K^+), resulting in a very weak bond. Water can easily enter between layers, causing them to expand considerably. Due to this characteristic, when placing pieces of dry Montmorillonite in water, they will significantly increase in volume (swell), without first losing their shape. Montmorillonite dos not withstand high temperature; it fuses at the temperature of approximately 982^0C [42]. Montmorillonite has the capacity to absorb a large amount of hydrogen, sodium, calcium, etc.; it has a base-exchange capacity in the range of 80 to 150 meq/100g [29]. These bases can absorb in a large quantity and may affect the properties of the material. To summarise, Montmorillonite has the highest swelling and shrinkage rates, as well as the highest exchangeable cations of the three clay minerals; however, its bonding characteristics are the weakest of the three clay mineral groups. A micrograph of natural montmorillonite is shown in Figure 2.8.

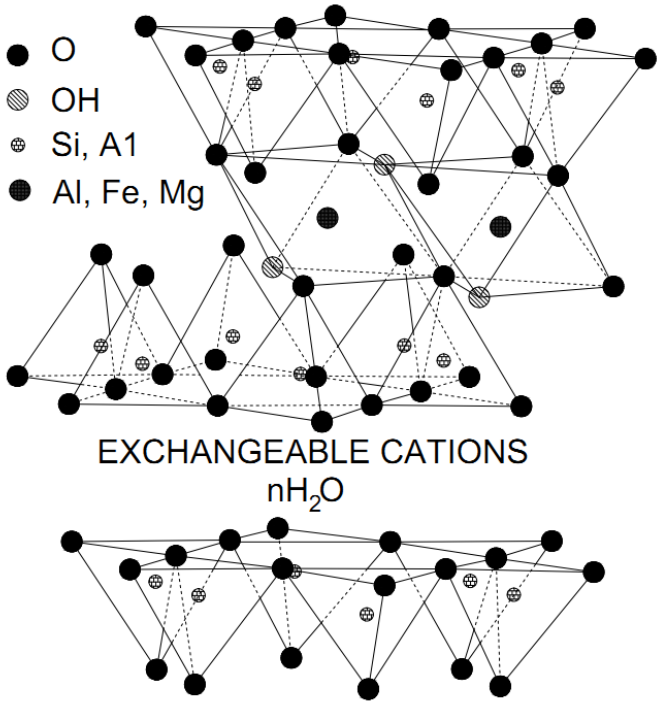

Figure 2.7: A sketch of the structure of Montmorillonite (Adapted from Mitchell [29])

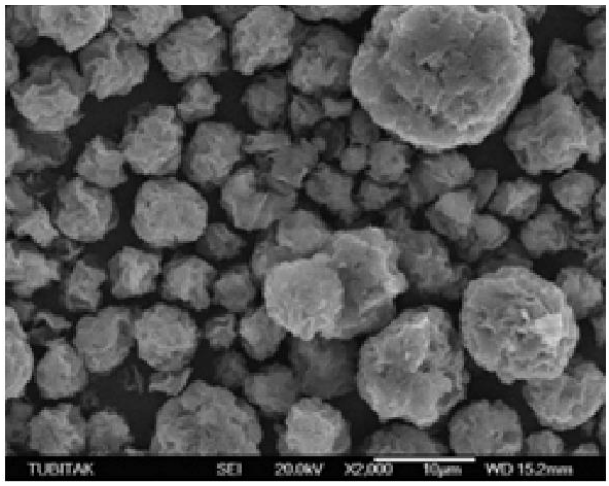

Figure 2.8: A SEM of natural Montmorillonite [43]

2.1.2 Fabric and anisotropy

Fabric

The term 'fabric' is associated with the arrangement of particles, particle assemblage, and pore spaces in a soil [29]. The classification of fundamental fabrics is presented in Craig [31]. They are flocculated fabric and dispersed fabric, associated with the combination of clay mineral particles; meanwhile bookhouse and turbostratic relate to the combination of elementary aggregation of particles (Figure 2.9).

Flocculated fabric is characterized by the net attraction between particles, due to short-range Van der Waals forces (electrical forces), resulting in an orientation where particles tends to be edge-to-face or edge-to-edge. If there is net repulsion force, the particles tend to be associated with face-to-face orientation, stimulating the formation of dispersed fabric. In natural clays, which normally contain a major proportion of bulky particles (elementary aggregation of particles), the arrangement may be significantly complex. The formation of the elementary aggregation of particles tends to be the arrangement face-to-face orientation of single clay mineral particles. The process of these element aggregates, forming larger assemblages, is influenced by the depositional environment. There are two possible forms of particle assemblages regarding bookhouse and turbostratic fabric, illustrated in Figure 2.9c and Figure 2.9d respectively. A sketch of fabrics in natural soil is presented in Figure 2.9e and an actual image of fabrics in Errol Clay is shown in Figure 2.10.

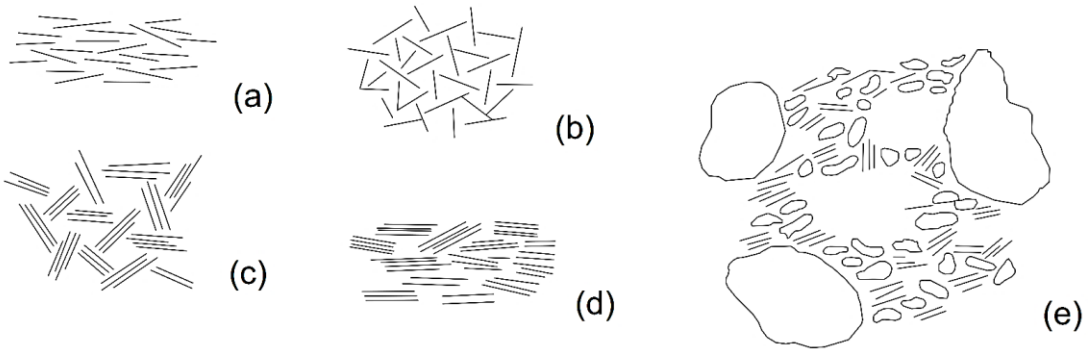

Figure 2.9: Classification of fabrics in Clay: dispersed (a), flocculated (b), bookhouse (c), turbostratic (d) and the fabrics in natural clay (e) [32]

Fabric stability is influenced by changes in stresses and chemical environment [29]. The chemical environment has significant effect on the initial stages of sediment fabric formation in water. The initial water content and ionic concentration yield four different types of settling behaviours in clay suspension: flocculated free settling, dispersed free settling, consolidation settling and zone settling [44]. Further research on settling behaviour states that the repulsive forces between clay platelets affect the settling behaviour of Montmorillonite, whereas the attractive forces control the settling behaviour of Kaolinite [45].

Figure 2.10: Structure of Errol Clay [32]

However, the effect of the chemical environment is much less important than the influence of loading in the subsequent states, when the initial flocculation of particles and deposition is complete [46]. The effect of external loading on the arrangement of clay particles has come under significant investigation and it has been concluded that the orientation of clay particles is random (i.e. flocculated fabric) before loading, but is modified to dispersed fabric when the external stress is greater than the pre-consolidation pressure [47]. Study of the transformation of the clay platelets of Kaolinite clay showed that the modification of the fabric arrangement of dispersed fabric under consolidation is much lower than for sample with the structure of flocculated fabric [48]. As a result, the structure of clay fabric has a significant effect on the shear strength, the volume change of natural clay. It was also reported that normally consolidated clay with the structure of dispersed fabric experiences dilation during shearing, whereas contraction is exhibited for samples with flocculated fabric structure [48]. Under static and cyclic load condition, the clays with a dispersed fabric structure reaches higher undrained strength, whereas their counterparts with flocculated fabric structure exhibits higher resistance to cyclic loading [49]. Therefore, it is important to understand the microstructure of natural clay, because of its relevance to engineering properties regarding volume change behaviour, permeability and water retention.

The arrangement of fabrics in soil is extremely complex due to the processes involved in soil deposition, previous stress history and soil composition. The anisotropy of clay fabrics results in the natural anisotropic behaviour of clay.

Anisotropy

As discussed above, the behaviour of natural clay is significantly anisotropic. This anisotropic feature can be categorised into two types 'inherent or structural anisotropy' and 'induced anisotropy' [50]. The former is defined as 'a physical characteristic inherent in the material and entirely independent of the applied stresses and strains'. The latter is defined as 'due exclusively to the strain associated with the applied stresses'.

For greater clarity, later research [51] categorized the anisotropy of natural clay into three different types, (1) inherent anisotropy, which results from the current fabric structure of clay and is used to determine the anisotropy of natural clay at its in-situ state; it might be related to the plastic strain history the soil has undergone during the soil deposition processes; (2) stress-induced anisotropy, which is an outcome from the anisotropy of the current stress condition only and is independent of the strain stress history of the clay; (3) strain-induced anisotropy is used for the anisotropy of reconstituted samples, which are recreated from slurry and so bonding is not an important factor. Its structure is expected to be modified predominantly under one-dimensional strain history, rather than the process of deposition. Other research (i.e. [52]) considered an additional type of anisotropy, namely azimuthal anisotropy, which is associated with the preferential alignments of crystals, cracks or heterogeneities in the clay deposit. However, this type of anisotropy is less noticeable due to its complicated formulation.

The inherent anisotropy not only depends on its natural structure, but is significantly attributed to the post-depositional processes [29]. During this time, the plate-shaped clay particles are arranged in such a manner that their long axes are perpendicular to the direction of major principal stress (vertical direction, due to the gravity effect). This encourages the clay to arrange in each layer at horizontal orientation.

As a result, the properties of natural clay can be assumed identical at horizontal direction but different in the vertical direction, referred to as "cross anisotropy". This makes the numerical modelling of fabric anisotropy of soil more convenient, but it still realistically reflects natural soil with anisotropy characteristics. The plastic strain in natural clay occurs during the post-depositional process and can stimulate the anisotropy in clay, which is called 'plastic strain-induced anisotropy'. Moreover, current, waves or slope can contribute to the preferred orientation of clay platelets. The

combination of both inherent and induced anisotropy may be termed ‘initial anisotropy’ [53]. The degree of ‘initial anisotropy’ in natural clay is normally more significant than in sand. It is clear that constitutive models, which do not concern themselves with anisotropic characteristics, can lead to incorrect predictions of a soil’s response under loading, particularly for natural clay.

For the strain-induced anisotropy of clay, it is asserted that anisotropic fabric may be produced by anisotropic consolidation, shear and directional transportation components, method of remoulded or compacted soil preparation. However, the strength of remoulded clay is less than that of natural clay, due to the loss of some fabrics [29].

The anisotropy of natural clay is not fixed. It changes under different external loading conditions, which is called “evolving anisotropy”. Some advanced constitutive models make efforts to capture the evolution of soil anisotropy ([54]–[57]). The result of modelling an embankment, concerning inherent anisotropy and evolutionary anisotropy, showed that the evolution of anisotropy has more impact on horizontal deformation than on the vertical deformation [58]. In summary, a model which has the capacity to describe both inherent anisotropy and evolving anisotropy will provide better prediction, with results close to taking data from natural soil [58].

2.1.3 Bonding and destructuration

Bonding

Bonds in natural clay result from various factors, ranging from gravity force, electrostatic forces between clay particles, various chemical glues (i.e. iron dioxides and cementation), fibrous organic materials and arrangement of gels and gums.

Bonding in microstructure is associated with the bonds between the particles by the inter-particle forces. There are two main categorizable bonds in the microstructure of clay, primary bonds and secondary bonds ([29],[59]).

Primary bonds, referred to as interatomic bonds, occur when there is a transfer or sharing electrons in adjacent atoms based on the electrostatic attraction between the protons and electrons in such a way their energy levels are lowered. The more the energy level is reduced, the stronger the primary bonds. Primary bonds are classified into three main types, namely the covalent bond, ionic bond and metallic bond ([29],[59],[60]).

Covalent bonds result from two nuclei sharing one or more electrons, to complete their outer shell. Therefore, the electrons located between the nuclei are the bonding electrons. The stable balance of attractive or repulsive force between atoms sharing the electrons is named covalent bonding. Taking the hydrogen molecule as an example for the covalent bond, the electron in its outer shell is represented by dot: H. + H. = H : H.

Ionic bonds involve sharing a pair of electrons between two nuclei, which has opposite charged ions. Ions are the atoms that have positive or negative charge due to either their gain or loss of one or more electrons. It is called anion if the ion gains more electrons and has negative charge. Alternatively, a cation that has lost one or more electrons has positive charge. The ionic bonds typically occur between two distinct nuclei which have different electronegativity, resulting in the bonding being more polar (ionic) than in covalent bonding (where electrons are shared equally). Due to this dipole characteristic, the ionic compounds tend to be soluble in a dipole environment like water.

Metallic bonding involves electrons which are running free among the nuclei. This type of bonding is normally present in metal and alloy material [59]. Metal has loose valence electrons, which hold the positive metal ions together but are freely running in a confined space through the solid metal. This can be described as an array of positive ions in a sea of electrons. This feature results in the nondirectional metallic bonding and some principal characteristic of metal, such as thermal and electrical conductivity, ductility, strength, opacity and lustre.

Following the explanation of three different types of primary bonds, it should be noted that metallic bonds have little importance in clay minerals. A combination of covalent and ionic bond is typically present in non-metal material. It is well established that the abundant constituent of clay is silicate minerals (SiO_2), where the interatomic bond is about half covalent and half ionic [29].

Secondary bonds, referred to as intermolecular bonds, are involved in the interaction between molecules, including the forces of attraction or repulsion between molecules, or the adjacent particles such as atoms or ions. Secondary bonds are weak when compared to the primary bonds, e.g. covalent bonds. However, they might nevertheless be strong enough to define the final arrangement of molecules atoms in solids, and they may be a source which attracts the small particles together or solid

particles and liquids together. These attraction forces can typically be represented by Hydrogen bonding and van der Waals forces [29].

The Hydrogen bond involves the attraction of a positive hydrogen ion to the negative end of an adjacent molecule that creates a hydrogen bond. The strength of this bond is significantly greater than that of the van de Waals bond. Therefore, it considerably affects the characteristics of the clay minerals, particularly in its interaction with water. This clarifies why Kaolinite minerals with hydrogen bonding are stable with water; meanwhile, Montmorillonite minerals bonded by van de Waals force are susceptible to water.

Van der Waals bond is the interaction between the dipole molecules or atoms, where there might be attractions or repulsions between atoms or molecules to form bonds. A Van der Waals bond looks similar to an ionic bond but is much different, since they are caused by correlations in the fluctuating polarisations of adjacent particles. Therefore, its strength is minimal and easily vanquished by disturbants. However, it still strong enough to determine the final arrangement of groups of particles in solids [60], and may be responsible for the small cohesion in clay.

In terms of macro-structure, bonding results from the frictional nature of soil due to gravity force, fibrous organic materials, cementation and thixotropic hardening [29]. These bonds have been developed and altered during the geological life of soil, as a result of physio-chemical effects.

Destructuration

The term ‘destructuration’ refers firstly to the post-yield degradation of the natural structure of clay [61]. It was later and more specifically explained as the progressive degradation of bonding in soil, as a result of plastic straining, mechanical energy or thermal energy effect [62]. Plastic straining involves slippage at inter-particle contacts and encourages the re-arrangement of the particles. Therefore, it not only induces a change of anisotropy but also stimulates the destructuration process of soil. Soil with stronger bonding requires more energy to break down. Its strength is higher accordingly.

It was assumed that the ‘destructured state’ may be the ‘reconstituted state’, in which soil powder has been mixed with water at equal content to or greater than the liquid limit, without air and has undergone one dimensional consolidation [23]. Burland defined the properties of a reconstituted state as ‘intrinsic’, since it is related to the inherent characteristics of clay. This statement is supported by the data of

oedometer tests of the structured and reconstituted samples of Bothkennar clay in Figure 2.11a. It shows that the behaviour of structured clay after experiencing the destructuration process is similar to the compressed behaviour of a reconstituted sample. Looking at the data of some undrained triaxial compression and extension tests of structured Bothkenanar clay in Figure 2.11b, it shows a loss of strength due to the destructuration process; many current constitutive models have not described this important feature. It can be seen from Figure 2.11 that the destructuration process is manifested as a sudden post-yield increase in compressibility, or a post peak decrease in strength under shearing. This performance is also corroborated by other research, which tested different clays: Leda clay [63], Pisa clay [64], Pietrafitta clay [65], Valericca clay ([65], [66]), and Pappadai clay [67]. The destruction of bonding in natural clay can result from plastic volumetric straining and plastic shearing straining [62].

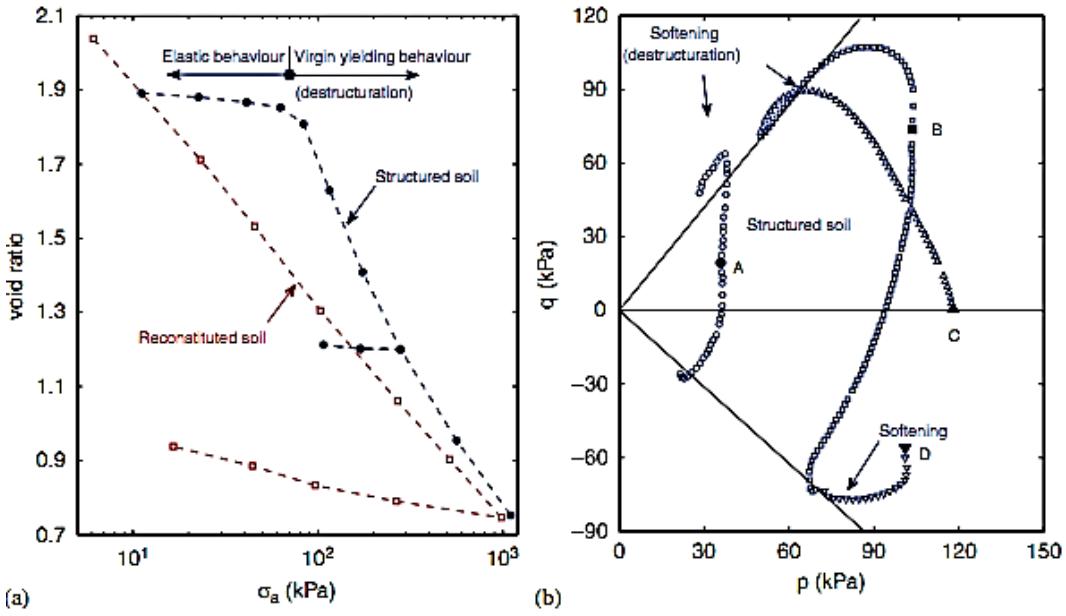

Figure 2.11: Behaviour of structured and reconstituted samples of Bothkennar clay (a) Oedometer tests; (b) undrained triaxial compression and extension tests (Adapted from [68])

Therefore, a constitutive model cannot provide an appropriate prediction if the destructuration feature is neglected.

2.2 Time dependent behaviour of soft clay

2.2.1 Overview

Soft clay deposits have been found to exhibit considerable time-dependent behaviour as an example of large deformation, or rupture over long periods, which

may cause significant damage to any construction projects built on it [69]; comparably it is not noticeable that sand shows significant time-dependent behaviour ([70]–[72]). Therefore, in the past, construction projects, e.g. buildings, road embankments, dams, or bridges, typically avoided construction on soft clay deposit, to limit possible damage over the time. However, world-wide socio-economic development has led to an increase in population, which has generally condensed in specific areas, especially in coastal areas, or riversides, where the availability of the appropriate soil for construction without special treatment is meagre. It is reported that various projects in Australia have been constructed on inappropriate soil deposit, for example Ballina Bypass [73], Port Botany Expansion [74] and Port of Brisbane Expansion [75] (covered respectively in the next paragraph). This requires geotechnical engineering, to address the complicated time-dependent behaviour of such soft clay deposits so that a safe solution can be delivered.

An illustration of this effort can be seen in two instrumented embankments constructed in 1998 on Ballina clay deposit to investigate the behaviour of this soft clay deposit over a long-term and it was reported that this soft clay exhibited large creep deformation [4]. Ballina bypass is an upgrade 12 km long four-way dual carriageway, connecting the Pacific Highway in North Ballina with the Bruxner Highway Intersection in South Ballina [73]. Most of this highway is constructed on coastal deposit, constituted of various soft clay thicknesses. Therefore, the stability of this road over long-term usage is a significant challenge to geotechnical engineering. The soft clay deposit must be treated to provide a ground strong enough to bear the external loading applied to it. Another example is Port Botany Expansion project, an important infrastructural development in New South Wales, which was constructed on a deep layer of marine clay underlaid by a 15m layer of dense sand [74]. This project included reclamation of 63 hectares at Botany Bay for developing a new container terminal. The major structure of this project is 1,850 metres of additional wharf face for the berth, which includes more than 200 precast counterfort units with 20m height and 640 tonnes weight per unit. It requires that the geotechnical engineer treat the clay deposit carefully, to bear this considerable loading. Lastly, the Port of Brisbane Expansion project was developed to cater for the increased trade activities in Brisbane and Queensland [75]. The project involved the reclamation of 230 hectares and a remarkable challenge was presented by the construction of a seawall of 4.6 kilometres long, on 9 metres of soft dredge materials overlying 30 metres of deep soft to firm seabed clays. Vacuum preloading, with vertical drain technique was used to accelerate

the dissipation of the excess pore pressure so that the clay deposit became over-consolidated. However, determination of the optimised over-consolidation ratio was a challenge because the behaviour of soft clay during the secondary process is complex and hard to predict due to the adjustment of the internal structure of soft clay. It is reported that soft clay still exhibits excessive settlement even when the applied pressure is in the over-consolidation range after investigating some projects constructed on Coode Island constituted of a deep soft silty clay layer in Melbourne [76].

The above mentioned are merely examples of many projects which have been constructed on inappropriate ground, typically soft clay deposit, where the long-term dependent behaviour presents a considerable challenge for geotechnical engineering since it is not only associated with the time effect but is also relevant to the mechanism of the adjustment of the internal structure of soft clay. This indicates the importance of the advanced study of soft clay engineering in general and the time-dependent behaviour in particular. A model for this must be able to describe not only the time effect but also the evolution of some advanced features of soft clay, regarding fabric anisotropy or destructuration under applied loading.

The term “time-dependent behaviour” as used in this research is only relevant to the viscous effects in the soil skeleton, such as the rate effect, ageing effect, creep and stress relaxation. These four time-related phenomena are respectively addressed in the next sections so that a clear definition and precise understanding of each time-related phenomenon is reached. This provides the crucial knowledge-base for the numerical solution in the development of a time dependent mode.

2.2.2 Aging effect

The aging effect is related to time, whereby the mechanical and physical properties of soil change significantly [77]. Reliable models which reflect the aging effect on soft clay have been developed by many researchers ([1], [78]–[86]). However, the aging process is still a complex and difficult to control phenomenon.

In general, the aging effect causes an improvement in soft clay properties. It can be categorised into two stages: pure aging and creep or secondary consolidation aging [85]. The former refers to a phenomenon which involves the depositional environment, such as chemical weathering, water interaction, freezing-thawing, swelling dessication, and cementation; called in-situ processes. The latter stage is related to the creep or secondary compression and has captured the attention of much research.

The improvement of pre-consolidation pressure due to the aging effect is shown in Figure 2.12. It shows that clay of 3000 years will gain an improvement of pre-consolidation pressure from p_0 to p_c. Therefore, if an additional load, for instance the weight of a building, is applied to that clay, only the part of loading exceeding the pre-consolidaton p_c leads to large instant settlement. This aging effect phenomenon has been proved by researchers – such as in Mitchell [79], Graham [87], and Ltifi [77]. The mechanism of aging is associated to thyxotropic hardening process which can occur without a volume change and without chemical alteration ([78], [88]).

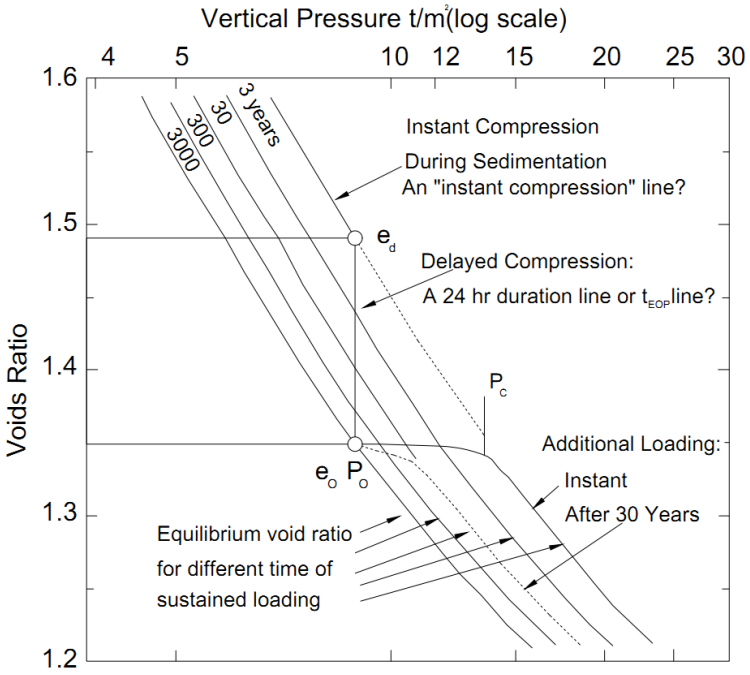

Figure 2.12: Compressibility of a clay exhibiting delayed compression (Adapted from [1])

Studying the aging effect on the permeability of clay from existing research shows a disparity of results. Ltifi [77] carried out tests to investigate the effect of aging on the strength and permeability of four different groups of samples with different storage times after compaction: immediate, 50 days, 142 days, 232 days after compaction. The results show an increase in the undrained shearing strength, but a decline in the permeability with the increase of aging days, as shown in Figure 2.13. Other research supports the decrease of the permeability of clay with the increase of storage time, due to the alteration of the micro-structure under secondary compression. For example, Dunn and Mitchell [89] noted that the decrease of permeability is induced by various factors, including the growth in microstructure and progressive filling by very fine particle migration. However, Mitchell et al. [90] argue that the

permeability increases over the aging period because the soil structure changes, in particular the flocculation is established, gradually leading to the increase in strength and permeability capacity. In short, this issue remains contentious among researchers in the field.

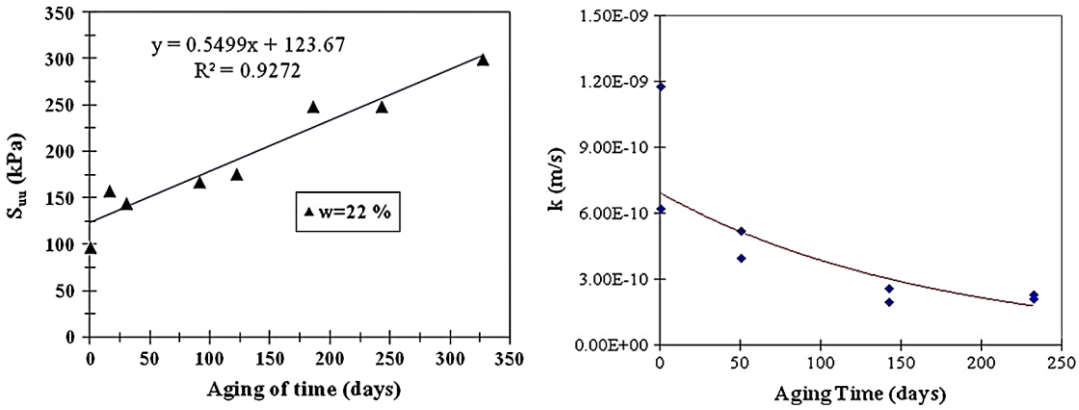

a. Effect on the undrained shearing strength b. Effect on the permeability

Figure 2.13: The effect of aging period on mechanical and physical properties of clay [77]

2.2.3 Rate effect

The rate effect refers to how soft clay reacts to different rates of loading or straining. In favour of simplicity, conventional analysis of soft clay behaviour has often ignored this feature. However, the effect of rate on the stress-strain relationship of soft clay has recently gained more attention in recognition that this effect has great influence on the stress-strain behaviour of soft clay ([7], [91]–[93]).

The typical strain rate effect on the stress-strain relationship of soft clay is illustrated in Figure 2.14. It shows that the faster the loading rate results, the higher stresses at a certain strain. This statement is supported by the results from a series of undrained triaxial tests at different constant strain rates on Haney clay samples, as shown in Figure 2.15 [94]. It shows that the undrained shear strength of soil increases corresponding to the higher rate of strain applied to the sample.

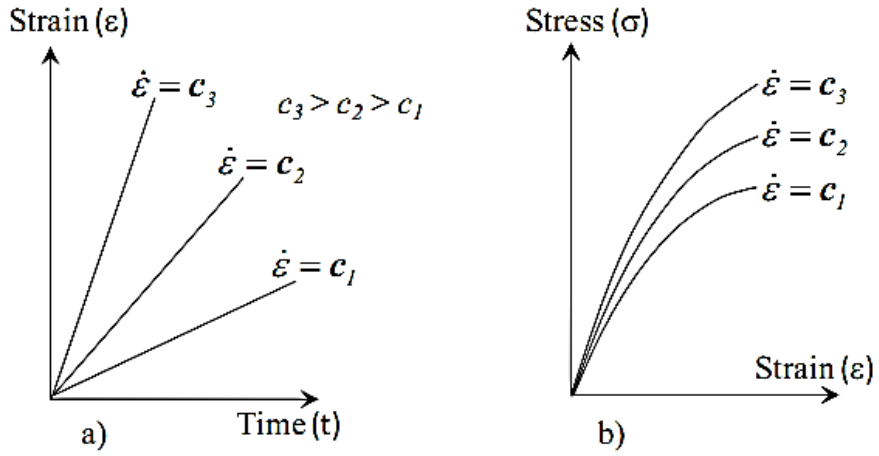

Figure 2.14: Illustration of the effect of strain rate on the stress-strain-time relation in CRS tests

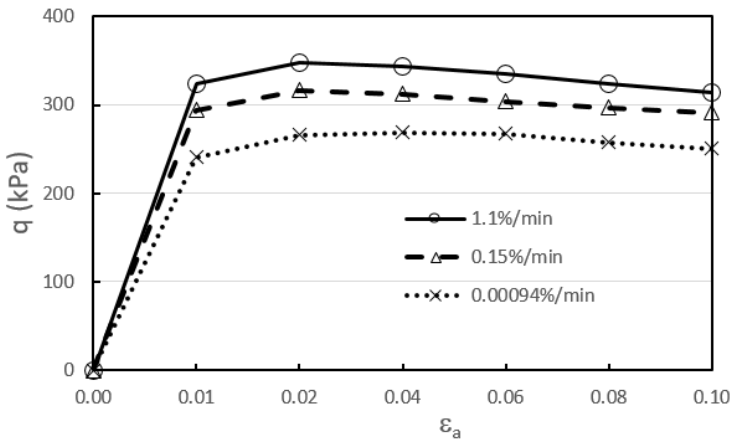

Figure 2.15: Illustration of the effect of strain rate on the stress-strain-time relation in CRS tests

In order to investigate the effect of strain rate on the compressibility of soft clay, constant rate of strain (CRS) tests have been broadly adopted to show the rate-dependency of soft clay under one-dimensional testing conditions. Detail of CRS tests has been discuseed in the research ([95]–[100]). Compared to the conventional Oedometer test, there are many advantages for the application of CRS test with respect to the continuous loading, which makes the testing conditions easier and provides a more direct and accurate relationship between stress and strain. Moreover, the CRS test can operate automatically after some initial setting steps. However, a major challenge in the application of CRS is the selection of an appropriate value of the imposed strain rate, in order to determine the consolidation parameters such as compression index, coefficient of secondary compression, permeability, or the stress-strain curve corresponding to the conventional Oedometer test. Different researchers have proposed different expressions to determine an appropriate value of strain-rate for CRS test (e.g. [95]–[100]). For example, Mesri and Feng [99] suggested an expression to determine the strain rate of the CRS test for studying end of primary (EOP) e-logσ_v' curves.

$$\dot{\varepsilon}_a = \frac{k_{v0}}{2^{C_c/C_k} H^2} \frac{\sigma_p'}{\gamma_w} \frac{C_\alpha}{C_c} \qquad [2.1]$$

where k_{v0} is the initial vertical coefficient of permeability, $C_k = \Delta e/(\Delta log k_v)$, H is the maximum drainage distance, σ_p' is the preconsolidation pressure corresponding to EOP e-logσ_v' curve, γ_w is the unit weight of water. Equation [2.1] requires some consolidation parameters such as compression index C_c, coefficient of secondary compression C_α obtained from conventional oedometer tests. Moreover, Equation [2.1] reveals that the increase of the height of sample leads to the decrease of vertical strain rate applied for the CRS test. This begs the question of whether the results from CRS tests at different rates and at various sample heights can produce a unique EOP e-logσ_v' curve. Regarding this, the vertical strain rate used for the CRS test in practice is adequately selected so that the ratio of excess pore-water pressure at the bottom of specimen to total axial stress between 2% and 7% throughout the test [99]. Resulting from many CRS tests with different types of clays at Norwegian Geotechnical Institute (NGI), a recommendation for an adequate rate of axial strain rate of CRS test is between 1.4×10^{-6} and 2.8×10^{-6} (s^{-1}) [100].

To study the effect of strain rate on the compressibility of clay, Leroueil et al. [91] carried out a set of CRS oedometer tests on Batiscan clay samples with strain rates varying from 1.69×10^{-8} to 1.43×10^{-5} (s^{-1}). The physical properties of clay samples are

as follows: unit weight $\gamma = 17.5$ kN/m^3, water content $w = 80\%$, liquid limit $w_L = 43\%$, plastic limit $w_p = 21\%$, clay size particle content 80%. The initial stress is 65kPa equal to the in-situ vertical effective stress by depth of collecting the specimens. The results from CRS tests are illustrated in Figure 2.16. It can be seen that the compression curve moves to the right side for higher strain rates. This means that the resistance to compression increases with an increasing rate of strain. It is notable that at very slow strain, the compression curve deviates from the other tests, which can be explained by the effect of structure of soft clay [91]. The yielding stress or pre-consolidation stress increases corresponding to the higher rate of loading, hence selection of an appropriate rate of CRS oedometer test to determine the adequate consolidation parameters presents a significant challenge. As a result, it is possible that the compressibility of in-situ soil is different from the data obtained from the laboratory. Leroueil [101] reported that the strain rates in the laboratory tests are typically higher than in-situ strain rates, as shown in Figure 2.17. From this, it can be argued that the rate of loading in conventional oedometer test is the closest rate to in-situ among laboratory tests. This explains why 24 hour incremental loading in the conventional oedometer test is normally carried out to determine the compressibility properties of soil.

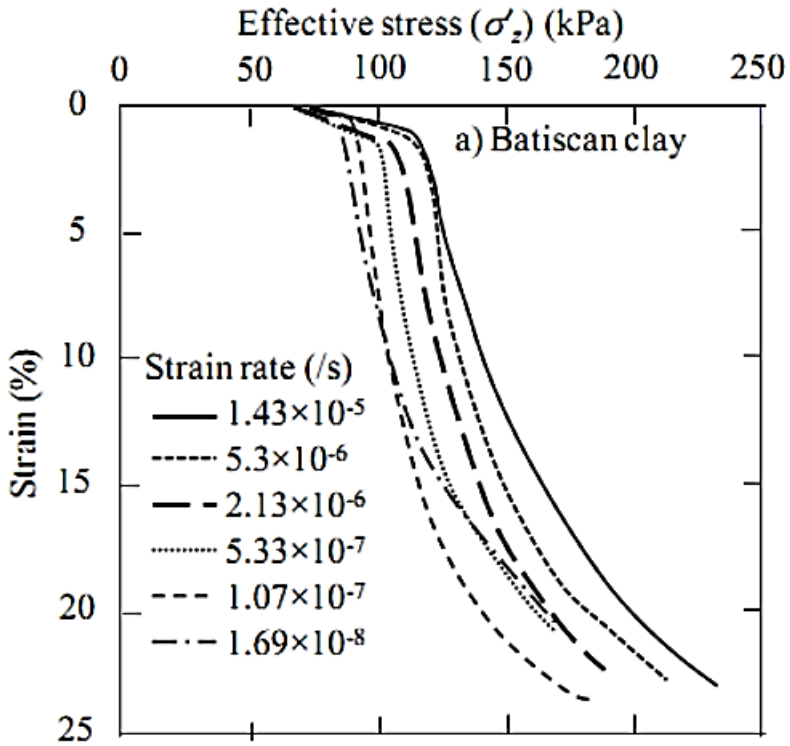

Figure 2.16: Typical constant rate of strain oedometer test on Batiscan clay. Solid line represents compression curves at different strain rates. (adapted [91])

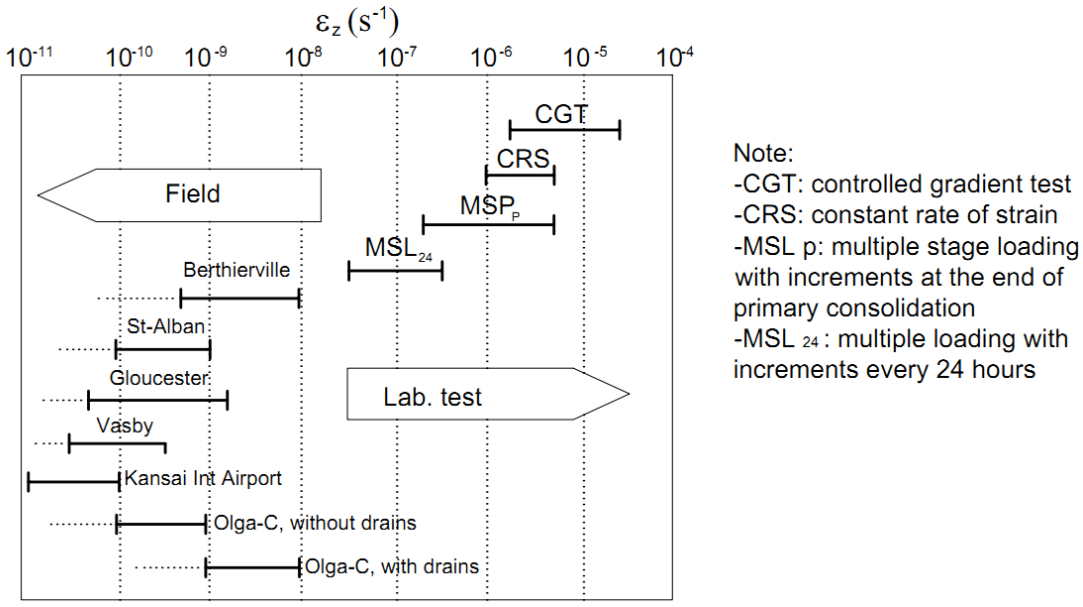

Figure 2.17: Range of strain rates in laboratory tests and in-situ (adapted from Leroueil [101])

Strain rate not only influences the compressibility of soft clay, it also has an effect on the strength of soil, as mentioned above in Figure 2.15. To sudy the effect of rate of loading on the strength of soil, Richardson and Whitman [102] conducted a

series of undrained triaxial compression tests on normally consolidated remoulded clay samples. The experiemental data showed that the undrained shear strength is improved corresponding to the samples which are applied by higher loading rate, as shown in Figure 2.18. They also reported that the effect of strain rate on soil strength of the overconsolidated specimens is more significant than that of the normally consolidated samples. The noticeable effect of strain rate on soil strength, in particular the peak strenth has also been supported by the work of Lo and Morin [103] .

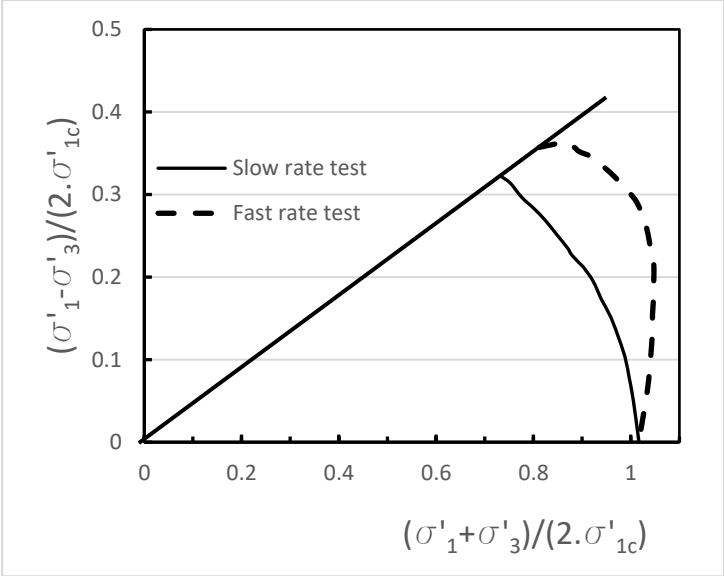

Figure 2.18: Effect of strain rate on the undrained effective stress path (adapted from [102])

2.2.4 Creep

2.2.4.1 Overview

The creep behaviour of soft clay is a phenomenon in which natural clay experiences deformation under a constant stress. This is clay's most typical, pronounced and observable behaviour. Observation of the deformation of some structures and natural slopes shows the existence of creep in natural clay, which may cause damage to construction projects. A typical example of this phenomenon is the Leaning Tower of Pisa, an iconic tourist destination for any visitor to Italy. There are, however, many other documented examples of in-situ creep behaviour; some of which exemplify that creep failure can lead to significant damage. An example for this is the disaster of Vayron reservoir in Italy. Due to the gravitational creep by slope, the reservoir's side slid and caused the loss of 3000 lives in 1963 [104]. Although creep deformation has attracted attention for centuries, real investigation started in the

middle of 19th century when many residential buildings were constructed on weak deposits such as soft clay. In the present time, geotechnical engineers consider the creep behaviour of soil to be an important factor in the design process.

The term creep is linked with the background of Terzaghi's theory of one dimensional consolidation of soils; however, it had not been fully explained until Taylor [105] accounted for secondary compression in a theory of consolidation. While the rate of primary consolidation is controlled by the velocity of water capable of escaping from the soil, the rate of secondary consolidation is controlled by the viscous resistance of soil structure. Therefore, the secondary consolidation is defined as the reduction of the volume of soil mass under sustained loading. Secondary compression refers to a special case of creep volumetric strain. To measure the magnitude of the secondary effect on the consolidation process of soil, Mesri [106] suggested a now popular parameter, namely coefficient of secondary compression which can be determined directly from the conventional oedometer test, via the relationship of the logarithm of time and void ratio.

The complete creep response is shown in the upper curve in Figure 2.19. It is often divided into three stages. In the initial stage (primary), the magnitude of strain is quite high, however, the strain rate gradually decreases to become steady during the second stage. This constant creep rate is called the minimum creep rate, since it is the slowest creep rate during the test. In the third stage (tertiary), the creep rate increases until failure occurs (creep rupture). Looking at the different deviatoric stress levels, it is obvious that at low deviatoric stress, creep rates are very small and of little practical importance. At high deviatoric stress, however, the strain rate is very large and rupture is noticeable. Related to creep rupture, the concept of rupture life has been an attraction of many researchers.

It is important to understand the mechanisms of creep deformation because it enables a better solutions for predicting the soft clay behaviour over the long term. The literature proposed different types of creep mechanism, which can be categorised into five groups: (1) breakdown the interparticle bonds; (2) sliding between the inter-particle bonds; (3) jumping bonds; (4) water flow in a double pore system, and (5) structural viscosity [107]. The detail of each creep mechanism group is presented in the following section.

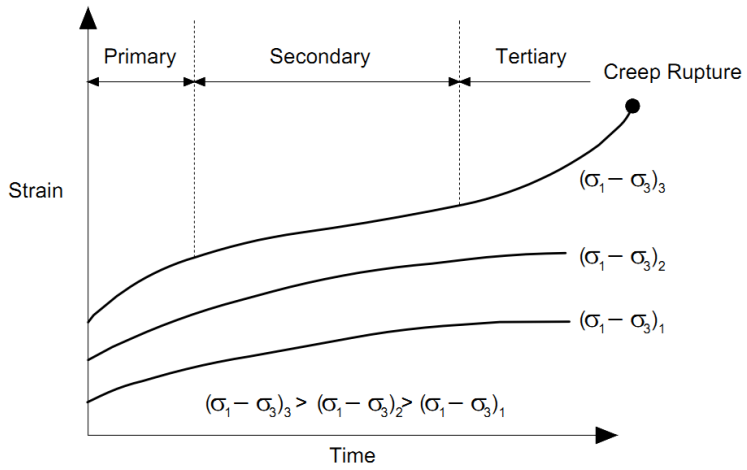

Figure 2.19: Creep response at different level of deviatoric stress (Adapted from [29])

2.2.4.2 Creep mechanisms

Terzaghi's influential theory of consolidation is based on the main assumption that the relationship between void ratio and effective stress is time independent; the theory focuses on the rate of excess pore water pressure dissipation. However, observation from many experiments shows that settlement continues after the completion of the dissipation of water pressure. This settlement is time and viscosity dependent, associated with the change of the structure of soft clay, called creep deformation or secondary consolidation. Unfortunately, the mechanism of creep deformation has been the subject of few experimental investigations [108]. Therefore, this section reviews the possible mechanisms of creep deformation and categorises them to make them more accessible.

a. The breakdown of inter-particle bonds

The processes of primary and secondary (creep) compression are associated with the transfer of stress from the external loading to the soil skeleton, leading to the movement of soil particles ([105], [109]). Under the application of external stress, free water is dissipated, causing the possible increase of the contact between the soil particles and the reduction of void ratio. The increase of effective stress results in the breakage of some inter-particles forces, such as primary valence bonds, van der Waals forces or even hydrogen bonds. This causes further rearrangement of soil particles, leading to further settlement or compression called creep deformation.

b. The movement of atoms and molecules

The creep mechanism due to the movement of atoms and molecules (called the flow unit) to a new equilibrium position is caused by the application of external stress,

as explained by Murayama and Shibata [110], Christensen and Wu [111], Mitchell [112], and Kwok and Bolton [113]. The flow unit, which is resisted by virtual energy barriers, requires active energy large enough to conquer the barriers. In clay, the flow unit concerns the displacement of oxygen atoms within the surface of the clay minerals [114]. It is suggested that the required activation energy, E_{act}, is subject to the elapsed time of creep and the deviatoric stress.

The concept of activation energy is specifically expressed by Low [115] as illustrated in Figure 2.20. The figure shows an atom (represented by solid grey) is surrounded by the water molecules (white circle). If the atom moves from position a to b, it must break the bond with the adjacent molecules and pull back the molecule in position b to secure that place. This process requires an activation energy Ea equal to the sum of the different bond's energies. The deformation of soil is estimated by the activation energy and the number of inter-particle bonds [116].

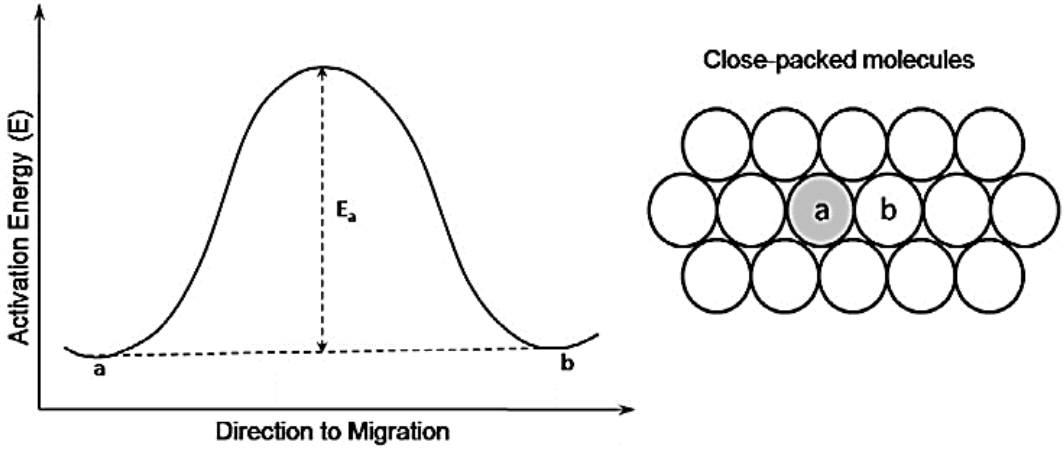

Figure 2.20: Illustration of the required activated energy for the movement of an atom surrounded by water molecules (after [115]) .

To study the effect of shear stress on creep, a number of undrained creep tests have been observed and reported that creep behaviour is dependent on the applied shear stress ([20], [116]). It is found that with a deviatoric stress approximately 30% of shear strength, the creep strain is at small creep strain rate decreasing to zero in the long term with deviatoric stress up to 70% of strength, the creep strain increases at a constant rate; and for the deviatoric stress over 70% of the shear strength, the rate of creep strain is accelerated and possibly leads to the failure or creep rupture.

c. Slipping among particles

As defined by Grim [117], creep is the reduction of volume mostly due to the slippage of the soil grains. However, this process occurs slowly, owing to the frictional

resistance of soil particles against the slipping. This concept is further investigated by Kuhn and Mitchell [114], who detailed the process of sliding movement between particles. Although this process is quite similar to the process of inter-particle bonding breakage as presented above, this section mainly focuses on the breakage of inter-particle bonds under deviatoric stress, which causes the tangential component of inter-particle force, called f_t as shown in Figure 2.21. The resistance of the inter-particle forces to the external applied loading has two components, the normal contact force f_n and the tangential contact force f_t. Due to the viscous behaviour of soft clay, the mechanism of creep deformation is defined by a system including the linear string which represents the stiffness of the normal force (Figure 2.21a) and a combination of dashpot and linear spring which represents the stiffness of the tangential force (Figure 2.21b). The creep sliding between individual particles occurs within the visco-frictional dashpot. The sliding occurs when the activation energy E_a obtains the range from 84 to 190 kJ/mol [114] .

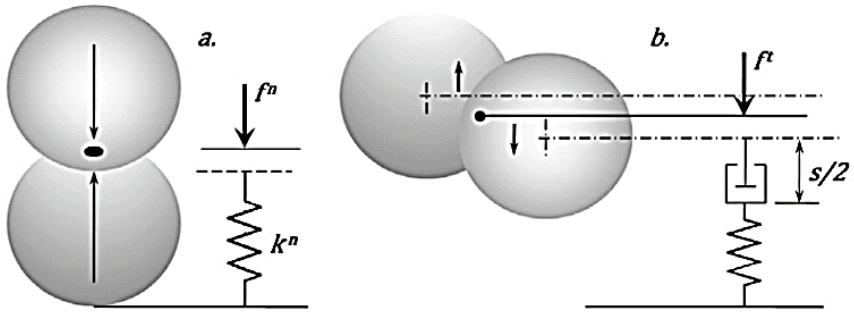

Figure 2.21: Illustration of the mechanism of inter-particle forces : (a) normal force; and (b) tangential force (adapted from [114])

d. The flow of water from micropores to macropores

The flow of water from micropores to macropores is believed to be a mechanism of creep by many researchers (e.g. [29], [118]–[121]). Micropores are defined as the pores existing within the clay clusters, while macropores are the pores created in the whole structure of soft soil, in which a primary structure is considered continuous skeleton formed by coarse grains surrounded by the clay plaletes and the secondary structure is formed by clay clusters, as shown in Figure 2.22 ([121]). Water in the micropores, which are constituted by the layer waters, have viscosity different from water in the macropore. The creep deformation or secondary compression results from the reduction of micropore water and primary consolidation is subject to the

dissipation of the macropore water [122]. It is reported that the micropore water is expelled out of the clay clusters to the macropores that not only is resulted from the application of external pressure, but also the interaction of chemical potentials of water in micropore and macropore to reach an equilibrium state [119].

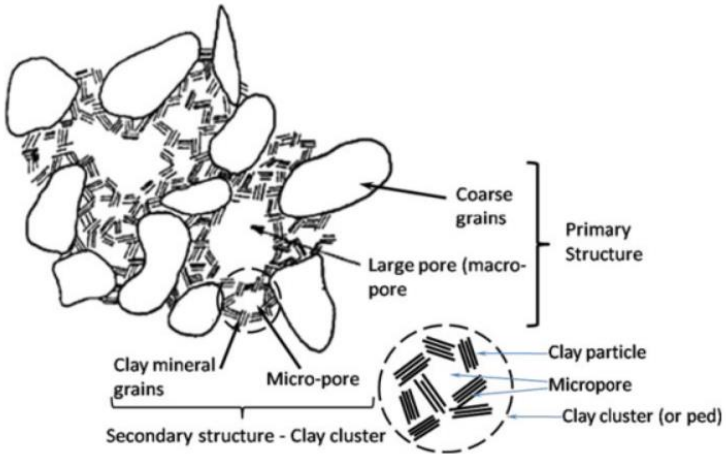

Figure 2.22: Schematic concept of micropore and macropore (adapted from Zeevart 1986)

e. Viscous resistance

Viscous resistance is defined as the obstruction of the flow of fluid or the deformation under an applied stress. It is the frictional drag of one particle sliding over another particle. Viscous resistance against the relative movement between clay particles is believed to be subject to the double layer of water surrounding the surface of clay particles ([123]–[127]). The absorbed water layers are very different from the free water layers, since they constitute different cations and anions and so the absorbed water exhibits electrochemical properties ([45], [117]). The absorbed water within the microstructure of clay can be categorised into three groups: (1) water absorbed on the internal surfaces of clay mineral, (2) water absorbed between the clay particles (called double layer water) and (3) capillary water located in the space between the clay particles [128]. The water layer in the first group is considered to be the solid state and is dependent on the distance from the clay particle surface [129]. The viscosity of the double layer of water is reported to be higher than the free water and increases with the proximity to the clay surface [117].

Taking the effect of the absorbed water on the rearrangement of soil structure, Bjerrum [124] proposed the concept of instant compression and delayed compression during the consolidation process. He believed that it is inadequate to divide the consolidation process into two stages, primary consolidation and secondary

consolidation, in which the secondary occurs after the completion of the excess pore pressure dissipation in primary consolidation. An instant compression occurs simultaneously with the increase of applied effective stress to get an equilibrium state; while the delayed compression is defined as the volume change under sustained effective stress.

Yin [130] suggested that the creep deformation is mainly induced by the combination of two processes: (1) viscous flow of the double layer of water, and (2) viscous adjustment of clay structure to reach another equilibrium state under an application of a sustained effective stress. Therefore, creep is continuous as long as the effective stress is sustained.

2.2.4.3 Creep rupture

Creep can be divided into three stages, the primary stage, secondary stage and tertiary stage – as shown in Figure 2.23. While the creep strain rate decreases or is constant during the primary stage and secondary stage respectively, the strain rate at the tertiary stage is accelerated, which may lead to a failure, namely creep rupture. Therefore, creep rupture is defined as the failure of soil due to an accelerated creep rate at a constant deviatoric stress. Following the creep response at different values of deviatoric stress in Figure 2.19, it is obvious that at low stress, the creep strain is small and has a tendency toward a constant value; there is little practical importance at the low value of the deviatoric stress. However, at the high deviatoric stress, the strain acceleration is very large and potentially catastrophic. For this reason creep rupture has been studied by many researchers (e.g. [15], [131], [132]).

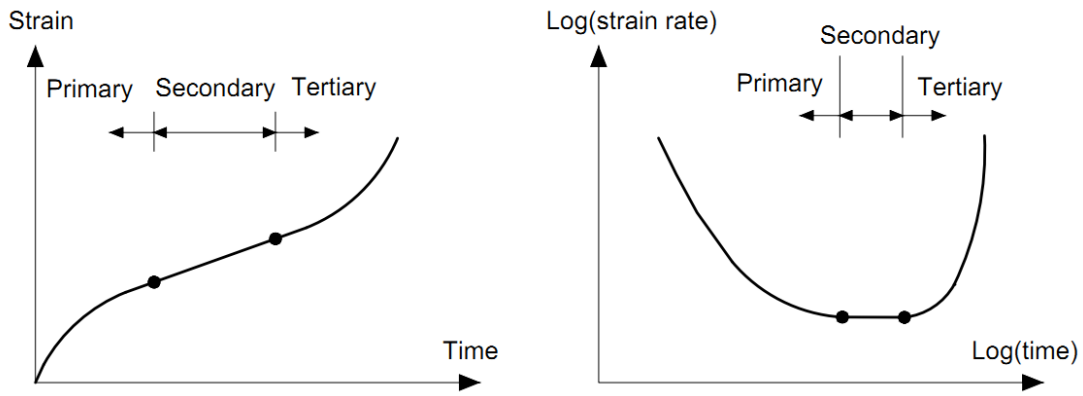

Figure 2.23: Creep rupture at the tertiary stage

Related to creep rupture, the concept of rupture life has been of interest to many researchers. Fin and Shead [133] conducted a series of undrained triaxial creep tests to investigate the relation between rupture life and creep strain rate, measuring the relationship between creep rate and elapsed time – shown in Figure 2.24. The straight light drawn by connecting the minimum axial strain rates is represented for the relation between time (t_m) and the minimum creep strain rate ($\dot{\varepsilon}_m$). Futher investigation of the minimum creep strain rate line for over-consolidated samples (OCR-2, OCR=6 or OCR=25), concluded that the minimum creep strain rate line (t_m, $\dot{\varepsilon}_m$) is uniquely determined and independent of consolidation history and the stress level. This line was noted earlier by Singh and Mitchell [134] in the discussion about predicting rupture life.

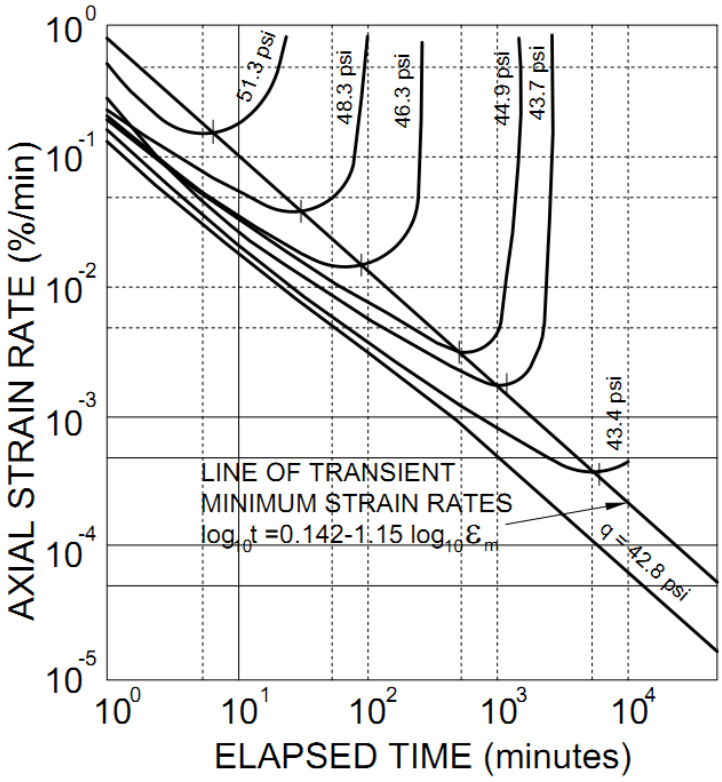

Figure 2.24: Variation in the axial strain rate with time in the undrained creep test (adapted from [133])

The correlation between the rupture life (t_f) and minimum creep rate ($\dot{\varepsilon}_m$) became well-recognized after the work of Saito ([135]–[137]), as shown in Figure 2.25.

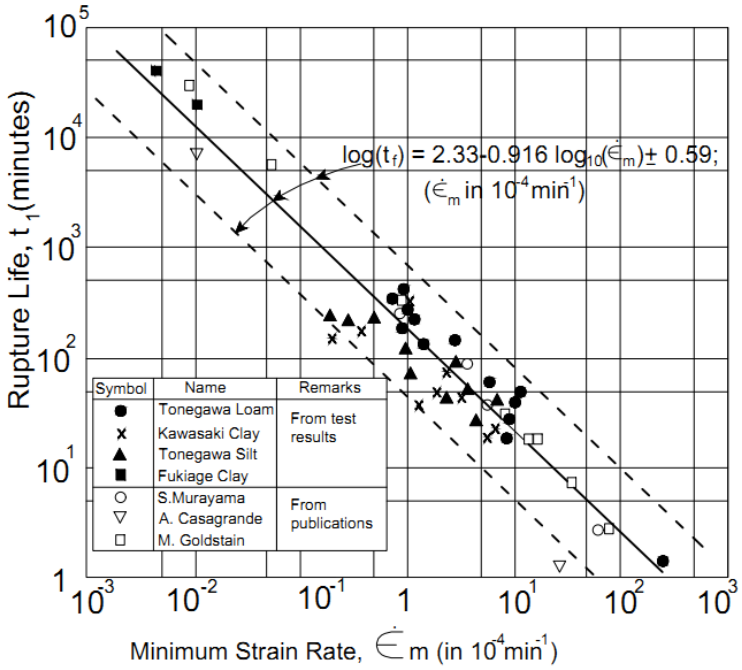

Figure 2.25: Correlation between rupture life and the minimum creep rate (adapted from [135])

Following the experimental result shown in Figure 2.25, the relation between rupture life (t_f) and minimum creep strain rate ($\dot{\varepsilon}_m$) can be expressed as:

$$\dot{\varepsilon}_m . t_f = constant \qquad [2.2]$$

Campanella and Valid [94] have conducted extensive investigation into undrained creep rupture behaviour of normally consolidated Haney Clay under triaxial and plane strain condition. Their test results show that the correlation in the form of [2.2] is reasonable. The value of the constant of Eq. 2.2 for K_0 triaxial condition is around 4, smaller than that of isotropic conditions.

2.2.4.4 Coefficient of secondary compression

According to Terzaghi's theory of one-dimensional consolidation, soft soil settlement would continue even after the dissipation of excess pore pressure is complete. Classical theory of consolidation distinguished between the two types of deformations, using the terms as primary consolidation and secondary consolidation. The former is used to describe the time-dependent deformation because of the volume change due to the dissipation of excess pore pressure whereas the latter is used to describe the time-dependent deformation under the constant effective stress (Figure 2.26).

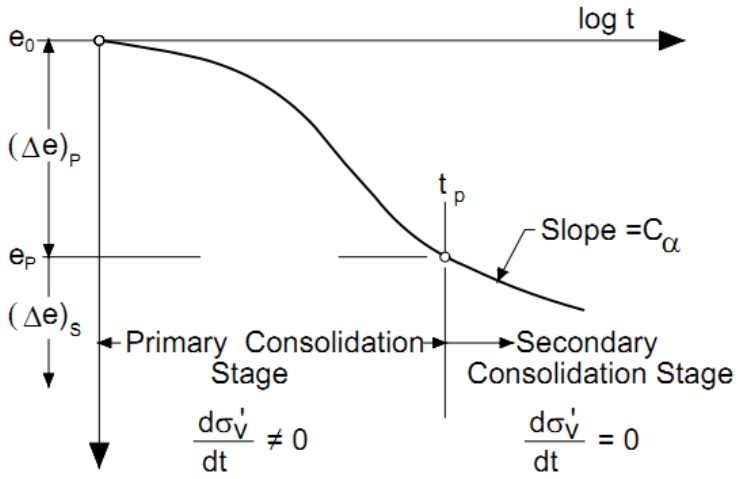

Figure 2.26: Primary and secondary consolidation (adapted from [6])

Many engineers find it convenient to consider that primary consolidation in the field occurs first, followed by secondary settlement. In the laboratory, with relatively thin samples, the concept that secondary effects follow the primary effects may be reasonable since the time testing is relatively short. However, it is not persuasive in-situ, where the thickness of the soil layer is quite large and the primary consolidation process is experienced over weeks, months and years. In addition, recent research into the microstructure of soil shows that soil structure, which has an important effect on secondary compression, changes from the initial stage of loading. Therefore, Buisman [6] proposed the term 'secular time effect', which was used to emphasize that secondary effects should not be thought of as following primary settlement. Taylor [138] proposed two hypotheses related to secondary effects. Hypothesis A assumes that the completion of primary consolidation is followed by secondary consolidation (creep deformation), while hypothesis B proposes that creep deformation occurs during the excess pore pressure dissipation period. The majority of creep models have been developed based on hypothesis B. The fundamentals of secondary compression have been the focus of a number of researchers (e.g. [6], [80], [106], [124], [138]–[140]).

To measure the magnitude of the secondary effect on the consolidation process of soil, Mesri [106] suggested the now popular parameter, namely coefficient of secondary compression (C_α) which can be directly determined from the conventional oedometer test, via the relationship of the logarithm of time and void ratio – as shown in Figure 2.26.

Many studies have been conducted to investigate the value of C_α (e.g. [6], [106], [140], [141]). Buisman [6] reported that C_α followed a linear relationship when void

ratio is plotted against logarithm of time (Figure 2.26). However other researchers argue that C_α is not constant (e.g. [91], [140]). In the interest of simplicity, C_α is assumed as a constant and determined by Mesri [106]:

$$C_\alpha = \frac{de}{d\log(t)} \qquad [2.3]$$

Or, C_α can be determined directly from the result from conventional oedometer test by the slope of the secondary compression line. So, it can be derived from the curve of void ratio and logarithm of time. C_α can also be estimated by empirical correlation suggested by some researches. An example is the proposed empirical correlation between C_α and the isotropic compression index λ as ${C_\alpha}/{\lambda} = 0.05 \pm 0.029$ for Clay and ${C_\alpha}/{\lambda} = 0.07 \pm 0.02$ for peat [142].

There are many factors affecting the coefficient of secondary compression including temperature, time, sample thickness, consolidation pressure, remolding, pre-compression, loading rate, and shear stress [106]. It has been found that at the consolidation pressures close to the critical pressure, C_α has a high value and decreases when the consolidation pressures goes away the critical pressure. The peak value of Cα is obtained at the range of critical pressure as shown in Figure 2.27. It was also reported from Figure 2.27 that remoulded specimens of natural clays are not dependent on critical pressure due to its destroyed structure.

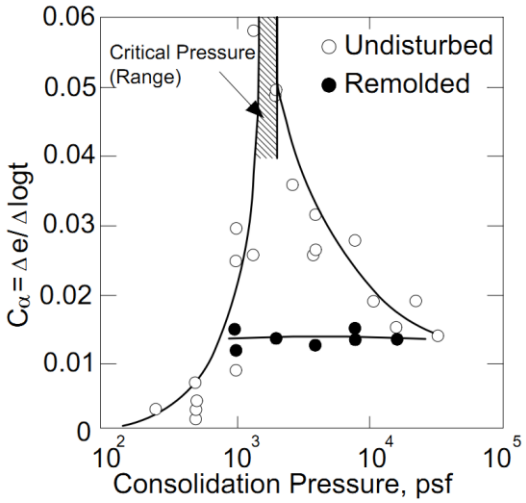

Figure 2.27: The effect of consolidation pressure for undisturbed and remoulded specimens [142]

2.2.5 Stress relaxation

Stress relaxation is a time related phenomenon in which the stress decreases while strain is kept constant over a period of time, as illustrated in Figure 2.28 [29]. Creep and stress relaxation are two important time-dependent phenomena in soft clay. Moreover, this process can be responsible for bringing about others. If creep is defined as the increase of deformation of material over time at constant effective stress, stress relaxation is the process by which effective stress tends to decrease at constant strain.

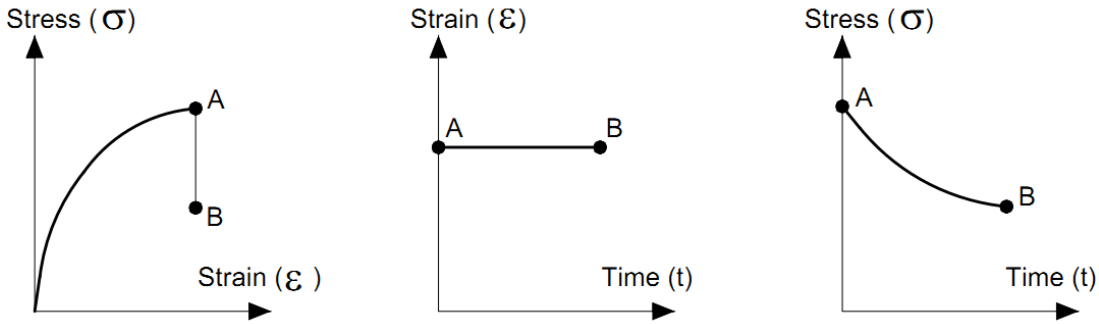

Figure 2.28: Illustration of stress relaxation process

2.3 Approaches for modelling time dependent behaviour of soft clay

2.3.1 Overview

Addressing practical solutions for time-dependent engineering problems, a constitutive model is an effective tool to predict the stress/strain/time behaviour of soft clay. A number of constitutive models have been proposed in the literature, based on different concepts and different theories but with a common aim to describe the time-dependent behaviour of soft clay, which would be as close to real-world behaviour as possible. Existing models can be categorised into three groups as follows [143]:

(1) Empirical models developed following data from experimental results.
(2) Rheological models typically given as closed-form solutions. They normally serve for conceptual understanding.
(3) General stress/strain time models are three dimensional and are often given in incremental form. Therefore, they are readily employed in numerical solutions. All stress paths can be simulated with this group of models. Hence, they are widely applied to model the behaviour of soil.

Expanding on the definitions above, the first group of models requires that specific conditions apply; the second is often limited to describing conceptual matters. Among the three group of models, the last is capable of addressing widely practical

geotechnical engineering. The aim of this thesis is to develop a constitutive model capable of describing practical soft clay behaviour, focusing on the general stress/strain/time approach. Therefore, this section focuses on reviewing this approach.

Most general stress-strain time models have been developed using the overstress theory and the nonstationary flow surface (NSFS) theory. Therefore, these two theories are reviewed and analysed, to explore some of the advantages and limitations of each, before one theory is selected for the development of a time dependent constitutive model.

2.3.2 Overstress theory

Overstress theory has been developed by Perzyna [8]. He assumed the existence of a rate sensitive loading surface, namely dynamic loading surface (DLS) and a static loading surface (SLS) or time independent plasticity yield surface. The different between DLS and SLS is associated with the rate of sensitivity or the viscosity of soil. It is represented by a function, called the overstress function, which is used to determine the viscoplastic strain rate. The total strain rate is composed of elastic strain rate and viscoplastic strain rate:

$$\dot{\varepsilon} = \dot{\varepsilon}^{e} + \dot{\varepsilon}^{vp} \qquad [2.4]$$

A key assumption in connection with Perzyna's overstress theory is that viscous effects are negligible in the elastic region and it is computed based on generalised Hooke's law (time – independent).

The viscoplastic strain rate in Eq. 2.4 is expressed as:

$$\boldsymbol{\varepsilon}_{ij}^{vp} = \boldsymbol{\gamma}.\boldsymbol{\Phi}(\boldsymbol{F}).\frac{\partial \boldsymbol{G}}{\partial \boldsymbol{\sigma}_{ij}'} \qquad [2.5]$$

Where γ is the viscosity parameter; G is the plastic potential; σ_{ij} is effective stress state tensor and Φ(F) is the overstress function representing the difference between the dynamic loading surface (DLS) and the static loading surface (SLS) (Figure 2.29). The core of this theory is determination the overstress function $\Phi(F)$ and its overstress index F. The overstress index is widely defined based on the dynamic yield surface [3]. This might cause an overestimation of the volumetric deformation under shearing if the expansion of yield surface is unequal. To address this issue, Hinchberger and Rowe [144] proposed a projection method to determine F as the distance between the original stress state and the projection stress state on the static yield surface. This makes for mathematical complexity. The overstress function

normally employs the form as exponential function ([17], [145], [146]) or the form power overstress function ([21], [144]). Other research has suggested that the overstress function can be determined from drained creep test behavior and it is able to simplify the determination of model parameters ([147], [148]).

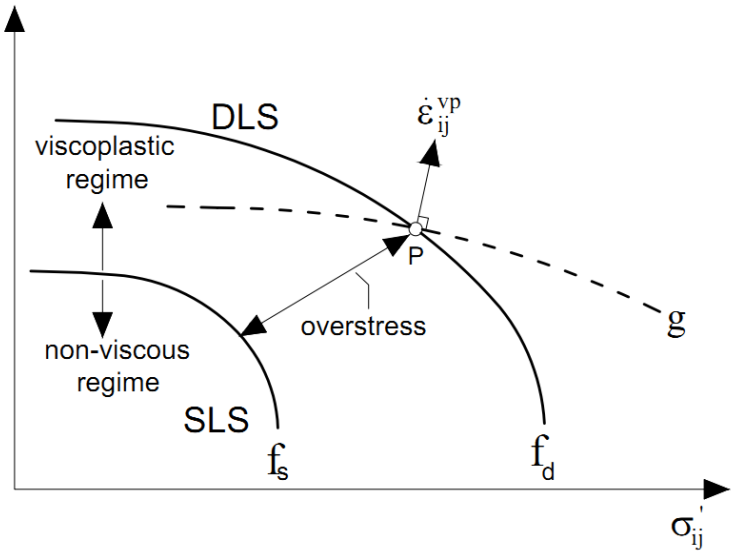

Figure 2.29: Illustration of overstress theory (After [8])

The difference between overstress theory and general elastoplasticity framework is that viscoplastic strain is not derived from the consistency condition, while plastic strain in the conventional elastoplastic model is computed from the consistency condition. This implies that inelastic strains in the overstress model are not dependent on the stress history but the current stress point, while inelastic strains in classical elastoplasticity are related to the stress rate.

Overstress theory has been commonly employed in modelling the viscoplastic behaviour of soil. The earliest viscoplastic model using overstress theory is the Adachi and Okano model [145], which modelled fully saturated normally consolidated clay. Further development of the Adachi and Okano model, in combination with the work of Oka [149], proposed a series of viscoplastic models ([17], [150]–[152]) with the capacity of describing more time-related phenomena such as creep, stress relaxation and strain rate effects, as well as secondary consolidation. Katona ([153], [154]) proposed a viscoplastic cap model, capable of modelling a wide range of geological materials, in particular soils and rocks. Recently, there have been some advanced models with the capacity of describing not only the viscosity of soil, but also some advanced features of natural soft soil including fabric anisotropy, inter-particle bonds

and the degradation of those bonds, such as EVP-SCLAY1S [155], and EVP-SANICLAY [156].

Most overstress-based models follow Perzyna's theory that the viscoplastic strain rate associated with the overstress function is only related to the current stress state but not to the stress history. Therefore, the consistency rule is invalid. Many researchers ([153], [157], [158]) report limitation of the overstress theory, arguing that it is unable to properly capture the creep behaviour of soil, in particular the acceleration creep process which leads to creep rupture. The latter drawback can be addressed by using a stress-state-dependent fluidity parameter [152], the destructuration effect [21] or the damage rule [159].

To study the overstress theory in more detail, an elasto-vicoplastic SaniClay (EVP-SANICLAY) model is taken for review and modification. The detail of the modification of this model and its capacity for predicting the long-term behaviour of natural soft clay is presented in the author's paper [160]. In the following, important points and a discussion of some limitation of the modified EVP-SANICLAY are presented.

The model EVP-SANICLAY was recently developed by Rezania et al. [156], in which not only the viscous behaviour of soil is modelled, but two other advanced features of natural soil are described: fabric anisotropy and destructuration; many time-dependent constitutive models [e.g. [3], [148], [161]] fail to account for these features. The overstress theory was employed in this model to account for the soil viscosity effects, so that the common practical issue, the time-dependent behaviour of soft soil, can be taken into consideration.

The rotational hardening (RH) law in EVP-SANICLAY has been further simplified and modified to define the evolution of the fabric anisotropy of natural clay. A new RH law proposed by Dafalias and Taiebat [162] is employed, which can be expressed as:

$$\dot{\alpha} = \langle L \rangle C p_{at} \frac{p}{p_0} (\alpha_b - \alpha) + \dot{\alpha}_f; \quad \alpha_b = \pm \frac{M}{z} \left[1 - \exp\left(s \frac{|\eta|}{M} \right) \right] \qquad [2.6]$$

where $\langle L \rangle$ is the plastic multiplier, a function of the stress rate or strain rate and the plastic modulus, obtained by the consistency condition $\dot{f} = 0$ and its relation with plastic volumetric strain rate can be expressed as $\langle L \rangle \left| tr \frac{\partial g}{\partial \sigma} \right| = \left| \dot{\varepsilon}_v^{vp} \right|$. C is a model parameter controlling the pace of evolution and z and s are model constants controlling

the equilibrium values of α under constant-stress-ratio η loadings. $\dot{\alpha}_f = (\dot{S}_f / S_f)\alpha$ controls the contribution of destructuration over the change of orientation of the yield surface.

The overstress function representing the difference between the dynamic loading surface and the static yield surface adopts an exponential form proposed by Fodil et al. [146]:

$$\Phi(F) = \exp(F) - 1 = \exp\left[N\left(\frac{p_0^d}{p_0^s} - 1\right)\right] - 1 \tag{3}$$

where p_0^d is the size of DLS, N is the strain-rate coefficient that together with μ are the two viscous parameters of this model.

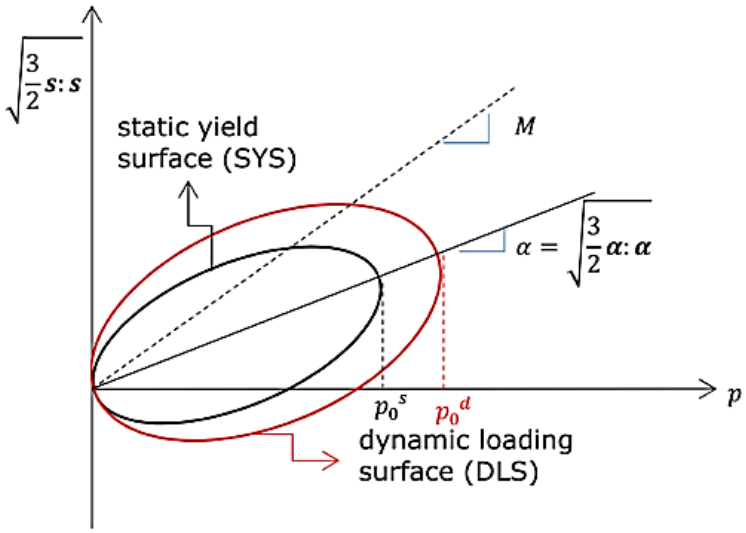

Figure 2.30: Schematic of modified EVP-SANICLAY model in the stress space

The model has a total of 10 parameters, which can be determined straight forwardly from standard laboratory tests such as oedometer test, triaxial undrained shearing test. The detail of how to determine the modified EVP-SANICLAY is presented in Rezania et al. [156]. Its prediction capacity was verified against the practical boundary value level by predicting the performance of a case study embankment built on a soft Ballina clay deposit in Australia and the results provided qualitatively and quantitatively similar predictions of embankment field data recorded for the long-term.

In spite of its outstanding capacity for capturing some complicated features of natural soil regarding fabric anisotropy, destructuration and time/rate dependent behaviour, modified EVP-SANICLAY nevertheless exhibits limitations due to the

mathematical structure of overstress theory and the hardening law using in SANICLAY model. For example, the model is unable to describe the creep behaviour of natural soil properly (it cannot account for tertiary creep) or the determination of model parameters is not truly straightforward from the laboratory results. Some model parameters have still been relied on for some calibration processes, in particular the two parameters of viscosity and destructuration. This challenges users to determine a set of appropriate parameters for the model. Therefore, a time-dependent model with the same capacity for capturing the advanced features of soft clay, but also properly capable of describing creep behaviour, with model parameters that have a clear physical meaning, determined directly from standard laboratory is demanded. To address this demand, another approach to modelling is considered: Nonstationary Flow Surface Theory.

2.3.3 Nonstationary Flow Surface Theory

The concept of Non-stationary Flow Surface (NSFS) Theory has been developed by Naghdi and Mursh [163] and Olszak and Perzyna [9],[10]; as reported by Matsui and Abe [18]. This theory is a result of further development of the inviscid theory of elastoplasticity. The significant difference between NSFS theory and classical elastoplasticity is the definition of yield condition. While the yield condition of the latter is time independent ($f\left(\sigma'_{ij}, \varepsilon^{p}_{ij}\right) = 0$) the yield condition associated with the NSFS theory depends on time expressed as $F\left(\sigma'_{ij}, \varepsilon^{vp}_{ij}, t\right) = 0$, where ε^{vp}_{ij}, t are the viscoplastic strain and time factor respectively.

According to the expression of NSFS yield surface, it is clear that the surface changes at every moment, even though the viscoplastic strains or stress state are kept constant leading to this yield surface called nonstationary flow surface. With this feature, the NSFS theory can easily describe two popular time-related phenomenon namely relaxation and creep of soft clay.

The nonstationary yield condition $F\left(\sigma'_{ij}, \varepsilon^{vp}_{ij}, t\right) = 0$ defines a surface in stress space. All possible stress states must lie on this nonstationary flow surface under consistency condition. If an initial stress state makes $F\left(\sigma'_{ij}, \varepsilon^{vp}_{ij}, t\right) < 0$ or $f\left(\sigma'_{ij}, \varepsilon^{p}_{ij}\right) < 0$), that stress state is located inside the flow surface (yield surface) and soil obeys elastic behaviour. However, keep loading and once the stress state reaches the yield surface, viscous behaviour is triggered, and soil is said to be an elasto-viscoplastic state.

Similar to overstress theory, the strain rate is decomposed into elastic strain rate and viscoplastic strain rate:

$$\dot{\varepsilon} = \dot{\varepsilon}^{e} + \dot{\varepsilon}^{vp} \quad [2.7]$$

The elastic strain rate is determined by generalised Hooke's law related to the effective stress rate as:

$$\dot{\boldsymbol{\varepsilon}}^{\boldsymbol{e}} = D_{ijkl}^{-1}.\dot{\sigma}'_{kl} \quad [2.8]$$

and the viscoplastic strain rate is defined according to the flow rule as in classical elastoplastic theory:

$$\dot{\varepsilon}_{ij}^{vp} = \langle\lambda\rangle \frac{\partial G}{\partial \sigma_{ij}} \quad [2.9]$$

where G is viscoplastic potential and $\langle\lambda\rangle$ is non-negative viscoplastic multiplier, which is determined from consistency condition $F\left(\sigma'_{ij}, \varepsilon_{ij}^{vp}, t\right) = 0$.

Looking at the eq.[2.9], it is clear that viscoplastic strain rate is determined in the same way as plastic strain. Therefore, the advantage of the NSFS concept is to be inherent from the framework of classical elastoplastic theory.

Consistency condition is derived as:

$$\dot{F} = \frac{\partial F}{\partial \sigma'_{ij}}\dot{\sigma}'_{ij} + \frac{\partial F}{\partial \varepsilon_{ij}^{vp}}\dot{\varepsilon}_{ij}^{vp} + \frac{\partial F}{\partial t} = 0 \quad [2.10]$$

Combining [2.7], [2.8], [2.9] and [2.10], the viscoplastic multiplier λ can be worked out as:

$$\langle\boldsymbol{\lambda}\rangle = -\frac{\frac{\partial F}{\partial \sigma'_{ij}}\dot{\sigma}'_{ij} + \frac{\partial F}{\partial t}}{\frac{\partial F}{\partial \varepsilon_{ij}^{vp}}\frac{\partial g}{\partial \sigma'_{ij}}} \text{ (for the stress loading path)} \quad [2.11a]$$

$$\langle\boldsymbol{\lambda}\rangle = -\frac{\frac{\partial F}{\partial \sigma'_{ij}}.D_{ijkl}.\dot{\varepsilon} + \frac{\partial F}{\partial t}}{\frac{\partial F}{\partial \varepsilon_{ij}^{vp}}.\frac{\partial g}{\partial \sigma'_{ij}} - \frac{\partial F}{\partial \sigma'_{ij}}.D_{ijkl}.\frac{\partial g}{\partial \sigma'_{ij}}} \text{ (for the strain loading path)} \quad [2.10\ b]$$

From equation [2.11a] and [2.10b], it can be seen that the viscoplastic multiplier has two parts, one part is related to stress/strain rate and one part is related to the time effect factor $\partial F/\partial t$. This implies that the viscoplastic strain occurs even under constant strain or constant of stress, which corresponds to the relaxation or creep process. The mechanisms of the creep and relaxation process are presented in detail in the following section.

The mechanism of a creep test is illustrated in Figure 2.31. The creep process is initiated from stress state P located on a yield surface. Taking a stress path from P to Q (Figure 2.31a), in which the stress is kept constant over the time t_0 to t_1, over time, the total strain gradually increases, while the elastic strain is constant due to the constant stress. Therefore, the increase of total strain is contributed by the development of viscoplastic strain. This is also confirmed by NSFS theory, since the initial stress state is located on the yield surface, triggering the viscous behaviour and leading to the development of the viscoplastic strain. At the time t_1, the increment of the viscoplastic strain is $\left|\Delta\varepsilon_{ij}^{vp}\right|$ (Figure 2.31a) making the expansion of the flow surface from $F\left(\sigma_{ij}', \varepsilon_{ij}^{vp}(t_0), t_0\right) = 0$ to $F\left(\sigma_{ij}', \varepsilon_{ij}^{vp}(t_1), t_0\right) = 0$ as illustrated by the dot line in Figure 2.31b, if the effect of time is ignored. However, following the consistency condition, stress state must be located in the flow surface that requires the flow surface to shrink back original yield locus so that the stress state at Q lies on the flow surface. This process occurs under the effect of the time factor ranging from t_0 to t_1. Therefore, it can be concluded that yield surface is hardened by the increment of viscoplastic strain, meanwhile time effect is considered a softening parameter. This statement differs from Linggard et al [143], who claim that time is a hardening factor, making the yield surface expand and that the stress state P will be located inside the yield surface at a subsequence time t_1. This claim is invalid with the case of creep rupture.

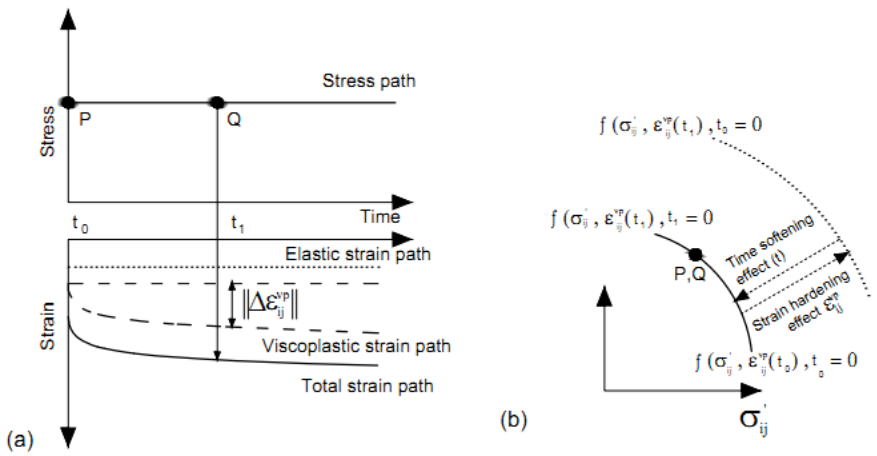

Figure 2.31a and b: Illustration of the mechanism of creep test

To study the mechanism of a relaxation process, a stress relaxation loading path from state P to state Q is illustrated in Figure 2.32. Assuming soil is loaded to the stress state P at the time t_0, the relaxation process is initiated by holding the total strain constant over the time t_0 to time t_1. Figure 2.32a shows that the stress gradually decreases from time t_0 to time t_1 by an amount $\|\Delta\sigma'_{ij}\|$. According to Hook Law, the corresponding amount of elastic strain is decreased by $\|\Delta\varepsilon^{e}_{ij}\|$, as shown by a dotted line in Figure 2.32a. Since the total strain is kept constant over time, the viscoplastic strain must increase by the same amount as elastic strain, $\|\Delta\varepsilon^{vp}_{ij}\|=\|\Delta\varepsilon^{e}_{ij}\|$ as shown by the dashed line in Figure 2.32a. The corresponding stress path presented in the stress space is illustrated in Figure 2.32b. The final flow surface must shrink to pass over the point Q at the time t_1 with the decrease of the stress by an amount of $\|\Delta\sigma'_{ij}\|$. To understand the mechanism of the relaxation process, the movement of the flow surface is divided into two stages, corresponding to the evolution of two parameters: viscoplastic strain playing a role in hardening parameters and time effect. Firstly, assuming the increase of viscoplastic strain without the effect of time, the flow surface moves outward corresponding to the accumulation of viscoplastic strain, as presented by the dotted line in Figure 2.32b . Then, only the effect of time is considered. At time t_1, the stress state Q is located inside the flow surface due to the decrease of stress. The yield locus must shrink to pass over point Q. Therefore, the effect of time here is considered as the softening factor, or as it is said: time softens the yield surface.

From the analysis of mechanism of the creep process and stress relaxation, it is revealed that the time-effect plays a role as softening rather than hardening parameter as explained in the literature review [143]. Alongside this, the increase of viscoplastic represents the hardening effect.

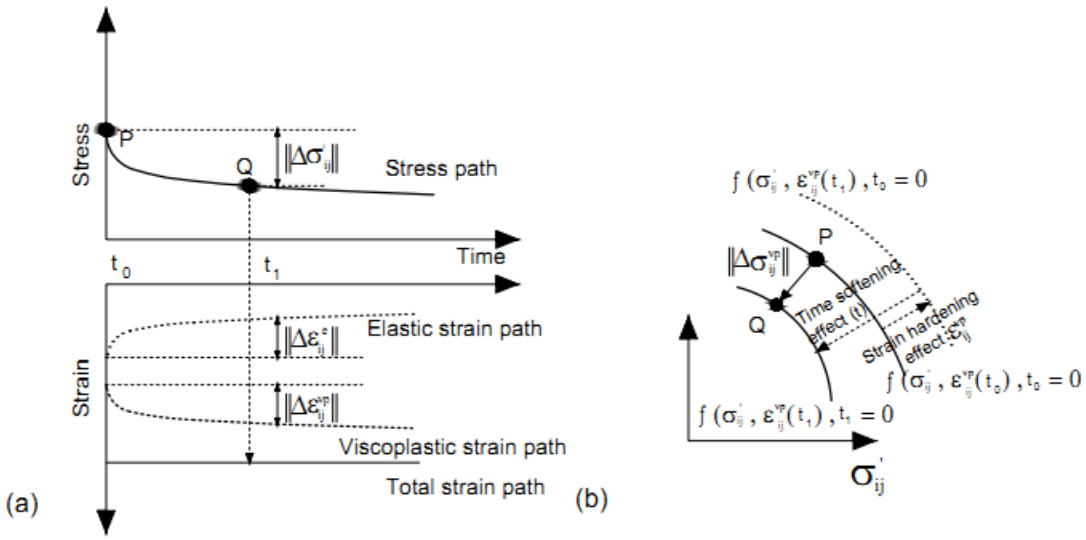

Figure 2.32: Schematic of the stress relaxation process

Despite some advantages of NSFS theory, as discussed above, such as the inherent framework from elastoplastic theory, satisfaction of the consistency condition and higher convergence rate [164], it is still not adopted widely for modelling the time-dependent behavior of soft clay. Only few constitutive models have been proposed using NSFS theory to model the time dependent behavior of soil (e.g. [16], [132], [165], [166]). Among them, the earliest model using NSFS theory to capture the full creep behavior of normally consolidated clay was proposed by Sekiguchi [161] in 1977 and the most recent model was proposed by Qiao [3] in 2016. Both models neglect the evolution of fabric anisotropy and the degradation of inter particle bonds.

2.4 Summary

Soft clay soil is characterised by its low shearing strength, low bearing capacity, high moisture content and high compressibility. However, there are now more constructions built on soft clay despite these characteristics, due to the increase of residential density on coastal areas and riverbanks. Clay ground typically exhibits large deformation over the longer term and this can potentially lead to serious damage to users. Therefore, current geotechnical engineers consider the long-term behaviour of soft ground an important factor in the design process. Addressing this challenge, many time-dependent constitutive models have been developed; however, there is still no constitutive model capable capturing all of the advanced features of soft clay under an external loading. With this ambition in mind, this chapter reviewed advanced features of soft clay, its time related behaviour and how to develop a time dependent constitutive model. This provides a knowledge-base for proposed model in subsequent chapters.

Soft clay constitutes different clay minerals which are normally the hydrated of aluminium, iron or magnesium silicate, combined in a manner to produce sheet-like structures. This determines the properties of soft clay. For example, clay composed of abundant mineral Montmorilonit exhibits high swelling and shrinkage rates, as well as very low strength; a clay composed of mostly Kaolinite, on the other hand, shows low shrinkage and swelling as well as high bearing capacity due to its strong inter-particle bonds.

Soft clay is obviously an imhomogeneous and cohesive material due to the random arrangement of clay particles, particle assemblage and pore space in soft clay which is called the fabric anisotropy. It is reported that the structure of clay fabric has a significant effect on the shear strength and volume change of natural clay. It is also reported that normally consolidated clay, with the structure of dispersed fabric, experiences dilation during shearing, whereas contraction is exhibited in samples with flocculated fabric structure [48]. The fabric anisotropy of soft clay can be categorised into two types including the inherent anisotropy and induced anisotropy; however, these are not fixed but change under the application of external loading. So, a model which has the capacity to describe both inherent anisotropy and evolving anisotropy will provide better predictions of creep. Another important characteristic of soft clay is the bonds between clay particles, which make clay material cohesive. These bonds are typically degraded by the post-yield stress, termed as the destructuration process which considerably reduces the strength of soil. Therefore, a constitutive model cannot provide an adequate prediction of soft clay behaviour if the destructuration feature is neglected.

To sum up, soft clay deposits have been found to exhibit considerable time-dependent behaviour. The most significant time-related phenomena have here been reviewed: the ageing effect, rate effect, creep and stress relaxation. If a model is to deliver reliable predications, it must address all of these time related phenomena. Among the time related phenomena, creep failure or creep rupture is an important issue requiring particular attention in geotechnical design. However, despite this, most of overstress-based constitutive models cannot capture the creep rupture process properly due to the limitation of the structure of theory formulation. Therefore, the non-stationary flow surface (NSFS) has been proposed as means of addressing this matter.

CHAPTER 3 :

DEVELOPING AN ISOTROPIC TIME-DEPENDENT CONSTITUTIVE MODEL USING NONSTATIONARY FLOW SURFACE

3.1 Introduction

Long-term deformation of soft soils can potentially cause excessive damage to geo-structures. Therefore, developing a practical model, which can provide accurate predictions of natural soil behaviour, has been the focus of many geotechnical engineers and researchers. Many constitutive models have been developed since the framework of critical state soil mechanics was introduced by Roscoe and Schofield in 1963 [11]. However, while a number of advanced models have attempted to capture different important features of soft soil behaviour, in particular regarding fabric anisotropy and inter-particle bonding (e.g. [62], [167], [168]), they have not yet described the time-dependent aspects of soft soil behaviour.

Over the past 50 years, the time dependency of soil response has been studied via various approaches; the resulting developed models can be categorised into different categories, most notably: empirical models (e.g., [1], [127], [134], [169] and overstress-based models (e.g. [156], [170]). The empirical models often require some restricting conditions and hence are not favoured for application in many practical problems; the overstress type models, despite the simplicity of their mathematical framework, are only able to capture the strain-rate effects and not the true creep response of soils. This is problematic because the creep deformation capacity of natural clays is known to be one of the most important and influential features of their behaviour.

This chapter proposes a time-dependent model based on the nonstationary flow surface (NSFS) theory ([10], [171]) in combination with the well-known Modified Cam Clay (MCC) model, namely NSFS-MCC. The NSFS theory is a further development of inviscid elasto-plastic theory, in which a time variable parameter is introduced in the yield surface equation to obtain the simultaneous description of strain hardening and the effect of time. This means that the yield surface can change at any moment. The inherent framework from the classical elasto-plastic theory is used in determining the viscoplastic strain, leading to the simplification of the numerical solution. However, defining the nonstationary yield surface is a significant challenge, that few constitutive models using this theory to model the time-dependent behaivour of soft soil achieve compared to overstress-based constitutive models. The NSFS-MCC model is capable of capturing the strain rate effects and creep response of soft clay. In particular, it is able to simulate tertiary creep response, which is an important phase of creep behaviour which leads to creep failure of soft soil deposits. In the following, a review of the MCC model is presented before introducing new model NSFS-MCC. The model is verified by some qualitative and quantitative simulations to show its capacity in describing the strain rate effects on strength and yield stress, as well as the creep behaviour of soft soil. Determination of model parameters using standard laboratory test data is also presented.

3.2 Modified Cam Clay model

The Modified Cam Clay (MCC) model was developed by Roscoe and Burland in 1968 [172]. It is a modification of the original Cam Clay (CC) model, to overcome some limitations; to be discussed in the next section. Both MCC and CC models are based on the critical state concept, a breakthrough in soil mechanics which provided a logical framework to develop a mathematical model capable of describing soil behaviour, based on the theories of plasticity, yield and flow – as proposed by the Cambridge soil mechanics school under the late Professor Roscoe [23]. The critical state concept was developed from the observed behaviour of reconstituted clay in triaxial compression tests and it is applicable to natural soils. Critical state is defined as a state in which plastic shearing could continue indefinitely, without changes in specific volume (v), deviatoric stress (q) or mean effective stress (p') [173]. This state can be mathematically expressed as:

$$\frac{\partial p'}{\partial \varepsilon_q} = \frac{\partial q}{\partial \varepsilon_q} = \frac{\partial v}{\partial \varepsilon_q} = 0 \qquad [3.1]$$

When soil reaches the critical state, it is accompanied by a unique line in $q - p' - v$ space, referred to as the Critical State Line (CSL).

The MCC is a an elasto-plastic model in which the permanent change in volume is associated with the change in size of the yield surface. It is assumed that when a stress state is located inside the yield surface, the behaviour of soil is purely elastic. Once the stress state reaches the yield surface, combination of elasticity and plasticity occurs. Hence the total strain is the combination of reversible strain and irreversible strain. Similar to an elasto-plastic model, the MCC model is defined by four principle aspects: elastic component, yield surface, flow rule and hardening law.

The elastic component is represented by bulk modulus $K' = \frac{(1+e)p'}{\kappa}$ and shear modulus $G = \frac{3(1+e)p'}{2\kappa}\frac{(1-2\mu)}{1+\mu}$ where the μ is the Poisson ratio and κ is the slope of the swelling line.

The yield surface adopted the elliptical shape as expressed by the formulation $q^2 = M^2(p'p'_m - p'^2)$. This is a significant modification from the CC model, since it prevents the indefinite possible number of strain increment vectors at the point q=0, and the discontinuity at the shape of yield surface, as shown in Figure 3.1. The modification of yield surface facilitates the numerical solution to analyse the behaviour of soil. For this reason, MCC model has been preferred for the development compared to the former CC model.

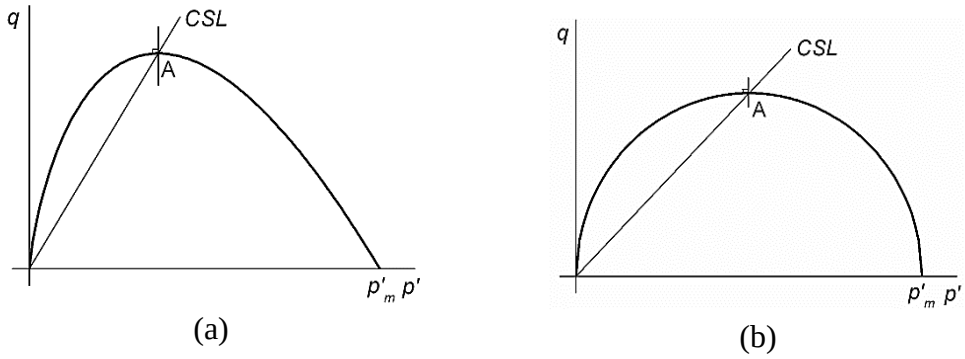

Figure 3.1: The yield surface of (a) CC model and (b) MCC model.

The flow rule in MCC model is assumed as associated flow rule. This means the plastic potential is identical to the yield surface. The yield surface is assumed to be

expanded uniformly and its size is controlled by the pressure p'_m, in other words the initial size of the yield surface. The expansion of the yield surface is associated with the change in volumetric strain via a relationship called the volumetric hardening law as expressed by $\Delta\varepsilon_v^p = \frac{\lambda-\kappa}{v}\frac{\Delta p'_m}{p'}$, where λ is the slope of normal compression line, κ is the slope of swelling line, and $\Delta\varepsilon_v^p$ is the volumetric strain increment.

MCC model follows the stability criteria of Drucker [174], hence the plastic incremental vector is normal to the slope of the plastic potential at the current stress state. This is mathematically expressed as follows:

$$d\varepsilon_{ij}^p = \langle\lambda\rangle\frac{\partial G}{\partial\sigma'_{ij}} \qquad [3.2]$$

where $\langle\lambda\rangle$ is the plastic multiplier determined from the consistency condition, and $\langle\ \ \rangle$ McCauley brackets which implies that only positive values are taken into consideration; the negative value are taken as zero.

3.3 NSFS-MCC model formulation in triaxial space

As explained above about the necessity of a time dependent constitutive model which is capable describing the creep behaviour fully, this section is an attempt to propose an isotropic time-dependent constitutive model using nonstationary flow surface (NSFS) in combination with the well-known inviscid Modified Cam Clay (MCC) model. The proposed model is named as NSFS-MCC. The formulation of NSFS-MCC model is presented in the triaxial stress space before extending to the general stress space which is presented in Appendix 1.

3.3.1 Elastic part of the model

According to NSFS theory ([171], [175]), if a stress state is located inside the yield surface, the behaviour of natural clay is purely elastic. Typically, the elastic properties of natural clay will be cross-anisotropic after deposition and consolidation. However, NSFS-MCC is intended to apply for the normally consolidated or lightly over-consolidated soft clays, where a small increase of stress will result in yielding. Therefore, elastic strains are often relatively unimportant. In the interest of simplicity, the elastic behaviour is assumed to be isotropic. The elastic components are similar to those in MCC model and expressed as

$$K' = \frac{(1+e)p'}{\kappa} \quad [3.3]$$

The elastic shear modulus G is defined as:

$$G = \frac{3(1+e)p'}{2\kappa}\frac{1-2\nu}{1+\nu} \quad [3.4]$$

with ν the Poisson ratio

The elastic strain increments are given as:

$$\begin{Bmatrix} d\varepsilon_v^e \\ d\varepsilon_q^e \end{Bmatrix} = \begin{bmatrix} 1/K' & 0 \\ 0 & 1/3G \end{bmatrix} \begin{Bmatrix} dp' \\ dq \end{Bmatrix} \quad [3.5]$$

3.3.2 Flow surface

The term "flow surface" refers to the nonstationary flow surface or nonstationary yield surface. In terms of developing a time-dependent constitutive model of soft clay using NSFS theory, the definition of the nonstationary flow surface is the core step and presents the biggest challenge. The following is an attempt to present such a definition of the nonstationary flow surface in NSFS-MCC model.

- **Creep from one dimensional compression**

Creep law for clay was first proposed by Buisman [6], after many observations of soil settlements behaviour which were different from classical consolidation theory. The work on one dimensional (1D) creep has been continued by many researchers, in particular Bjerrum [124], Taylor [105], Garlanger [127] , and Mesri [176]. This work has been extended to three dimensional (3D) creep behaviour, with support from the powerful computational calculation at the disposal of modern researchers, such as Sekiguchi [161], Adachi and Oka [150], Borja et al.[177] and Vermeer [178].

Buisman [6] proposed the following expression to define the creep behaviour of soil under a constant stress,

$$\varepsilon = \varepsilon_p + C\ log\frac{t}{t_p} = \varepsilon_p + C\ log\frac{t_p + t_c}{t_p} \quad [3.6]$$

where ε_p is the strain up to the end of primary consolidation, t is the elapsed time from the initial loading, t_p is the time to the end of primary consolidation, $t_c$is the elapsed time of the creep process and C is the material constant.

Mesri [106] has argued that the important assumption in Terzaghi's theory of consolidation, that the relationship between void ratio and effective stress is time independent, is incorrect. Laboratory and field observation have showed that, after the primary consolidation or after the excess pore pressure has dissipated, the settlement is still continuous under constant effective stress. Therefore, the total deformation is additively composed by the change of volume related to the change of excess pore pressure, called primary compression; the remaining change of volume under a constant effective stress is called secondary compression. A plot of void ratio against logarithm of time, as shown in Figure 3.2 clearly indicates two different stages that the void ratio experiences over the time. At the first stage, the void ratio decreases sharply, which is then followed by a slight decrease of the void ratio at an almost constant rate. The first stage is associated with the primary compression, and the second stage is related to the secondary compression, as noted in Figure 3.2. It is assumed that the intersection of two tangents of the primary compression curve and secondary compression curve is the end of the primary compression (t_p). It is reported that the direct or indirect influence of the secondary compression on the whole consolidation process is noticeable ([105], [106]). To evaluate the magnitude of the secondary compression or the creep behaviour, the coefficient of secondary compression appears to be the most useful parameter and is defined as follows:

$$C_{\alpha e} = \frac{de}{d\log(t)} \qquad [3.7]$$

Where de is the change of void ratio and $d\log(t)$ is the change of the logarithm of time under the secondary consolidation stage as shown in Figure 3.2.

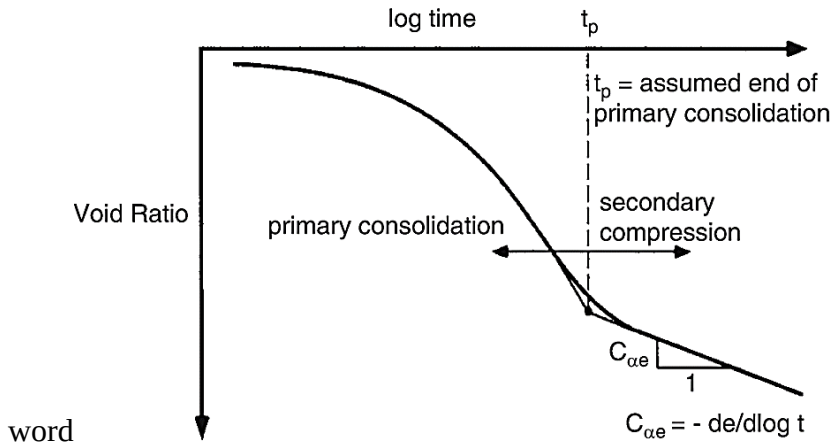

Figure 3.2: Illustration of the relationship between void ratio and logarithm of time

If C_α is assumed as constant over the secondary consolidation stage, the total void ratio change is defined as:

$$\Delta e = \Delta e_p + \Delta e_c = \Delta e_p + C_{\alpha e} \log\left(\frac{t_p + t_c}{t_p}\right) \quad [3.8]$$

Under 1D compression, the strain is defined as:

$$\varepsilon = \frac{\Delta V}{V_0} = \frac{\Delta V / V_s}{V_0 / V_s} = \frac{\Delta e}{1 + e_0} \quad [3.9]$$

with e_0 is the initial void ratio

Combining [3.8] and [3.9], the total strain can be expressed as follows,

$$\varepsilon = \varepsilon_p + log\frac{t}{t_p} = \varepsilon_p + \frac{C_{\alpha e}}{(1+e_{0})} log\left(\frac{t_p+t_c}{t_p}\right) \quad [3.10]$$

Expression of [3.10] in the natural logarithm shows:

$$\varepsilon = \varepsilon_p + \frac{C_\alpha e}{(1+e_{0})}\frac{1}{ln10} ln\left(\frac{t_p+t_c}{t_p}\right) \quad [3.11]$$

Comparing [3.11] and [3.8], the creep strain under 1D compression, termed the creep volumetric strain, can be defined as:

$$\varepsilon_v = \frac{C_{\alpha e}}{(1 + e_{0})}\frac{1}{ln10} ln\left(\frac{t_p + t_c}{t_p}\right) = \mu ln\left(\frac{t}{t_0}\right) \quad [3.12]$$

$$with\ \mu = \frac{C_{\alpha e}}{(1 + e_{0})}\frac{1}{ln10} \quad [3.13]$$

where μ is named as the creep index, t is the elapsed time from the beginning of loading, $t_0 = t_p$ is the time at the end of the primary consolidation.

Taking derivative of creep volumetric strain at the time t and t_0, it shows:

$$\dot{\varepsilon}_v = \mu\frac{1}{t} \quad [3.14]$$

$$\dot{\varepsilon}_{v0} = \mu\frac{1}{t_0} \quad [3.15]$$

Combining [3.12], [3.14] , and [3.15], it yields

$$\varepsilon_v = \mu ln\left(\frac{\dot{v}_0}{\dot{\varepsilon}_v}\right) \quad [3.16]$$

where $\dot{v}_0$ is named as the initial volumetric strain rate and μ is the modified coefficient of secondary compression.

- **Volumetric strain from the plastic behaviour**

The yield surface in MCC model is expressed as:

$$f_y = q^2 - M^2(p'_m - p')p' = 0 \qquad [3.17]$$

After some manipulations, the yield surface is yielded as:

$$f_y = ln\left(\frac{p'}{p'_m}\right) + ln\left(\frac{M^2 + \eta^2}{M^2}\right) = 0 \qquad [3.18]$$

where p'_m is the size of the yield surface and η is the stress ratio of the deviatoric stress q and the mean effective stress p'.

Taking a normally consolidated clay into consideration, a loading path from initial state causes the size of yield surface change from initial value p'_0 to the current value p'_m corresponding to the total volume change $dv = \lambda ln\left(\frac{p'_0}{p'_m}\right)$, in which the elastic volume change is $dv^e = \kappa ln\left(\frac{p'_0}{p'_m}\right)$. Hence the plastic volumetric change is $dv^p = (\lambda - \kappa) ln\left(\frac{p'_0}{p'_m}\right)$. It yields the change of plastic volumetric strain as:

$$d\varepsilon_v^p = -\frac{dv^p}{v} = \frac{(\lambda - \kappa) ln\left(\frac{p'_m}{p'_o}\right)}{1 + e_0} \qquad [3.19]$$

Taking some manipulations from equation [3.19], with a note that the plastic volumetric strain at the initial state is zero yielding:

$$p'_m = p'_0 . exp\left(\frac{(1 + e_0)}{(\lambda - \kappa)} \varepsilon_v^p\right) \qquad [3.20]$$

Combining [3.20] and [3.18] gives the plastic volumetric strain as:

$$\varepsilon_v^p = \frac{\lambda - \kappa}{1 + e_0} ln\left(\frac{p'}{p'_0}\right) + \frac{\lambda - \kappa}{1 + e_0} ln\left(\frac{M^2 + \eta^2}{M^2}\right) \qquad [3.21]$$

- **Viscoplastic strain**

According to NSFS theory, once the stress state reaches the yield surface, viscoplasic behaviour is triggered. Following this, the behaviour of soil at this state is a combination of viscosity and plasticity. Therefore, the visoplastic volumetric strain is additively decomposed of the creep volumetric strain and plastic volumetric. Combining [3.16 and [3.21], the viscoplastic volumetric strain can be defined as:

$$\varepsilon_v = \frac{\lambda-\kappa}{1+e_0} ln\left(\frac{p'}{p'_0}\right) + \frac{\lambda-\kappa}{1+e_0} ln\left(\frac{M^2+\eta^2}{M^2}\right) + \mu ln\left(\frac{\dot{v}_0}{\dot{\varepsilon}_v}\right) \quad [3.22]$$

- **Finding the equation of the nonstationary flow surface (F)**

  Given $f(p', q)$ a scalar function of stress state as shown

$$f = \frac{\lambda-\kappa}{1+e_0} ln\left(\frac{p'}{p'_0}\right) + \frac{\lambda-\kappa}{1+e_0} ln\left(\frac{M^2+\eta^2}{M^2}\right) \quad [3.23]$$

  and substituting into [3.22] yielding:

$$\varepsilon_v = f + \mu ln\left(\frac{\dot{v}_0}{\dot{\varepsilon}_v}\right) \quad [3.24]$$

Manipulating [3.24] so that one side is a function of the viscoplastic volumetric strain and the other side is a constant, it yields:

$$\dot{\varepsilon}_v e^{\frac{\varepsilon_v}{\mu}} = \dot{v}_0 e^{\frac{f}{\mu}} \quad [3.25]$$

Taking an integration of [3.25] with an increment of time dt, it yields:

$$\int \dot{\varepsilon}_v e^{\frac{\varepsilon_v}{\mu}} dt = \int \dot{v}_0 e^{\frac{f}{\mu}} dt \Leftrightarrow \int e^{\frac{\varepsilon_v}{\mu}} d\varepsilon_v = \int \dot{v}_0 e^{\frac{f}{\mu}} dt \quad [3.26]$$

Carrying out some manipulations of [3.26], it leads to definition of the viscoplastic volumetric strain dependent on time t,

$$e^{\frac{\varepsilon_v}{\mu}} = \frac{\dot{v}_0 e^{\frac{f}{\mu}} t}{\mu} + c \Leftrightarrow \varepsilon_v = \mu ln\left(\frac{\dot{v}_0 e^{\left(\frac{f}{\mu}\right)} t}{\mu} + c\right) \quad [3.27]$$

Where c is the integral constant determined by the boundary condition.

At t=0, there is no viscoplastic strain, [3.27] is equivalent to $\varepsilon_v = \mu ln(c) = 0$, yielding c=1, so the viscoplastic volumetric strain is determined as:

$$\varepsilon_v = \mu ln\left(\frac{\dot{v}_0 e^{\frac{f}{\mu}} t}{\mu} + 1\right) \Leftrightarrow \mu ln\left(\frac{\dot{v}_0 e^{\frac{f}{\mu}} t}{\mu} + 1\right) - \varepsilon_v = 0 \quad [3.28]$$

If F is given by the left side of the equation [3.28], so:

$$F = \mu ln\left(\frac{\dot{v}_0 e^{\frac{f}{\mu}} t}{\mu} + 1\right) - \varepsilon_v = 0 \qquad [3.29]$$

The expression of F in [3.29] can be transformed to a scalar function of stress state and a function of time and viscoplastic volumetric strain as follows:

$$F = f(p', q) - \varkappa(\varepsilon_v, t) = f - \mu ln\left(\frac{\mu}{\dot{v}_0 t}\left(e^{\frac{\varepsilon_v}{\mu}} - 1\right)\right) = 0 \qquad [3.30]$$

From [3.29] and [3.30], if time factor 't' is kept constant, F is a surface in the triaxial stress space, which is called the yield surface and $\varkappa(\varepsilon_v, t)$ plays a role of hardening parameters. This yield surface is not stable due to the change of time (t) so it is called nonstationary yield surface or nonstaionary flow surface. Therefore, the nonstationary flow surface of NSFS-MCC is proposed as:

$$F = \mu ln\left(\frac{\dot{v}_0 e^{\frac{f}{\mu}} t}{\mu} + 1\right) - \varepsilon_v = 0 \qquad [3.31]$$

where t is not allowed to be zero, since there is no viscous behaviour at the beginning time t=0. The initial yield surface is the yield surface of the inviscid model MCC, and f is a scalar function of stress state as shown in [3.23]:

$$f = \frac{\lambda - \kappa}{1 + e_0} ln\left(\frac{p'}{p'_0}\right) + \frac{\lambda - \kappa}{1 + e_0} ln\left(\frac{M^2 + \eta^2}{M^2}\right)$$

and $\dot{v}_0$ is the initial volumetric strain rate, μ is the creep index, and ε_v is the initial viscoplastic volumetric strain, which can be determined from an assumption that the hardening parameter is equal to zero at a very small time elapsed during the initial state, for example time t=1E-7. From [3.30], taking the hardening parameter as zero yields:

$$\varkappa(\varepsilon_v, t) = \mu ln\left(\frac{\mu}{\dot{v}_0 t}\left(e^{\frac{\varepsilon_v}{\mu}} - 1\right)\right) = 0 \ (at\ t = 1e - 7) \qquad [3.32]$$

The initial viscoplastic volumetric strain can be derived as,

$$\varepsilon_v = \mu ln\left(\frac{\dot{v}_0 t}{\mu} + 1\right) = 0 \ (at\ t = 1e - 7) \qquad [3.33]$$

3.3.3 Flow rule

Evidence from the laboratory experiments (e.g. [179], [180]) suggests that the flow rule for natural clays is reasonably assumed as an associated flow rule. However, other researchers (e.g. [181], [182]) argue for a non-associated flow rule. For the interest of simplicity and due to the lack of conclusive evidence to support the non-associated flow rule, the associated flow rule is assumed within the NSFS-MCC model which coincides with the flow rule assumed in the MCC model, leading to the nonstationary yield surface, which is identical to the plastic potential, or $F = G$.

3.3.4 Stress-strain-time relation

According to NSFS theory, the total strain increment may be additively composed of an elastic strain increment $d\varepsilon^e$ and a viscoplastic increment $d\varepsilon^{vp}$

$$d\varepsilon = d\varepsilon^e + d\varepsilon^{vp} \qquad [3.34]$$

where the superscripts *e* and *vp* denotes the elastic component and viscoplastic component, respectively.

The elastic strain increment can be determined, following the Modified Cam Clay (MCC) model, and expressed in a general form as:

$$d\varepsilon^e = D^{e^{-1}} d\sigma' \qquad [3.35]$$

where D^e is the elastic stiffness matrix and $d\sigma'$ is the effective stress increment.

The viscoplastic strain increment is obtained following Drucker's stability criterion [174]:

$$d\varepsilon^{vp} = \langle\lambda\rangle \frac{\partial G}{\partial \sigma'} = \langle\lambda\rangle \frac{\partial F}{\partial \sigma'} \qquad [3.36]$$

where G is viscoplastic potential identical to nonstationary flow surface F due to the associated flow rule and $\langle\lambda\rangle$ is a non-negative viscoplastic multiplier, if λ is negative, $\langle\lambda\rangle$ is taken as zero.

Similar to elasto-plasticity, viscoplastic behaviour is initiated and continuous once the stress state reaches the initial yield surface. It is noted that the stress state is not allowed to be located outside of the yield surface (the stress state must always be located on the nonstationary flow surface) to satisfy the consistency condition, yielding an expression as follows:

$$dF = \frac{\partial F}{\partial \sigma'_{ij}} d\sigma'_{ij} + \frac{\partial F}{\partial \varepsilon_{ij}^{vp}} d\varepsilon_{ij}^{vp} + \frac{\partial F}{\partial t} dt = 0 \quad [3.37]$$

Combining [3.36] and [3.37], the viscoplastic multiplier can be derived in relation to the stress increment as:

$$\lambda = -\frac{\frac{\partial F}{\partial \sigma'_{ij}} d\sigma'_{ij} + \frac{\partial F}{\partial t} dt}{\frac{\partial F}{\partial \varepsilon_{ij}^{vp}} \frac{\partial F}{\partial \sigma'_{ij}}} \quad [3.38]$$

To find the viscoplastic multiplier in relation to the strain increment, combining [3.35] and [3.37] yields,

$$\frac{\partial F}{\partial \sigma'_{ij}} D^e_{ijkl}(d\varepsilon_{ij} - d\varepsilon_{ij}^{vp}) + \frac{\partial F}{\partial \varepsilon_{ij}^{vp}} d\varepsilon_{ij}^{vp} + \frac{\partial F}{\partial t} dt = 0 \quad [3.39]$$

Then subtituting [3.36] into [3.39] followed by some manipulations will produce the definition of the viscoplastic multiplier in relation to strain increment as below:

$$\lambda = \frac{\frac{\partial F}{\partial \sigma'_{ij}} D^e_{ijkl} d\varepsilon + \frac{\partial F}{\partial t} dt}{\frac{\partial F}{\partial \sigma'_{ij}} D^e_{ijkl} \frac{\partial F}{\partial \sigma'_{ij}} - \frac{\partial F}{\partial \varepsilon_{ij}^{vp}} \frac{\partial F}{\partial \sigma'_{ij}}} \quad [3.40]$$

where some auxiliary derivatives can be defined as follows:

$$\frac{\partial F}{\partial \sigma'_{ij}} = \begin{bmatrix} \left(1 - exp\left(-\frac{\varepsilon_v^{vp}}{\mu}\right)\right) \frac{\partial f}{\partial p'} \\ \left(1 - exp\left(-\frac{\varepsilon_v^{vp}}{\mu}\right)\right) \frac{\partial f}{\partial q} \end{bmatrix} \quad [3.41]$$

$$\frac{\partial F}{\partial t} = \dot{v}_0 exp\left(\frac{f - \varepsilon_v^{vp}}{\mu}\right) \quad [3.42]$$

$$\frac{\partial F}{\partial \varepsilon_{ij}^{vp}} = \frac{\partial F}{\partial \varepsilon_v^{vp}} = -1 \quad [3.43]$$

where F is the nonstationary flow surface as shown in [3.31],

$$F = ln\left(\frac{\dot{v}_0 e^{\frac{f}{\mu} t}}{\mu} + 1\right) - \varepsilon_v = 0,$$

and f is a scalar function as shown in [3.23] expressed as:

$$f = \frac{\lambda - \kappa}{1 + e_0} ln\left(\frac{p'}{p'_0}\right) + \frac{\lambda - \kappa}{1 + e_0} ln\left(\frac{M^2 + \eta^2}{M^2}\right)$$

Following the equations [3.38] and [3.40], the viscoplastic multiplier is dependent on stress (strain) increment and time increment. This implies that the viscoplastic strain increment occurs even when the stress or strain is constant. Hence the NSFS-MCC model is capable of describing the creep behaviour and stress relaxation, typical time related phenomena of natural clays.

From the conventional constitutive relation between stress and strain increment, inherent from elasto-plasticity theory, $d\sigma = D^e(d\varepsilon - d\varepsilon^{vp})$, in combination with equation [3.36] and [3.40], the complete constitutive stress-strain-time relationship in NSFS-MCC model is described as follow,

$$d\sigma = D^e_{ijkl} d\varepsilon - D^e_{ijkl} \left[\frac{\frac{\partial F}{\partial \sigma'_{ij}} D^e_{ijkl} d\varepsilon + \frac{\partial F}{\partial t} dt}{\frac{\partial F}{\partial \varepsilon^{vp}_{ij}} D^e_{ijkl} \frac{\partial F}{\partial \sigma'_{ij}} - \frac{\partial F}{\partial \varepsilon^{vp}_{ij}} \frac{\partial F}{\partial \sigma'_{ij}}} \right] \frac{\partial F}{\partial \sigma'_{ij}} \qquad [3.44]$$

3.3.5 Hardening law

The evolution of the nonstationary flow surface incorporates the volumetric hardening law, which is related to the change in size of yield surface similar to the volumetric hardening law in the MCC model, expressed as:

$$dp'_m = p'_0 \frac{1 + e_0}{\lambda - \kappa} d\varepsilon^{vp}_v \qquad [3.45]$$

The equation [3.45] shows that the change in size of the flow surface is controlled by viscoplastic volumetric strain increment ε^{vp}_v . λ and κ are the slope of isotropic compression line and swelling line in $e - lnp'$ space respectively.

3.4 Determination of model parameters

The NSFS-MCC model requires a total of six parameters. They can be categorised into three groups:

- Elastic parameters κ and ν';
- Critical state parameters M and λ;
- Creep parameters μ and $\dot{v}_0$.

$\kappa,\ \nu', M$, and λ parameters are determined based on the MCC model. In terms of the creep parameters, the creep index, μ, is related to the coefficient of secondary compression, $C_{\alpha e}$. The other creep parameter is the initial volumetric strain rate, $\dot{v}_0$.

The creep index μ has a clear physical meaning and can be determined from the coefficient of secondary compression which has been well presented in the literature and can be determined directly from the result of conventional oedometer as shown in [3.7]. The expression of creep index μ is related to coefficient of secondary compression as:

$$\mu = \frac{C_{\alpha e}}{(1 + e_{0)}} \frac{1}{ln10}$$

Another creep parameter is the initial volumetric strain rate $\dot{v}_0$ which can be defined based on the relation with creep index, since it is complex to derive this from the laboratory test:

$$\dot{v}_0 = \frac{\mu}{t_0} \qquad [3.46]$$

where t_0 is the end of the primary (EOP) consolidation which can be estimated by Taylor's square root method [183] from Terzaghi's theory of consolidation:

$$t_0 \approx t_{90} = \frac{H^2 T_v(90\%)}{C_v}$$

in which C_v is coefficient of consolidation, H is the drainage distance, and T_v (90%) is a constant.

3.5 Numerical solution

The NSFS-MCC was implemented in MATLAB software to qualitatively verify the behaviour of model and validate the model at the elementary level.

The model was implemented in MATLAB software, using the explicit algorithm in which the stress increment is computed directly from the constitutive relationship with strain increment as shown in []. The application of the explicit integration scheme

to conventional elastoplastic model demonstrated by Sloan ([184], [185]) is adopted in this model.

The constitutive relationship between stress and strain is employed for the implementation NSFS-MCC model and is presented as:

$$d\bar{\sigma}'_{ij} = \left[D^e_{ijkl}\right]d\bar{\varepsilon}_{ij} - \left[D^e_{ijkl}\right]\left[\frac{\frac{\partial F}{\partial \bar{\sigma}'_{ij}}\left[D^e_{ijkl}\right]d\bar{\varepsilon}_{ij} + \frac{\partial F}{\partial t}dt}{\frac{\partial F}{\partial \bar{\sigma}'_{ij}}\left[D^e_{ijkl}\right]\frac{\partial F}{\partial \bar{\sigma}'_{ij}} - \frac{\partial F}{\partial \bar{\varepsilon}^{vp}_{ij}}\frac{\partial F}{\partial \bar{\sigma}'_{ij}}}\right]\frac{\partial F}{\partial \bar{\sigma}'_{ij}} \qquad [3.47]$$

In explicit (Euler's forward) algorithm, the constitutive equation is integrated directly from the previously known stress point $\bar{\sigma}'_n$, called the initial state of the current calculation step. The stress at the next increment $\bar{\sigma}'_{n+1}$ is calculated as follows:

$$\bar{\sigma}'_{n+1} = \bar{\sigma}'_n + d\bar{\sigma}'_{ij}$$

where $\bar{\sigma}'_n$ is the current stress and $d\bar{\sigma}'_{ij}$ is the incremental stress, which is computed using Eq. [] in which all derivatives are taken about the previously known state. The corresponding viscoplastic strain $d\bar{\varepsilon}^{vp}$ is obtained by the following formula:

$$d\bar{\varepsilon}^{vp} = \left[\frac{\frac{\partial F}{\partial \bar{\sigma}'_{ij}}\left[D^e_{ijkl}\right]d\bar{\varepsilon}_{ij} + \frac{\partial F}{\partial t}dt}{\frac{\partial F}{\partial \bar{\sigma}'_{ij}}\left[D^e_{ijkl}\right]\frac{\partial F}{\partial \bar{\sigma}'_{ij}} - \frac{\partial F}{\partial \bar{\varepsilon}^{vp}_{ij}}\frac{\partial F}{\partial \bar{\sigma}'_{ij}}}\right]\frac{\partial F}{\partial \bar{\sigma}'_{ij}}$$

In order to obtain an acceptable accuracy and allow the consistency condition at the end of each increment, the explicit algorithm requires very small increment size.

3.6 Qualitative verification of the model implementation

To illustrate the capabilities of the model in capturing the rate and time-dependency of soil behaviour, the following three hypothetical loading scenarios are considered and the model performance in each scenario is numerically examined. The values of model constants and state variables used for the hypothetical soil is presented as follows:

$\kappa = 0.05$; $\nu = 0.2$; $M = 1.51$; λ =0.3;

$\mu = 1.15e-2$; $\dot{v}_0 = 3.5e-6$

e_0=2, OCR=1

Strain rate effect on undrained shear strength

Simulations of the model prediction for undrained compression of a hypothetical clay at four different strain rates of 1%/min, 0.1%/min, 0.01%/min and 0.001%/min have been carried out. The results, presented in Figure 1, show that the model is able to capture the effect of different strain rates and predict different undrained shear strengths for the soil. With increasing strain rates, the soil shows higher strength values, which is the expected soil response as supported by many experimental observations.

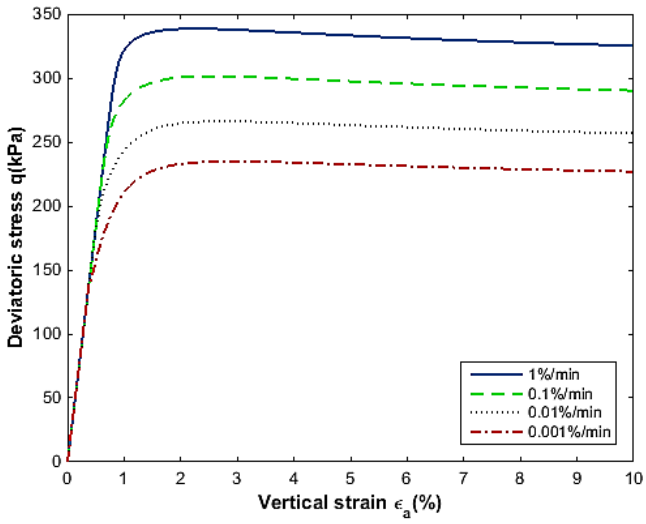

Figure 3.3 Undrained compression tests at different strain rates

Strain rate effect on pre-consolidation pressure

To study the effect of strain rate on the yield stress value, simulations of three constant strain rate tests under one dimensional compression condition have been carried out. The results are displayed in Figure 3.4. It shows that the higher the strain rate, the greater the value of apparent pre-consolidation pressure. For example in these simulations, the yield stress of a sample, which is compressed at a constant strain rate of 1×10^{-5} (%/s) is nearly 125 kPa; whereas, the sample compressed at a constant strain rate of 1×10^{-7} (%/s) yields at a stress of about 78 kPa.

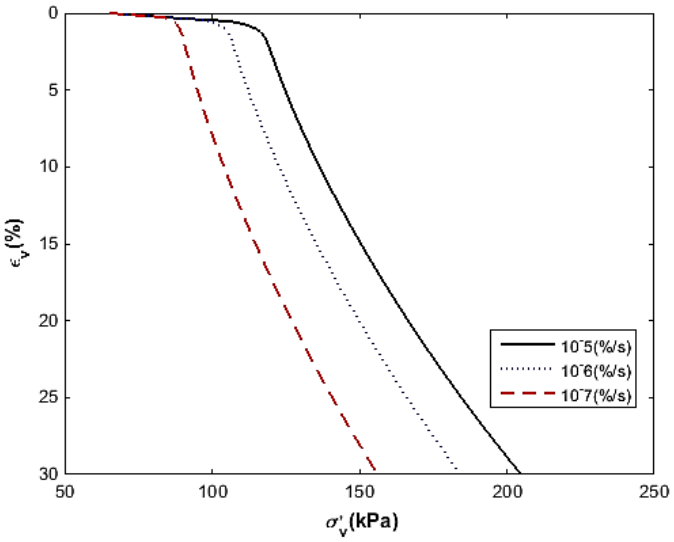

Figure 3.4. Strain rate effect on yield stress

Creep rupture

Creep rupture, which occurs at the tertiary creep stage, is the failure of soil as creep rate increases at a constant deviatoric stress. Capturing this phenomenon is vital for modelling the long-term stability of embankment and slopes. Simulations of creep deformation at three different constant deviatoric stresses have been conducted to study the creep rupture occurrence of a hypothetical clay. The results are shown in Figure 3.5. It can be seen that at a low deviatoric stress (193 kPa), creep rate has a slight increase and then tends towards a rather stable state. However, at higher deviatoric stress values of 267 kPa or 329 kPa at some stage accelerating strain rate occurs, signalling the tertiary creep phase. These results confirm the elegance and capacity of the model in capturing the eventual long-term rupture failure of natural clay deposits.

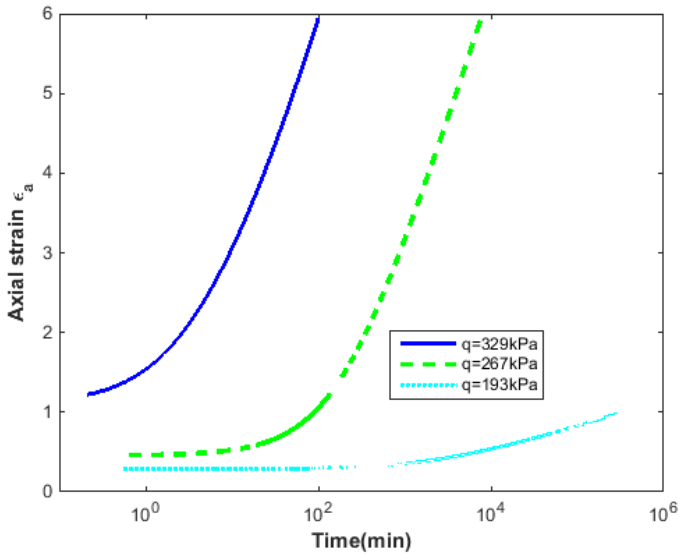

Figure 3.5: Creep rupture simulations at different constant deviatoric stresses.

3.7 Model verification at elementary test levels

3.7.1 Undrained triaxial tests on Haney clay

Vaid and Campanella [94] conducted a series of undrained triaxial compression tests on undisturbed saturated sensitive marine clay known as Haney Clay. The undrained shearing stage of tests was performed at different constant strain rates varying from 0.00094%/min to 1.1%/min to investigate the rate depenency. Haney Clay properties are reported as follows: Liquid limit $w_L = 44\%$, plastic limit $w_P = 26\%$, preconsolidation pressure at 340 kPa and sensitivity S_t between 6 and 10. All test samples were normally consolidated under an isotropic confining pressure of 515 kPa for a period of 36 hours and then were left undrained for 12 hours under consolidation stresses prior to shearing.

The conventional parameters $(\kappa, \lambda, e_0, and\ \nu')$ of Haney clay are determined following the report by Vermeer and Neher [178]. The slope to critical state line $M_c$was estimated from triaxial tests and taken as $M_c = 1.28$. The creep index value was provided by Vermeer et Neher [178] , and the value of the initial volumetric strain rate $\dot{\upsilon}_0$ is estimated from the creep index by relation: $\dot{\upsilon}_0 = \mu/t_0$. All model parameters are presented in Table 3.1.

Table 3.1:NSFS-MCC model parameters for Haney clay

$\kappa = 0.05$	$\lambda = 0.32$	$\mu = 0.004$	$e_0 = 2$
$\nu = 0.03$	$M = 1.28$	$\dot{\upsilon}_0$=2.78e-7 (s^{-1})	

The implementation NSFS-MCC model to simulate the undrained triaxial shearing tests at different constant rates of strain 1.1%/min, 0.15%/min and 0.00094%/min is presented in Figure 3.6. It can be seen that the result from the simulation underestimated the undrained strength of Hanney clay compared to the laboratory test result. This is resulted from the lack of describing the inter-particle bonding and the effect of fabric anisotropy in NSFS-MCC model. However, the shape of the deviatoric stress (q) and vertical strain (ε_a) curve from the simulation captures quite well the experimental data, in particular, the pattern of this curve after the peak of shearing strength shows the softening effect by time factor that inviscid model, such as MCC cannot exhibit.

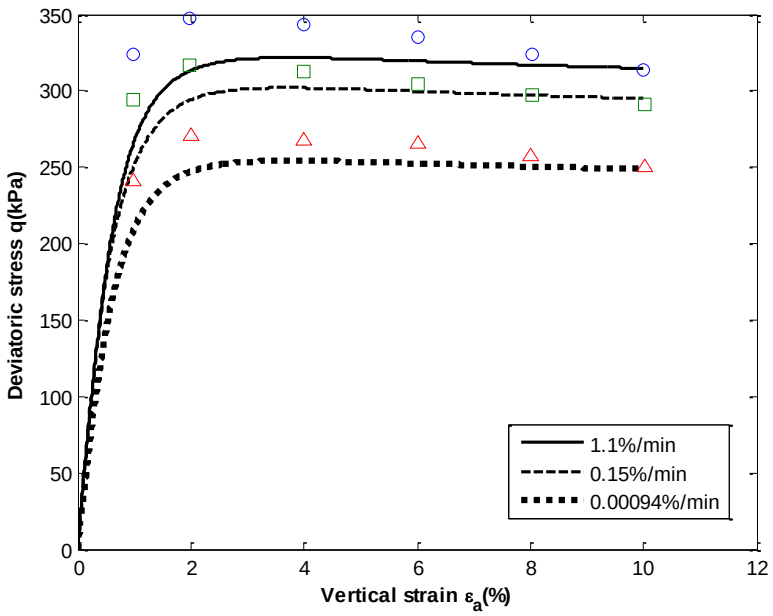

Figure 3.6: Undrained triaxial shearing tests at different constant rates of strain against the experiemental results of Haney clay.

3.7.2 Creep rupture of Haney Clay

The parameters of Haney clay obtained from the undrained triaxial compression tests above are employed to simulate the undrained triaxial creep tests conducted on the same Haney clay samples with the same procedure of consolidation process. The deviatoric stress applied to the sample and kept constant over the creep test period are 193 kPa, 267kPa and 329kPa respectively. The result from the simulation of these triaxial creep tests against the experimental data are illustrated in Figure 3.7. It can be seen implementation to NSFS-MCC model can describe well the creep behaviour of

Haney clay, especially the tertiary stage of creep behaviour at high deviatoric stress value of 329 kPa. Against the undrained triaxial creep tests, the proposed model captures very well the experimental data, especially the creep rupture scenario in this test. This is an important objective when developing this model using non stationary flow surface since other overstress-based time dependent constitutive models are unable to capture the creep rupture behaviour. This verifies the model to describe the creep behaviour of soft clay properly. However, looking prediction by NSFS-MCC model at the deviatoric stress q=267 kpa, it is noticeable that the NSFS-MCC underestimates the induced creep strain.

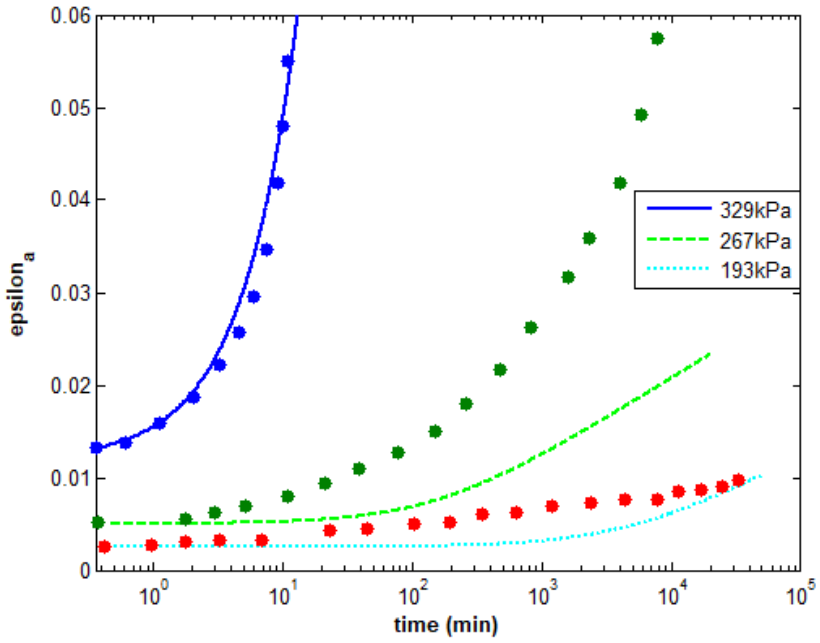

Figure 3.7: Creep rupture simulations at different constant deviatoric stresses.

3.7.3 CRS oedometer tests on Batiscan clay

Leroueil et al. (1985) conducted a series of constant rate of strain (CRS) oedometer tests on Batiscan clay samples which were taken at depth of 7.25-7.46m within Batiscan area, about 110km west of Quebec City. The geotechnical properties of Batiscan clay were reported that the water content is around 79.6% while the liquid limit w_L= 43%, the plasticity index I_p=21, the liquid index I_L=2.7, and clay-sized particle content 81%. The initial state was taken as $\sigma'_{v0} = 65kPa$, equal to the in-situ vertical effective stress at the depth of samples taken. The preconsolidation pressure was reported as 88 kPa, determined by conventional oedometer test. The CRS

oedometer tests were performed in the range between 1.7x10^{-8} (s^{-1}) and 4x10^{-5} (s^{-1}). In which, three CRS tests at strain rates 1.07e-7 (s^{-1}), 1.43e-6 (s^{-1}), and 2.14e-6 (s^{-1}) were employed to verify the proposed model.

The parameters $\kappa, \lambda, e_0, \mu, \dot{v}_0 \; and \; x_0$ shown in Table 3.2 were determined from the result of oedometer tests on natural Batiscan clay samples. The slope to critical state line $M_c$was taken as $M_c = 0.98$ as suggested by Rocchi et al. [187]. Poisson's ratio v was assumed to be 0.3.

Table 3.2: NSFS-MCC model parameters for Batiscan clay

$\kappa = 0.037$	$\lambda = 1.04$	$\mu = 0.019$	$e_0 = 1.92$
$v = 0.3$	$M = 0.98$	$\dot{v}_0$=1.32e-6 (s^{-1})	

The simulation of CRS oedometer tests of Batiscan clay at three different rates 1.43e-5, 2.13e-6 and 1.07e-7 (%/s) against the experimental data are displayed in Figure 3.8. It is seen that the prediction from the NSFS-MCC model can describe the effect of strain rates on the preconsolidation of soft clay. However, it underestimates the yield stress at corresponding strain rate. For example, it estimates the yield stress at strain rate 1.43e-7 %/s at around 108 kPa while the experimental data shows approximately 118 kPa. In ddition; the post yield behaviour of the vertical stress and strain is not predicted well. This might result from the limitation of describing the inter-particle bonding and fabric anisotropy of Batiscan clay in this model. Although, the model exibits qualitative performance in accordance with the literature, its underestimation for both shearing strength and preconsolidation of soil requires a further development which includes the advanced features of soft clay such as fabric anisotropy and the destructuration of inter-particle bonding during straining.

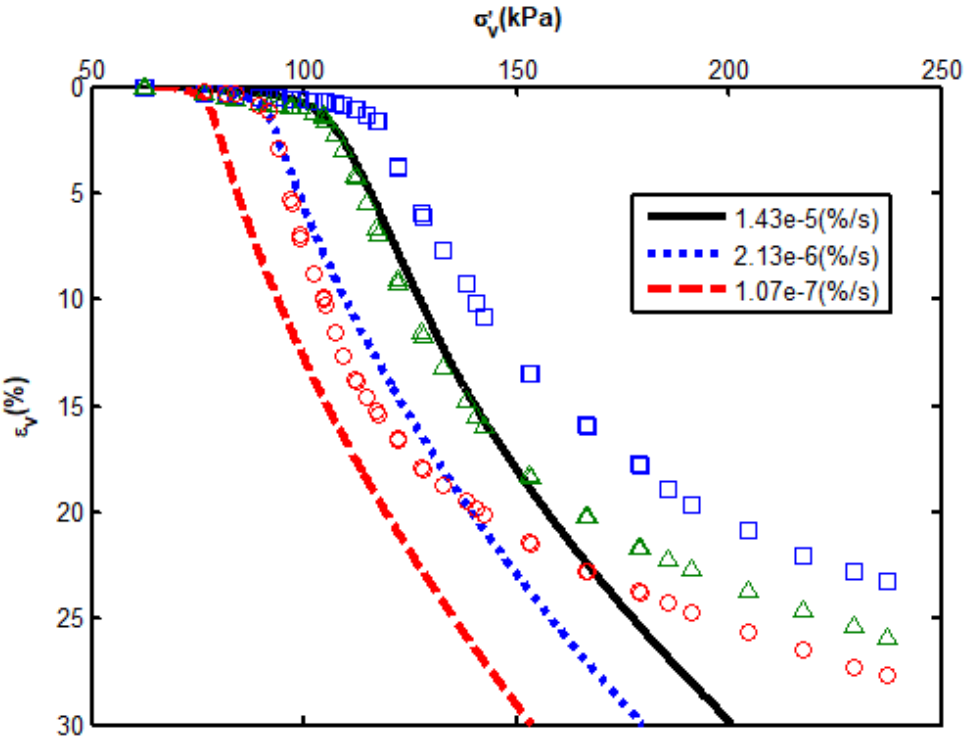

Figure 3.8 : Simulations of CRS oedometer tests of Baiscan clay.

3.8 Concluding points

In this chapter, a time-dependent constitutive model has been proposed, based on nonstationary flow surface theory. The MCC model has been employed as the base model but was developed to an isotropic creep model using the nonstationary flow surface. With a modification in yield condition, so that it can describe the time effects, the model took advantage of classical elasto-plasticity framework for numerical implementation. The simulations showed that the new model is capable of describing the time and rate effects on the behaviour of natural clays. It also indicates that the model provides a promising solution for the simulation of the long-term creep deformations in soft ground. Quantitative verification of the model at elementary levels was carried out. The results showed NSFS-MCC model can reproduce quite well the experimental data of some standard laboratory tests to some natural clays with regard to undrained triaxial compression test of Haney clay, CRS oedometer tests of Batiscan clay, and undrained triaxial creep tests of Haney clay. However, the prediction from the model is not good enough to provide a reliable solution to a practical geotechnical problem. It irequires some additional developments to enable the model capacity of describing other fundamental features of natural clay behaviour;

in particular with respect to fabric anisotropy and destructuration, so that a more accurate prediction can be obtained. The following chapter attempts to extend NSFS-MCC model so that the evolution of fabric anisotropy and the degradation of inter-particle under loading can be fully described.

CHAPTER 4 :

FURTHER DEVELOPMENT OF NSFS-MCC MODEL WITH FABRIC ANISOTROPY AND DESTRUCTURATION FEATURE

4.1 Introduction

Natural soft clays are structured materials, which exhibit the degree of anisotropy developed during the clay deposition, sedimentation and consolidation history as well as during plastic strain development ([169], [188]). The anisotropy feature can be categorised into two types: inherent anisotropy and induced anisotropy. While the former is associated with the natural structure of soil and its post-depositional processes, the latter is attributed to the anisotropic consolidation, shear and directional transportation component [29]. The anisotropy of natural clay is not fixed; it changes under different external loading conditions called "evolving anisotropy". Some advanced constitutive models make efforts to capture the evolution of soil anisotropy ([54]–[57]). The result of modelling an embankment, including inherent anisotropy and evolutionary anisotropy, showed that the evolution of anisotropy has more impact on horizontal deformation than on the vertical deformation [58] . In general, a model with a capacity to describe both inherent anisotropy and evolving anisotropy will provide better prediction of natural soil behaviour.

Natural clays also exhibit some inter-particle bond, which is gradually degraded as a result of plastic straining, the mechanical energy or thermal energy effect ([23], [62]). This process is referred as destructuration. After the observations of data of many undrained triaxial compression and extension tests of structured Bothkenar clay, Taiebat [62] stated that there is a loss of strength due to the destructuration process. This statement is supported by other researchers testing different clays (e.g. [63], [64], [65], and [67]). This explains why a constitutive model with destructuration feature will provide a closer prediction to the natural clay behaviour. Many constitutive models have been proposed based on the framework of critical state concept, however;

very few models can describe fully the advanced features of soft clay. Some models only describe the yield surface change due to the change of volume with an assumption of isotropic condition that contradicts the anisotropy of natural clay (e.g.[11], [172]). Some other models get an improvement with an inclusion of the inclination of the yield surface to capture the fabric anisotropy of natural clay but still neglect the bonding or destructuration feature of natural clay (e.g. [12], [56], [161]). Only the latest advanced constitutive models include both advanced features with respect to fabric anisotropy and destructuration features (e.g. [13], [14]).

Another important feature of natural clay that has significant attention recently is time dependent behaviour, in particular the creep deformation that many constitutive models have not covered properly. There are many well documented reports in literature about the serious damage of creep deformation on the structure or even the safety of the lives [104]. So taking this feature into consideration is a requirement for any developed constitutive model to provide an adequate prediction of the long term behaviour of soft clay. Many constitutive models have been developed to describe the time dependent behaviour. However they are either the isotropic extended overstress models (e.g. [3], [19], [126], [178], [189]) or only inherent anisotropy, neglecting the evolution of anisotropy (e.g. [57], [150], [190]). Some latest advanced model with an attempt to describe both advanced features of natural clay regarding anisotropy and destructuration were developed based on the overstress theory (eg. [156], [191]). Hence, they cannot fully describe the creep behaviour of soft clay due to the limitation of the overstress formula structure.

To address the abovementioned matters, the author made an attempt to propose a time dependent constitutive model using non stationary flow surface (NSFS) theory in combination with an advanced inviscous model, namely S-CLAY1S [13] an extension from S-CLAY1 model [12]. With an interest of simplicity and ability of practical application, S-CLAY1S is the first option compared to the other advanced model, for example SANICLAY [14]. Detail of S-CLAY1S is presented in the next section. The proposed model, namely NSFS-SCLAY1S is capable describing the inherent anisotropy and the involving anisotropy attributable to irrecoverable straining. It enables the model to provide a better prediction to the natural anisotropic clay behaviour. The NSFS-SCLAY1S model also concerns the effects from destructuration process once the viscoplastic behaviour is triggered. Using the NSFS theory as a base, a time factor is included in the yield condition enabling the NSFS-SCLAY1S to describe the viscous behaviour of soft clay, particularly the creep

behaviour that many overstress-based constitutive models are limited. While determination the input parameters of overstress models is complicated and requires some calibrations [192], NSFS-SCLAY1S model parameters are determined straightforwardly from some standard laboratory work. This is an outstanding point of this model. With the consideration of inherent and induced anisotropy, destructuration and time dependent stress-strain behaviour, the proposed model is applicable to sensitive soft clay ground on which many structures have been built recently due to the demand of residential development.

This chapter firstly introduces the advanced inviscous model, namely SCLAY1S that is employed in developing NSFS-SCLAY1S model. Then, formulation of NSFS-SCLAY1S model in triaxial stress space and general stress space are presented before the numerical solution and some verifications are expressed.

4.2 SCLAY-1S model

The SCLAY1S model developed by [13] is an extension of the SCLAY-1 model [12] with incorporation of the influence of both anisotropy and destructuration. This is the outstanding point of SCLAY1S model since the recent advanced constitutive models only describe the inherent anisotropy (e.g. [57], [55]) or describe the evolution of anisotropy of soil as consequence of plastic straining, (e.g. [53], [193]. Some models incorporate the destructuration of soil, however; the procedure to determine the model parameters is not easy. SCLAY-1S, in contrast, requires some standard laboratory experiments to determine the model parameters.

The elastic behaviour of SCLAY-1S model is assumed to be isotropic since plastic deformations are likely to dominate in practice with the application to normally consolidated clay while elastic deformation is relatively unimportant. Elastic increments of volumetric and deviatoric strain have the same formulation as that from MCC model:

$$d\varepsilon_v^e = \frac{dp'}{K'} \; with \; K' = \frac{(1+e)p'}{\kappa} \qquad [4.1]$$

$$d\varepsilon_q^e = \frac{dq}{3G} \; with \; G = \frac{3(1+e)p'}{2\kappa}\frac{(1-2\nu)}{1+\nu} \qquad [4.2]$$

where e is void ratio, ν is Poisson's ratio, and κ is the slope of the swelling line.

Yield surface

In triaxial stress space, the yield surface of SCLAY1S is relatively similar to SCLAY1 [12]. The proposed yield curve is a sheared ellipse, identical to that suggested by Dafalias [55]:

$$f = (q - \alpha p')^2 - (M^2 - \alpha^2)(p'_m - p') = 0 \qquad [4.3]$$

where M is the slope to critical state line, p'_m and α define the size and inclination of the yield curve respectively.

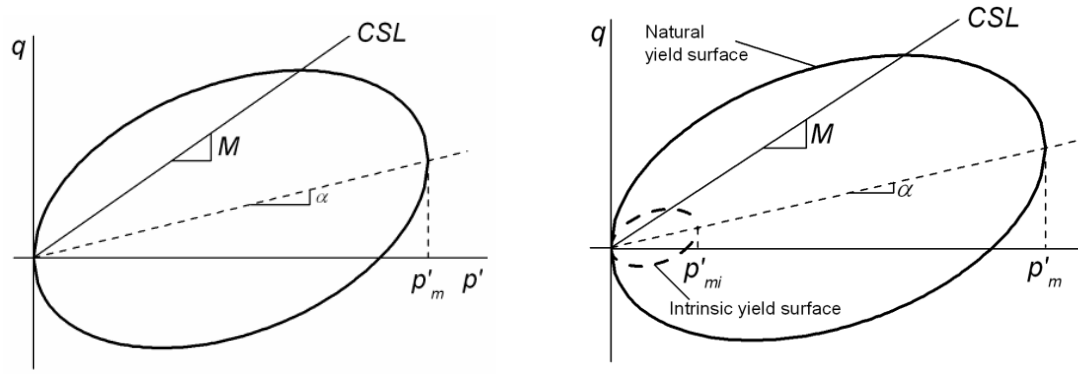

a. Yield curve of SCLAY1 model

b. Yield curve of SCLAY1S model

Figure 4.1: Yield curves of SCLAY1 model and SCLAY1S model

The effect of bonding in SCLAY1S is illustrated by the difference between intrinsic yield surface and natural yield surface by the amount of bonding x [167] and the relation between the size of natural yield loci p'_m and intrinsic yield loci p'_{mi} as follows:

$$p'_m = (1 + x)p'_{mi} \qquad [4.4]$$

Flow rule

SCLAY-1S assumes the flow rule for plastic flow as 'associated flow rule'. Similarly MCC model, plastic strain is expressed as follows:

$$d\varepsilon^p = \lambda \frac{\partial f}{\partial \sigma'} \qquad [4.5]$$

Hardening law

SCLAY1S employs three hardening rules to describe the changes of yield surface.

Firstly, the increase in size of the intrinsic yield surface resulting in the change in size of natural yield surface is adopted from the volumetric hardening law similar MCC model:

$$dp'_{pi} = \frac{\upsilon p'_{mi}}{\lambda_i - \kappa} d\varepsilon_v^{vp} \quad [4.6]$$

where υ is specific volume, λ_i and κ are the slope of intrinsic normal compression line and swelling line in the compression space (lnp'- υ space) respectively.

The second hardening law is used to describe the evolution of the rotation of yield surface due to plastic straining:

$$d\alpha = \omega \left(\left[\frac{3\eta}{4} - \alpha \right] \langle d\varepsilon_v^{vp} \rangle + \omega_d \left[\frac{\eta}{3} - \alpha \right] d\varepsilon_d^{vp} \right) \quad [4.7]$$

where parameters ω and ω_d are used to control the absolute rate of the viscoplastic strain increment on the rotation of the flow surface and relative influence of the viscoplastic deviatoric strain increment $d\varepsilon_d^{vp}$ respectively; $d\varepsilon_v^{vp}$ is the viscoplastic volumetric strain increment.

The third hardening law describes the degradation of bonding during viscoplastic straining where the viscoplastic volumetric strains and viscoplastic deviatoric strains tend to reduce the bonding parameter x towards a target value of zero as follows:

$$dx = -\xi \left(\left| d\varepsilon_v^{vp} \right| + \xi_d \left| d\varepsilon_d^{vp} \right| \right) \quad [4.8]$$

Where ξ and ξ_d are two additional soil constants that control the absolute rate of destructuration and control the relative effectiveness of viscoplastic deviatoric strains and viscoplastic volumetric strains in destroying the bonding respectively.

4.3 NSFS-SCLAY1S model formulation in triaxial space

To address the advanced features of soft clay with respect to fabric anisotropy, destructuration and time dependency, this section attempts to propose an advanced time dependent constitutive model using non stationary flow surface (NSFS) in combination with recently developed inviscid SCLAY1S model presented above. The proposed model is termed as NSFS-SCLAY1S and its formulation is expressed in the triaxial stress space before an extension to the general stress space in the following section.

4.3.1 Elastic part of the model

Following the NSFS theory ([171], [175]), the viscoplastic behaviour only occurs if a stress state is located on the yield surface, otherwise the behaviour of natural clay is purely elastic. Typically, the elastic properties of natural clay will be cross-anisotropic after deposition and consolidation. However, to simplify, the elastic behaviour is assumed to be isotropic. This assumption is widely acceptable for predicting the behaviour of normally consolidated or lightly overconsolidated soft clays which experience a significant amount of viscoplastic strain compared to elastic strain with a small increment of stress.

The elastic bulk modulus K' is defined as

$$K' = \frac{(1+e)p'}{\kappa} \qquad [4.9]$$

The elastic shear modulus G is defined as

$$G = \frac{3(1+e)p'}{2\kappa}\frac{1-2\nu}{1+\nu} \qquad [4.10]$$

with ν is the Poisson ratio

The elastic strain increments are given as

$$\begin{Bmatrix} d\varepsilon_v^e \\ d\varepsilon_q^e \end{Bmatrix} = \begin{bmatrix} 1/K' & 0 \\ 0 & 1/3G \end{bmatrix} \begin{Bmatrix} dp' \\ dq \end{Bmatrix} \qquad [4.11]$$

4.3.2 Flow surface

The term “flow surface” refers to the nonstationary flow surface or nonstationary yield surface. Definition of the nonstationary flow surface is the core step and the most challenging matter in developing a time dependent constitutive model of soft clay using NSFS theory. This part attempts to present how to define the nonstationary flow surface in NSFS-SCLAY1S model.

- **Creep from one dimensional compression**

The creep volumetric strain is determined following the creep law proposed by Mesri [106] explained in detail at Chapter 3, expressed as

$$\varepsilon_v = \mu ln\left(\frac{\dot{\upsilon}_0}{\dot{\varepsilon}_v}\right) \quad [4.12]$$

where $\dot{\upsilon}_0$ is named as the initial volumetric strain rate and μ is the modified coefficient of secondary compression.

- **Volumetric strain from the plastic behaviour**

  According to the plasticity theory, the change of yield surface induces the change of the plastic volumetric strain. Following the SCLAY1S model, the yield surface is expressed as

$$f_y = (q - \alpha p')^2 - (M^2 - \alpha^2)(p'_m - p')p' = 0 \quad [4.13]$$

where p'_m indicates the size of the yield surface, q is the deviatoric stress and p' represents the mean effective stress.

p'_m has a relation with the size of intrinsic yield surface [194] by

$$p'_m = p'_{mi}(1 + x) \quad [4.14]$$

where x is the amount of bonding.

An increase in the size of the intrinsic yield surface is related to the increment of plastic volumetric ($d\varepsilon_v^p$) by a volumetric hardening law for unbonded (reconstituted) soil which is similar to that in Modified Cam Clay (MCC)

$$dp'_{pi} = \frac{(1 + e)p'_{mi}}{\lambda_i - \kappa} d\varepsilon_v^{vp} \quad [4.15]$$

Taking integration of equation [4.15] from the initial state to current state, we have:

$$p'_{mi} = p'_{mi0}.\exp\left(\frac{1 + e_0}{\lambda_i - \kappa}\varepsilon_v^{vp}\right) \quad [4.16]$$

substituting $p'_{mi0} = {p'_{m0}}/{(1 + x^0)}$ and $p'_{mi} = {p'_m}/{(1 + x)}$ into [4.16], yielding:

$$p'_m = \frac{1 + x}{1 + x0} p'_{m0}.\exp\left(\frac{1 + e_0}{\lambda_i - \kappa}\varepsilon_v^{vp}\right) \quad [4.17]$$

Sustituting [4.17] into [4.13] and doing some manipulations, we have:

$$\varepsilon_v^{vp} = \frac{\lambda_i - \kappa}{1 + e0}\left[ln\left(\frac{p'}{p'_{m0}}\right) + ln\left(1 + \frac{(q - \alpha p')^2}{(M^2 - \alpha^2)p'^2}\right) + ln\left(\frac{1 + x_0}{1 + x}\right)\right] \quad [4.18]$$

where :

ε_v^p : plastic volumetric strain

λ_i : slope of the intrinsic normal compression line in the compression plane (ln*p'*-*e* space), determined from an oedometer test on a reconstituted sample.

κ : slope of a swelling line in the compression plane

e_0 : initial void ratio

x_0, x : the initial and current amount of bonding

M : critical state value of the stress ratio in triaxial space

q : deviatoric stress

p' : mean effective stress

p'_{m0} : initial size of the yield surface for the natural clay

- **Viscoplastic strain**

According to NSFS theory, once the stress state reaches the yield surface, the viscoplasic triggers. It means that the behaviour of soil at this state is the combination of viscosity and plasticity. So, the visoplastic volumetric strain is additively composed of the creep volumetric strain and plastic volumetric. Combining [3.16] and [4.18], the viscoplastic volumetric strain can be defined as,

$$\varepsilon_v = \frac{\lambda_i - \kappa}{1+e_0} ln\left(\frac{p'}{p'_0}\right) + \frac{\lambda_i - \kappa}{1+e_0} ln\left(1 + \frac{(q-\alpha p')^2}{(M^2-\alpha^2)p'^2}\right) + \frac{\lambda_i - \kappa}{1+e_0} ln\left(\frac{1+x_0}{1+x}\right) + \mu ln\left(\frac{\dot{v}_0}{\dot{\varepsilon}_v}\right) \quad [4.19]$$

- **Finding the equation of the nonstationary flow surface (F)**

Solving the differential equation [3.22] with the arrangement

$$f = \frac{\lambda_i - \kappa}{1+e_0}\left[ln\left(\frac{p'}{p'_0}\right) + ln\left(1 + \frac{(q-\alpha p')^2}{(M^2-\alpha^2)p'^2}\right) + ln\left(\frac{1+x_0}{1+x}\right)\right] \quad [4.20]$$

, the viscoplastic volumetric strain is derived as

$$\varepsilon_v = \mu ln\left(\frac{\dot{v}_0 e^{\frac{f}{\mu}t}}{\mu} + 1\right) \Leftrightarrow \mu ln\left(\frac{\dot{v}_0 e^{\frac{f}{\mu}t}}{\mu} + 1\right) - \varepsilon_v = 0 \quad [4.21]$$

If F is given as left side of the equation [4.21, so $F = \mu ln\left(\frac{\dot{v}_0 e^{\frac{f}{\mu}t}}{\mu} + 1\right) - \varepsilon_v = 0$ is a surface in the stress space with constant t, or at a moment of time, F is yield surface This yield surface is not stable due to the change of time so it is called as the nonstationary yield surface or nonstationary flow surface.

Therefore, the nonstationary flow surface of NSFS-SCLAY1S is proposed as

$$F = \mu ln\left(\frac{\dot{v}_0 e^{\frac{f}{\mu}t}}{\mu} + 1\right) - \varepsilon_v = 0 \qquad [4.22]$$

where f is a scalar function of stress state as defined in [4.20]:

$$f = \frac{\lambda_i - \kappa}{1 + e_0} ln\left(\frac{p'}{p'_0}\right) + \frac{\lambda_i - \kappa}{1 + e_0} ln\left(1 + \frac{(q - \alpha p')^2}{(M^2 - \alpha^2)p'^2}\right) + \frac{\lambda_i - \kappa}{1 + e_0} ln\left(\frac{1 + x_0}{1 + x}\right)$$

,

$\dot{v}_0$ is the initial volumetric strain rate

μ is the modified coefficient of secondary compression

ε_v is the initial viscoplastic volumetric strain, which can be determined from an assumption that the hardening parameter is equal to zero at a very small time elapsed over the initial state, for example time t=1E-7 similar to equation [3.33] in chapter 3:

$$\varepsilon_v = \mu ln\left(\frac{\dot{v}_0 t}{\mu} + 1\right) = 0 \ (at\ t = 1e - 7) \qquad [4.23]$$

4.3.3 Flow rule

The associated flow rule is assumed within the NSFS-SLAY1S model, leading to the nonstationary yield surface is identical to the plastic potential or $F = G$. This assumption is based on the evidence from laboratory experiments (e.g. [179], [180]) that the associated flow rule for natural clays is reasonably assumed.

4.3.4 Stress-strain-time relation

According to NSFS theory, the total strain increment may be additively composed of an elastic strain increment $d\varepsilon^e$ and a viscoplastic increment $d\varepsilon^{vp}$

$$d\varepsilon = d\varepsilon^{e} + d\varepsilon^{vp} \quad [4.24]$$

where the superscripts *e* and *vp* denote the elastic component and viscoplastic component, respectively.

The elastic strain increment can be determined following the SCLAY1S model, and expressed in a general form as

$$d\varepsilon^{e} = D^{e-1} d\sigma' \quad [4.25]$$

where D^{e} is the elastic stiffness matrix and $d\sigma'$ is the effective stress increment.

The viscoplastic strain increment is obtained following Drucker's stability criterion [174]

$$d\varepsilon^{vp} = \langle\lambda\rangle \frac{\partial G}{\partial \sigma'} = \langle\lambda\rangle \frac{\partial F}{\partial \sigma'} \quad [4.26]$$

where G is viscoplastic potential identical to nonstationary flow surface F due to the associated flow rule and $\langle\lambda\rangle$ is a non-negative viscoplastic multiplier, if λ is negative, $\langle\lambda\rangle$ is taken as zero. The nonstationary flow surface F of NSFS-SCLAY1S model is shown in [4.22]

Similar to elasto-plasticity, viscoplastic behaviour triggers and continues once the stress state reaches the initial yield surface. It is noted that the stress state is not allowed to locate outside of the yield surface or the stress states always located on the nonstationary flow surface to satisfy consistency condition, yielding an expression as follows:

$$dF = \frac{\partial F}{\partial \sigma'_{ij}} d\sigma'_{ij} + \frac{\partial F}{\partial \varepsilon^{vp}_{ij}} d\varepsilon^{vp}_{ij} + \frac{\partial F}{\partial t} dt = 0 \quad [4.27]$$

Combining [4.26] and [4.27], the viscoplastic multiplier can be derived in relation to the stress increment as

$$\lambda = -\frac{\frac{\partial F}{\partial \sigma'_{ij}} d\sigma'_{ij} + \frac{\partial F}{\partial t} dt}{\frac{\partial F}{\partial \varepsilon^{vp}_{ij}} \frac{\partial F}{\partial \sigma'_{ij}}} \quad [4.28]$$

To find the viscoplastic multiplier in relation to the strain increment, combining [4.25] and [4.27] yields,

$$\frac{\partial F}{\partial \sigma'_{ij}} D^e_{ijkl}(d\varepsilon_{ij} - d\varepsilon^{vp}_{ij}) + \frac{\partial F}{\partial \varepsilon^{vp}_{ij}} d\varepsilon^{vp}_{ij} + \frac{\partial F}{\partial t} dt = 0 \quad [4.29]$$

Then subtituting [4.26] into [4.29] followed by some manipulations will produce the definition of the viscoplastic multiplier in relation to strain increment as below

$$\lambda = -\frac{\frac{\partial F}{\partial \sigma'_{ij}} D^e_{ijkl} d\varepsilon + \frac{\partial F}{\partial t} dt}{\frac{\partial F}{\partial \varepsilon^{vp}_{ij}} D^e_{ijkl} \frac{\partial F}{\partial \sigma'_{ij}} - \frac{\partial F}{\partial \varepsilon^{vp}_{ij}} \frac{\partial F}{\partial \sigma'_{ij}}} \quad [4.30]$$

where some auxiliary derivatives can be defined as follows

$$\frac{\partial F}{\partial \sigma'_{ij}} = \begin{bmatrix} \left(1 - exp\left(-\frac{\varepsilon^{vp}_v}{\mu}\right)\right) \frac{\partial f}{\partial p'} \\ \left(1 - exp\left(-\frac{\varepsilon^{vp}_v}{\mu}\right)\right) \frac{\partial f}{\partial q} \end{bmatrix} \quad [4.31]$$

$$\frac{\partial F}{\partial t} = \dot{v}_0 exp\left(\frac{f - \varepsilon^{vp}_v}{\mu}\right) \quad [4.32]$$

$$\frac{\partial F}{\partial \varepsilon^{vp}_{ij}} = \frac{\partial F}{\partial \varepsilon^{vp}_v} = -1 \quad [4.33]$$

where F is the nonstationary flow surface as shown in [4.22] and f is a function of current stress state as shown in [4.20].

Following the equation [4.28] and [4.30], the viscoplastic multiplier is dependent on stress (strain) increment and time increment. It implies that the viscoplastic strain increment occurs even when the stress or strain is constant. This results in NSFS-SCLAY1S model capable of describing the creep behaviour and stress relaxation, typical time related phenomena of natural clays.

From the conventional constitutive relation between stress and strain increment inherent from elasto-plasticity theory, $d\sigma = D^e(d\varepsilon - d\varepsilon^{vp})$, in combination with equation [4.26] and [4.30], the complete constitutive stress-strain-time relationship in NSFS-SCLAY1S model is described as,

$$d\sigma = D^e_{ijkl} d\varepsilon - D^e_{ijkl} \left[\frac{\frac{\partial F}{\partial \sigma'_{ij}} D^e_{ijkl} d\varepsilon + \frac{\partial F}{\partial t} dt}{\frac{\partial F}{\partial \varepsilon^{vp}_{ij}} D^e_{ijkl} \frac{\partial F}{\partial \sigma'_{ij}} - \frac{\partial F}{\partial \varepsilon^{vp}_{ij}} \frac{\partial F}{\partial \sigma'_{ij}}} \right] \frac{\partial F}{\partial \sigma'_{ij}} \quad [4.34]$$

4.3.5 Hardening law

The evolution of the flow surface incorporates three hardening laws. The first hardening law relates to the change in size of the intrinsic yield surface. The second hardeninng law decribes the evolution of orientation of the inclined flow surface with viscoplastic straining, which is called 'rotational hardening law' [12]. The third hardening law, which is proposed by Karstunen [194], is related to the degradation bonding process with viscoplastic straining.

- **The first hardening law: volumetric hardening law**

The model adopts the volumetric hardening law similar to the same formulation in MCC model as follows :

$$dp'_{pi} = \frac{vp'_{mi}}{\lambda_i - \kappa} d\varepsilon_v^{vp} \qquad [4.35]$$

The formulation shows that the change in size of the flow surface is controlled by viscoplastic volumetric strain increment $d\varepsilon_v^{vp}$. λ_i and κ are the slope of intrinsic compression line and swelling line in e-lnp' space respectively.

- **The second hardening law: rotational hardening law**

The model employs the rotational hardening law from the SCLAY1S model to control the rotation of flow surface due to soil anistropy. The rotational hardening law is defined by:

$$d\alpha = \omega \left(\left[\frac{3\eta}{4} - \alpha \right] \langle d\varepsilon_v^{vp} \rangle + \omega_d \left[\frac{\eta}{3} - \alpha \right] d\varepsilon_d^{vp} \right) \qquad [4.36]$$

where parameters ω and ω_d are used to control the absolute rate of the viscoplastic strain increment on the rotation of the flow surface and relative influence of the viscoplastic deviatoric strain increment $d\varepsilon_d^{vp}$ respectively; $d\varepsilon_v^{vp}$ is the viscoplastic volumetric strain increment.

- **The third hardening law: destructuration law**

The destructuration law describes the degradation of bonding during viscoplastic straining where the viscoplastic volumetric strains and viscoplastic deviatoric strains tend to reduce the bonding parameter x towards a target value of zero as follows:

$$dx = -\xi \left(\left| d\varepsilon_v^{vp} \right| + \xi_d \left| d\varepsilon_d^{vp} \right| \right) \qquad [4.37]$$

where ξ and ξ_d are two additional soil constants that control the absolute rate of destructuration and control the relative effectiveness of viscoplastic deviatoric strains and viscoplastic volumetric strains in destroying the bonding respectively.

4.4 NSFS-SCLAY1S model formulation in general space

NSFS-SCLAY1S is extended to general stress space to adapt the general practical geotechnical problem. The formulation in NSFS-SCLAY1S model in the general stress space is expressed in the following section.

4.4.1 Definition in general stress space

The generalisation form to NSFS-SCLAY1S model can be performed in general stress space using the following definitions.

$$\text{Stress vector } \bar{\sigma}'_{ij} \text{ is defined as } \bar{\sigma}'_{ij} = \begin{Bmatrix} \sigma'_{xx} \\ \sigma'_{yy} \\ \sigma'_{zz} \\ \tau'_{xy} \\ \tau'_{yz} \\ \tau'_{zx} \end{Bmatrix}$$

$$\text{Mean effective stress is defined as } p' = \frac{1}{3}\left(\sigma'_{xx} + \sigma'_{yy} + \sigma'_{zz}\right)$$

Deviatoric stress vector $\bar{\sigma}_d$ is defined as:

$$\bar{\sigma}_d = \begin{Bmatrix} \sigma'_{xx} - p' \\ \sigma'_{yy} - p' \\ \sigma'_{zz} - p' \\ \sqrt{2}.\,\tau'_{xy} \\ \sqrt{2}.\,\tau'_{yz} \\ \sqrt{2}.\,\tau'_{zx} \end{Bmatrix} = \begin{Bmatrix} \frac{1}{3}(2\sigma'_{xx} - \sigma'_{yy} - \sigma'_{zz}) \\ \frac{1}{3}(-\sigma'_{xx} + 2\sigma'_{yy} - \sigma'_{zz}) \\ \frac{1}{3}(-\sigma'_{xx} - \sigma'_{yy} + 2\sigma'_{zz} \\ \sqrt{2}.\,\tau'_{xy} \\ \sqrt{2}.\,\tau'_{yz} \\ \sqrt{2}.\,\tau'_{zx} \end{Bmatrix}$$

The scalar value of deviatoric stress q (used in the simplified version of the model for triaxial stress space) is defined by:

$$q^2 = \frac{3}{2}\{\bar{\sigma}_d\}^T\{\bar{\sigma}_d\}$$

$$\text{Strain vector } \bar{\varepsilon}_{ij} \text{ is defined as } \bar{\varepsilon}_{ij} = \begin{Bmatrix} \varepsilon_{xx} \\ \varepsilon_{yy} \\ \varepsilon_{zz} \\ \varepsilon_{xy} \\ \varepsilon_{yz} \\ \varepsilon_{zx} \end{Bmatrix}$$

Deviatoric strain increment vector $d\bar{\varepsilon}_d$ is defined as,

$$d\bar{\varepsilon}_d = \begin{Bmatrix} \frac{1}{3}(2d\varepsilon_{xx} - d\varepsilon_{yy} - d\varepsilon_{zz}) \\ \frac{1}{3}(-d\varepsilon_{xx} + 2d\varepsilon_{yy} - d\varepsilon_{zz}) \\ \frac{1}{3}(-d\varepsilon_{xx} - d\varepsilon_{yy} + 2d\varepsilon_{zz} \\ \sqrt{2}.d\varepsilon_{xy} \\ \sqrt{2}.d\varepsilon_{yz} \\ \sqrt{2}.d\varepsilon_{zx} \end{Bmatrix}$$

Volumetric strain increment $d\varepsilon_v$ is defined as:

$$d\varepsilon_v = d\varepsilon_{xx} + d\varepsilon_{yy} + d\varepsilon_{zz}$$

The scalar value of deviatoric strain increment $d\varepsilon_d^2$ is defined by:

$$d\varepsilon_d^2 = \frac{2}{3}\{d\bar{\varepsilon}_d\}^T\{d\bar{\varepsilon}_d\}$$

4.4.2 Elastic part of the model

According to NSFS theory [9], when the flow surface F has a negative value (F<0) then the predicted behaviour of soil is purely elastic. The elastic bulk modulus K' and elastic shear modulus G have the following definition,

$$K' = \frac{(1+e)p'}{\kappa}$$

$$G = \frac{3(1+e)p'}{2\kappa}\frac{1-2\nu}{1+\nu}$$

The elastic stiffness matrix can be expressed in terms of the elastic bulk modulus K' and elastic shear modulus G as follows (after [53], [173]),

$$[D^e] = \begin{bmatrix} 2G\frac{1-\nu'}{1-2\nu'} & 2G\frac{\nu'}{1-2\nu'} & 2G\frac{\nu'}{1-2\nu'} & 0 & 0 & 0 \\ 2G\frac{\nu'}{1-2\nu'} & 2G\frac{1-\nu'}{1-2\nu'} & 2G\frac{\nu'}{1-2\nu'} & 0 & 0 & 0 \\ 2G\frac{\nu'}{1-2\nu'} & 2G\frac{\nu'}{1-2\nu'} & 2G\frac{1-\nu'}{1-2\nu'} & 0 & 0 & 0 \\ 0 & 0 & 0 & G & 0 & 0 \\ 0 & 0 & 0 & 0 & G & 0 \\ 0 & 0 & 0 & 0 & 0 & G \end{bmatrix}$$

4.4.3 Flow surface

The flow surface in NSFS-SCLAY1S model in general stress space is a modification of the one expressed in the triaxial stress space as follow,

$$F(\bar{\sigma}'_{ij}, \bar{\varepsilon}'_{ij}, t) = \mu ln\left(\frac{\dot{v}_0 t}{\mu} e^{\left(\frac{f}{\mu}\right)} + 1\right) - \varepsilon_v = 0 \quad [4.38]$$

where f is a scalar function defined as

$$f = \frac{\lambda_i - \kappa}{1 + e_0} ln\left(\frac{p'}{p'_0}\right) + \frac{\lambda_i - \kappa}{1 + e_0} ln\left(1 + \frac{3}{2}\frac{\{\bar{\sigma}'_d - \overline{\alpha_d} p'\}^T \{\bar{\sigma}'_d - \overline{\alpha_d} p'\}}{(M^2 - \alpha^2) p'^2}\right) + \frac{\lambda_i - \kappa}{1 + e_0} ln\left(\frac{1 + x_0}{1 + x}\right)$$

where $\bar{\sigma}'_d$ and $\bar{\alpha}_d$ are the derivative stress tensor and the deviatoric fabric vector respectively; { } represents vector. M is the slope to the critical state line, p'_0 is the initial size of the yield surface of the natural clay; the scalar parameter α is a measure of the degree of anisotropy of natural clay.

4.4.4 Flow rule

An associated flow rule is assumed for the NSFS-SCLAY1S model, leading to the plastic potential (G) and non-stationary yield surface (F) identical. The flow rule is mathematically expressed as follows:

$$\dot{\varepsilon}_{ij}^{vp} = \langle \dot{\lambda} \rangle \frac{\partial G}{\partial \bar{\sigma}'_{ij}} = \langle \dot{\lambda} \rangle \frac{\partial F}{\partial \bar{\sigma}'_{ij}} \; or \; d\bar{\varepsilon}_{ij}^{vp} = \langle d\lambda \rangle \frac{\partial F}{\partial \bar{\sigma}'_{ij}} \quad [4.39]$$

where $\langle d\lambda \rangle$ is a non-negative viscoplastic multiplier, if $d\lambda$ is negative, $\langle d\lambda \rangle$ is taken as zero.

4.4.5 Stress-strain-time relation

The stress state is not allowed to be located outside of the yield surface in order to satisfy the consistency condition. This is expressed in formulation as,

$$F = F + \frac{\partial F}{\partial t} dt = 0 \quad [4.40]$$

$$or \; \frac{\partial F}{\partial \bar{\sigma}'_{ij}} \dot{\sigma}'_{ij} dt + \frac{\partial F}{\partial \bar{\varepsilon}_{ij}^{vp}} \dot{\varepsilon}'_{ij} dt + \frac{\partial F}{\partial t} dt = 0 \Leftrightarrow \frac{\partial F}{\partial \bar{\sigma}'_{ij}} d\bar{\sigma}_{ij} + \frac{\partial F}{\partial \bar{\varepsilon}_{ij}^{vp}} d\bar{\varepsilon}_{ij} + \frac{\partial F}{\partial t} dt = 0 \quad [4.41]$$

where $d\bar{\sigma}_{ij}$ and $d\bar{\varepsilon}_{ij}$ are the stress increment vector and strain increment vector respectively.

Subtituting [4.39] into [4.41], the viscoplastic multiplier can be derived in relation to the stress increment as:

$$\langle d\lambda \rangle = -\frac{\frac{\partial F}{\partial \bar{\sigma}'_{ij}} d\bar{\sigma}'_{ij} + \frac{\partial F}{\partial t} dt}{\frac{\partial F}{\partial \bar{\varepsilon}^{vp}_{ij}} \frac{\partial F}{\partial \bar{\sigma}'_{ij}}} \qquad [4.42]$$

To find the viscoplastic multiplier in relation to the strain increment, subtituting $d\bar{\sigma}'_{ij} = [D^e](d\bar{\varepsilon}_{ij} - d\bar{\varepsilon}^{vp}_{ij})$ into [4.42] and doing some manipulations, it yields the definition of the viscoplastic multiplier in relation to the strain increment as,

$$\langle d\lambda \rangle = -\frac{\frac{\partial F}{\partial \bar{\sigma}'_{ij}} \left[D^e_{ijkl}\right] d\bar{\varepsilon} + \frac{\partial F}{\partial t} dt}{-\frac{\partial F}{\partial \bar{\sigma}'_{ij}} \left[D^e_{ijkl}\right] \frac{\partial F}{\partial \bar{\sigma}'_{ij}} + \frac{\partial F}{\partial \bar{\varepsilon}^{vp}_{ij}} \frac{\partial F}{\partial \bar{\sigma}'_{ij}}} \qquad [4.43]$$

with F the nonstationary flow surface as shown in [4.38]:

$$F(\bar{\sigma}'_{ij}, \bar{\varepsilon}'_{ij}, t) = \mu ln\left(\frac{\dot{v}_0 t}{\mu} e^{\left(\frac{f}{\mu}\right)} + 1\right) - \varepsilon_v = 0$$

where f is a scalar function of stress state expressed as:

$$f = \frac{\lambda_i - \kappa}{1 + e_0} ln\left(\frac{p'}{p'_0}\right) + \frac{\lambda_i - \kappa}{1 + e_0} ln\left(1 + \frac{3}{2} \frac{\{\bar{\sigma}'_d - \overline{\alpha_d} p'\}^T \{\bar{\sigma}'_d - \overline{\alpha_d} p'\}}{(M^2 - \alpha^2) p'^2}\right) + \frac{\lambda_i - \kappa}{1 + e_0} ln\left(\frac{1 + x_0}{1 + x}\right)$$

Some auxiliary derivatives in [4.41] can be defined as follows:

$$\frac{\partial F}{\partial \bar{\sigma}'_{ij}} = \left(1 - exp\left(-\frac{\varepsilon_v^{vp}}{\mu}\right)\right)\frac{\partial f}{\partial \bar{\sigma}'_{ij}} \quad [4.44]$$

$$\frac{\partial F}{\partial t} = \dot{v}_0 exp\left(\frac{f - \varepsilon_v^{vp}}{\mu}\right) \quad [4.45]$$

$$\frac{\partial F}{\partial \bar{\varepsilon}_{ij}^{vp}}\frac{\partial F}{\partial \bar{\sigma}'_{ij}} = \quad [4.46]$$

Following the equation [4.42] and [], the viscoplastic multiplier is dependent on stress (strain) increment and time increment. This implies that the viscoplastic strain increment occurs even when the stress or strain is sustained. Hence the NSFS-MCC model is capable of properly describing the creep behaviour and stress relaxation which are the time related phenomena of natural clays.

Combining [4.42], [4.33] and the conventional stress-strain increment relationship, $d\bar{\sigma}'_{ij} = [D^e](d\bar{\varepsilon}_{ij} - d\bar{\varepsilon}_{ij}^{vp})$, the complete constitutive stress-strain-time relationship to NSFS-MCC model is defined:

$$d\bar{\sigma}'_{ij} = \left[D^e_{ijkl}\right]d\bar{\varepsilon}_{ij} - \left[D^e_{ijkl}\right]\left[-\frac{\frac{\partial F}{\partial \bar{\sigma}'_{ij}}\left[D^e_{ijkl}\right]d\bar{\varepsilon}_{ij} + \frac{\partial F}{\partial t}dt}{-\frac{\partial F}{\partial \bar{\varepsilon}_{ij}^{vp}}\left[D^e_{ijkl}\right]\frac{\partial F}{\partial \bar{\sigma}'_{ij}} + \frac{\partial F}{\partial \bar{\varepsilon}_{ij}^{vp}}\frac{\partial F}{\partial \bar{\sigma}'_{ij}}}\right]\frac{\partial F}{\partial \sigma'_{ij}} \quad [4.47]$$

4.4.6 Hardening laws

The hardening laws in generalised space incorporate the change of flow surface related to the volumetric change, the evolution of the inclination of the flow surface and the degradation of inter-particle bonding. They are adopted from ones in triaxial stress space but modified to adapt to the general stress space. Three hardening laws are presented as follows:

- **Volumetric hardening law**

The first hardening law relates to the change in size of the intrinsic yield surface, which is adopted from SCLAY1S and Modified Cam Clay model :

$$dp'_{pi} = \frac{vp'_{mi}}{\lambda_i - \kappa}d\varepsilon_v^{vp} \quad [4.48]$$

The formulation shows that the change in size of the flow surface is controlled by solely viscoplastic volumetric strain increment $d\varepsilon_v^{vp}$, λ_i and κ are the slope of intrinsic compression line and swelling line in e-lnp' space respectively.

- **Rotational hardening law**

The second hardeninng law decribes the evolution of orientation of the inclined flow surface with viscoplastic straining, which is called 'rotational hardening law' [12]. The rotational hardening law is defined by

$$d\alpha = \omega\left(\left[\frac{3\eta}{4} - \alpha\right]\langle d\varepsilon_v^{vp}\rangle + \omega_d\left[\frac{\eta}{3} - \alpha\right]d\bar{\varepsilon}_d^{vp}\right) \quad [4.49]$$

Where parameter ω and ω_d are used to control the absolute rate of the viscoplastic strain increment on the rotation of the flow surface and relative influence of the viscoplastic deviatoric strain increment $d\bar{\varepsilon}_d^{vp}$ respectively; $d\varepsilon_v^{vp}$ is the viscoplastic volumetric strain increment. $\langle\ \rangle$ are Macaulay brackets where $\left\langle d\varepsilon_v^{vp}\right\rangle = d\varepsilon_v^{vp}$ if $d\varepsilon_v^{vp} > 0$ and $\left\langle d\varepsilon_v^{vp}\right\rangle = 0$ if $d\varepsilon_v^{vp} < 0$.

- **Destructuration law**

The third hardening law, which is proposed by Karstunen [194], is related to the degradation bonding process with viscoplastic straining. The formulation is given by:

$$dx = -\xi\left(\left|d\varepsilon_v^{vp}\right| + \xi_d\left|d\varepsilon_d^{vp}\right|\right) \quad [4.50]$$

where ξ and ξ_d are two additional soil constants that control the absolute rate of destructuration and the relative effectiveness of viscoplastic deviatoric strains and viscoplastic volumetric strains in destroying the bonding respectively.

4.5 Determination of model parameters

The NSFS-SCLAYS model requires a total of twelve parameters as shown in the table below:

Table 4.1: NFST-SCLAY1S model's parameters

Category	Symbol	Explanation
Elasticity (MCC model)	κ	Swelling index
	ν	Poison's ratio
Critical state (MCC model)	λ_i	Intrinsic compression index
	M	Slope of critical state line
Rotational hardening law (SCLAY1S model)	α_0	Initial inclination of yield surface
	ω	Absolute effectiveness of rotational hardening
	ω_d	Relative effectiveness of rotational hardening
Destructuration law (SCLAY1S model)	x_0	Initial amount of bonding
	ξ	Absolute effectiveness of destructuration
	ξ_d	Relative effectiveness of destructuration
Creep parameters	μ	Modified coefficient of secondary compression
	$\dot{\upsilon}_0$ [s^{-1}]	Initial volumetric strain rate

Of the 12 parameters, there are only two new parameters (μ and $\dot{\upsilon}^0$) compared to the SCLAY1S model. Determination of modified coefficient of secondary comresion μ is direct from the well-known coefficient of secondary compression which is interpreted from the 1-D consolidation test. Regarding the initial volumetric strain rate ($\dot{\upsilon}_0$) , it is difficult to directly estimate from laboratory data. However, it can be determined in correlation with the other parameters based on its definition. The methodology which is employed to determine all parameters is summarised in this section.

Elasticity parameters

$\boldsymbol{\kappa}$ slope of a swelling line in the compression plane (lnp' – υ – space). It can be determined from oedometer test.

ν The Poisson's ratio is assumed constant value of material so that shear modulus G can be determined based on the relation with bulk modulus K' and

Critical state

$\boldsymbol{\lambda_i}$ the slope of the intrinsic normal compression line in the compression plane (lnp' – υ – space). Ideally, the value for $\boldsymbol{\lambda_i}$ should be determined from an oedometer test on a reconstituted sample otherwise it is the slope of the post-yield compression line in the (lnp'- υ) plane.

M Slope of critical state line. It can be determined from the value of critical friction angle ϕ_{cs} via their relationship $M = \frac{6\sin\phi_{cs}}{3-\sin\phi_{cs}}$

Anisotropy parameters

α_0 Initial inclination of yield curve. For the case of normally consolidated or lightly over consolidated, the value of α_0 can be determined based on this formulation [12]

$$\alpha_{K0} = \frac{\eta_{K0}^2 + 3\eta_{K0} - M^2}{3} \quad (4.51)$$

Where : $\eta_{K0} = \frac{3(1-K_0^{NC})}{(1+2K_0^{NC})}$

and $K_0^{NC} = 1-\sin\varphi'$ (Jaky's simplified formula)

ω The model parameter ω controls the rate at which α tends towards its current target value. Wheeler [12] found it difficult to have a direct method to derive this parameter. He suggested that an appropriate for the value of ω can be derived from the comparison between simulation of model at different values of ω with the experimental test which significantly involves the rotation of the yield curve, e.g. isotropic consolidation test. Zentar [195] suggested the value of ω will normally be in the range between $\frac{10}{\lambda}$ and $\frac{15}{\lambda}$.

ω_d The model parameter ω_d defines the relative effectiveness of plastic shear strains and plastic volumetric strains in rotating the yield curve. It is determined by the following formulation:

$$\omega_d = \frac{4(M^2-4\eta_{K0}^2-3\eta_{K0})}{8(\eta_{K0}^2-M^2+2\eta_{K0})}$$

Destructuration parameters

x_0 The parameter describing the amount of bonding, was estimated based on sensitivity [13] :

$x_0 \approx S_t - 1$ (with S_t is the sensitivity of soil)

ξ, ξ_d are the destructuration parameters which control the absolute effectiveness and relative effectiveness of destructuration. Determination of the parameters ξ and ξ_d requires an optimisation procedure [13]. It means that model simulation must be compared with the test results. Parameter ξ should be optimised based on isotropic loading tests and simulations at different values of ξ since the influence of parameter ξ_d in this case is relatively small and can be chosen by 0.2 (typical value for most clay [13]). In order to optimise ξ_d, a high stress ratio should be used to have significant influence of parameter ξ_d due to large plastic shear strain generated. Simulating models at the value of ξ (determined before) with different values of ξ_d (around 0.2 as suggested by [13]) then making comparison with the trixial compression test at high stress ratio to optimise the value of ξ_d.

Creep parameters

μ The modified coefficient of secondary compression is determined in equation [3.13], $\mu = \frac{C_{\alpha e}}{(1+e_0)} \frac{1}{ln10}$ where $C_{\alpha e}$ is the slope to secondary compression line (assumption of constant) depicted in the relationship of void ratio and logarith of time. Mesri and Godlewski [176] proposed an empirical correlation to determine $C_{\alpha e}$ as ${C_{\alpha e}}/{\lambda} = 0.05 \pm 0.029$ (Clay) and ${C_{\alpha e}}/{\lambda} = 0.07 \pm 0.02$ (peat).

$\dot{\upsilon}_0$ The initial volumetric strain rate at the time to the end of primary consolidation is expressed as $\dot{\upsilon}^0 = {\mu}/{t_0}$, where t_0 can be estimated by Taylor's square root method [138] based on Terzaghi's theory of consolidation : $t_0 \approx t_{90} = \frac{H^2 T_v(90\%)}{C_v}$

C_v is coefficient of consolidation with dimensions L^2T^{-1}. H is the drainage distance and T_v (90%) is a constant.

4.6 Numerical solution

The NSFS-SCLAY1S is implemented in MATLAB and FORTRAN software to verify the behaviour of the model and validate the model against the results from laboratory tests like oedometer, undrained triaxial compression & extension tests, triaxial creep tests.

The model is implemented in MATLAB software using the explicit algorithm in which the stresses are computed directly from the consistency condition, flow surface, viscoplastic volumetric strain at a previously known point. The application of the explicit integration scheme for conventional elastoplastic model demonstrated by Sloan ([184], [185]) is adopted in this model with the procedure as follows.

The stress increment is computed based on the constitutive stress-strain relationship from equation [4.52]:

$$d\bar{\sigma}'_{ij} = \left[D^e_{ijkl}\right]d\bar{\varepsilon}_{ij} - \left[D^e_{ijkl}\right]\left[-\frac{\frac{\partial F}{\partial \bar{\sigma}'_{ij}}\left[D^e_{ijkl}\right]d\bar{\varepsilon}_{ij} + \frac{\partial F}{\partial t}dt}{-\frac{\partial F}{\partial \bar{\sigma}'_{ij}}\left[D^e_{ijkl}\right]\frac{\partial F}{\partial \bar{\sigma}'_{ij}} + \frac{\partial F}{\partial \bar{\varepsilon}^{vp}_{ij}}\frac{\partial F}{\partial \bar{\sigma}'_{ij}}}\right]\frac{\partial F}{\partial \sigma'_{ij}} \qquad [4.52]$$

In explicit (Euler's forward) algorithm, the constitutive equations are integrated directly at the previously known stress point. It is also known as the tangential stiffness method. The stress at the next increment $\{\sigma_{n+1}\}$ is calculated as follows:

$$\{\sigma'_{n+1}\} = \{\sigma'_{n}\} + \{d\sigma'\}$$

where $\{\sigma'_{n}\}$ is the current stress and $\{d\sigma'\}$ is the incremental stress which is computed using Eq. 5.45 in which all derivatives are taken about the previously known state (see appendix 2). The corresponding viscoplastic strain $\{d\varepsilon^{vp}\}$ is obtained by the following formula:

$$d\bar{\varepsilon}^{vp} = \left[\frac{\frac{\partial F}{\partial \bar{\sigma}'_{ij}}\left[D^e_{ijkl}\right]d\bar{\varepsilon}_{ij} + \frac{\partial F}{\partial t}dt}{\frac{\partial F}{\partial \bar{\sigma}'_{ij}}\left[D^e_{ijkl}\right]\frac{\partial F}{\partial \bar{\sigma}'_{ij}} - \frac{\partial F}{\partial \bar{\varepsilon}^{vp}_{ij}}\frac{\partial F}{\partial \bar{\sigma}'_{ij}}}\right]\frac{\partial F}{\partial \bar{\sigma}'_{ij}}$$

In order to obtain acceptable accuracy and allow the consistency condition at the end of each increment, the explicit algorithm requires very small increment size.

4.7 Model verification against laboratory tests on different soils

4.7.1 Undrained triaxial shearing tests of Haney clay

Vaid and Campanella [94] conducted a series of undrained triaxial compression tests on undisturbed saturated sensitive marine clay known as Haney Clay. The undrained shearing stages of tests were performed at different constant strain rates

varying from 0.00094%/min to 1.1%/min to investigate the rate dependency. Haney Clay properties are reported as follows: liquid limit $w_L = 44\%$, plastic limit $w_P = 26\%$, preconsolidation pressure at 340 kPa and sensitivity S_t between 6 and 10. All test samples were normally consolidated under an isotropic confining pressure of 515 kPa for a period of 36 hours and then were left undrained for 12 hours under consolidation stresses prior to shear loading.

The conventional parameters ($\kappa, \lambda_i, e_0, and\ \nu'$) of Haney clay are determined following the report by Vermeer and Neher [178]. The slope of the critical state line $M_c$was estimated from triaxial tests and taken as $M_c = 1.28$. For rotational parameters, ω was calculated from λ_i as suggested by Zentar et al. [195][196] ($\omega = 15/\lambda_i$) and ω_d was determined from the relation with M_c and η_{K0} as proposed by Wheeler et al. [12], discussed in section 4.5. Related to the destructurational parameters, the initial bonding value was calculated from sensitivity as $x_0 = S_t - 1$; the parameters ξ and ξ_d are calibrated from curve fitting. The creep index value was provided by Vermeer and Neher [178] ($\mu = 0.004$) and the value of the initial volumetric strain rate $\dot{v}_0$ is estimated from the creep index via relation: $\dot{v}_0 = \mu/t_0$. All model parameters are presented in Table 4.2.

The implementation of simulating the undrained triaxial compression test of Haney clay samples at three different strain rates 1.1%/min, 0.15%/min and 0.00094%/min is presented in Figure 4.2. It shows that the NSFS-SCLAY1S model is able to reproduce the triaxial undrained compression laboratory tests very well. It can estimate correctly the peak of the strength of soil compared to the underestimation from the NSFS-MCC model. Furthermore, the destructuration of the inter-particle bonding of sensitive soft clay is very well captured after the peak of strength. With this performance, the NSFS-SCLAY1S model shows a significant improvement from the isotropic NSFS-MCC model. This promises the reliability of the application of this model in a practical geotechnical problem.

Table 4.2: Model parameters for Haney clay

Model parameters		**Haney clay**
Elasticity	κ	0.05
	ν	0.25
Critical state	M	1.28
	λ_i	0.32
Rotational hardening	α_0	0
	ω	47
	ω_d	0.84
Destructuration	x_0	8
	ξ	11
	ξ_d	0.3
Creep	μ	0.004
	$\dot{v}_0$ [s^{-1}]	2.78e-7
Initial state	p'_{m0} [kPa]	410
	e_0	2
	OCR	1

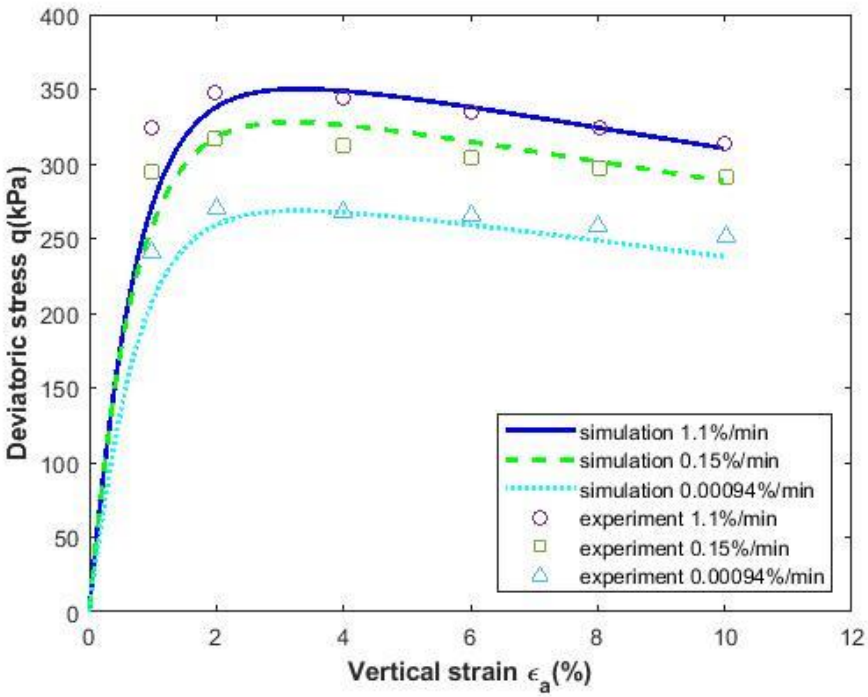

Figure 4.2 : NSFS-SCLAY1S verification against undrained triaxial shearing tests of Hanney clay at three different rates of loading.

4.7.2 Creep rupture of Haney clay

Vaid and Campanella [94] conducted a series of triaxial creep tests on the same specimens as those on the undrained shearing tests above. All specimens had the same consolidation stage with confining pressure of 515 kPa. The applied deviatoric stresses of a 329kPa, 267kPa and 167kPa were kept constant for creep tests.

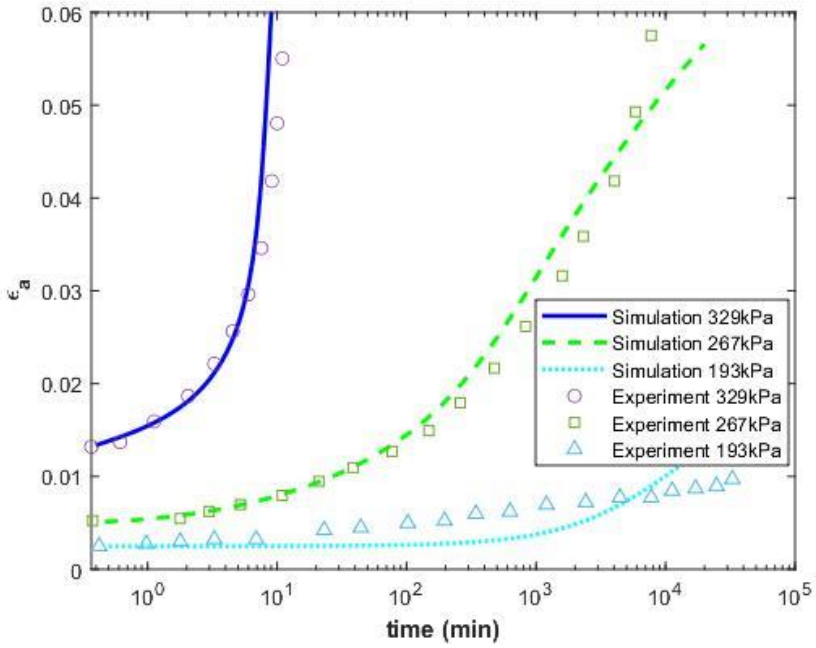

Figure 4.3 : NSFS-SCLAY1S verification against undrained triaxial shearing tests of Hanney clay at three different rates of loading.

The simulation of undrained triaxial creep tests by NSFS-SCLAY1S model at three different constant deviatoric stresses against the laboratory test results is presented in Figure 4.3. It shows that NSFS-SCLAY1S can reproduce the result of undrained triaxial creep tests correctly. At low deviatoric stress, there is a slight increase of axial strain. When the deviatoric stress reaches a certain value large enough, such as 267 kPa or 329 kPa, the strain rate tends to accelerate over time resulting in a potential failure, called creep rupture. At the highest value of deviatoric q=329 kPa, the strain rate increases sharply over just under 5 mins, while at q=267 kPa, the strain starts to rocket after a longer period at around 300 mins. This explains why some failures of geo-structures occur in the short term, but some others reach a failure after a long period under a constant loading condition. These results confirm the elegance and capacity of the NSFS-SCLAY1S model in capturing the eventual

long-term failure of natural clay deposits. This is an important feature that the other overstress-based time dependent constitutive models are unable to replicate.

4.7.3 Constant rate of strain oedometer test of Batiscan clay

Leroueil et al. [2] conducted a series of constant rate of strain (CRS) oedometer tests on Batiscan clay samples which were taken at a depth of 7.25m - 7.46m in Batiscan area, about 110km west of Quebec City. The geotechnical properties of Batiscan clay were reported that the water content is around 79.6% while the liquid limit w_L= 43%, the plasticity index I_p=21, the liquid index I_L=2.7, and clay-sized particle content 81%. The initial state was taken as $\sigma'_{v0} = 65kPa$, equal to the in-situ vertical effective stress at the depth of samples taken. The preconsolidation pressure was reported as 88 kPa, determined by conventional oedometer test. The CRS oedometer tests were performed in the range between 1.7x10^{-8} (s^{-1}) and 4x10^{-5} (s^{-1}). Three CRS tests at strain rates 1.07e-7 (s^{-1}), 1.43e-6 (s^{-1}), and 2.14e-6 (s^{-1}) were employed to verify the developed model NSFS-SCLAY1S.

The parameters $\kappa, \lambda_i, e_0, \mu, \dot{v}_0 \; and \; x_0$ shown in Table 4.3 were determined following the process which is detailed in section 4.5 from the result of oedometer tests on natural Batiscan clay samples. The slope of the critical state line $M_c$was taken as $M_c = 0.98$ as suggested by Rocchi et al. [187]. For rotational parameters, ω was calculated from λ_i as suggested by Zentar et al. [195][196] ($\omega = 15/\lambda_i$) and ω_d was determined from the relation with M_c and η_{K0} as proposed by Wheeler et al. [12], discussed in section 4.5. The initial bonding value was calculated from sensitivity as $x_0 = S_t - 1$. The destructuration parameters χ and χ_d were determined via curve fitting similar to the report by Yin and Karstunen [155] . Poisson's ratio ν was taken to be 0.3.

The result of simulating the CRS oedometer tests of Batiscan clays at three constant rates 1.43e-5, 2.13e-6, and 1.07e-7 (%/s) is presented against the laboratory test data in Figure 4.4. It can be seen that the predictions from the NSFS-SCLAY1S model get along quite well with the experimental data. It shows the model capacity of describing the rate effect on the preconsolidation pressure that has been discussed widely in the literature similar to the effect of strain rate on the undrained shear strength of soil ([91], [94]).

Table 4.3: Model paramaters for Baiscan clay

Model parameters		**Batiscan clay**
Elasticity	κ	0.037
	ν	0.3
Critical state	M	0.98
	λ_i	0.41
Rotational hardening	α_0	0.184
	ω	14
	ω_d	1.21
Destructuration	x_0	5
	ξ	10
	ξ_d	0.3
Creep	μ	0.019
	$\dot{v}_0$ [s^{-1}]	1.32e-6
Initial state	p'_{m0} [kPa]	81.84
	e_0	1.92
	OCR	1.354

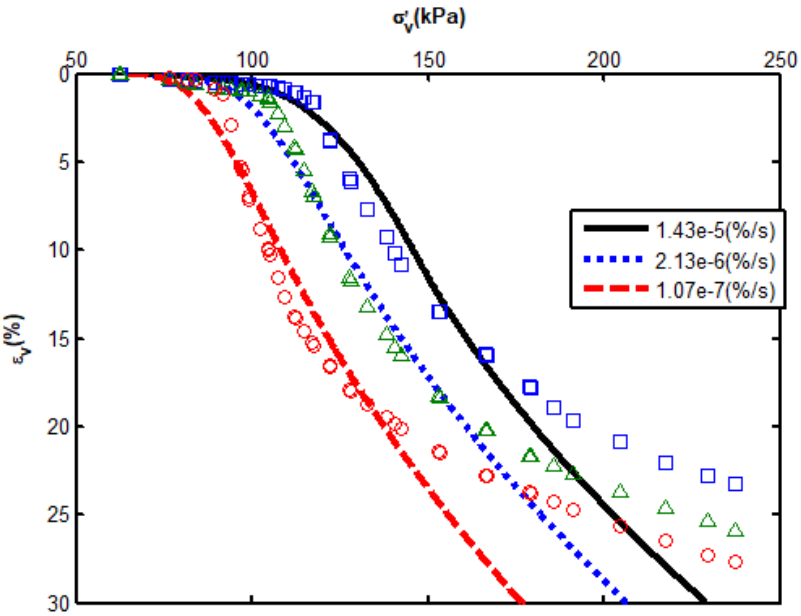

Figure 4.4 : NSFS-SCLAY1S verification against CRS oedometer tests on Batiscan clay at three different rates of loading.

4.7.4 Oedometer tests on Saint -Herblain Clay

Rangeard [197] conducted a particular constant strain rate oedometer test on St. Herblain clay. The clay samples were collected from a depth of 6.5m – 7.5m with the properties as reported: water content 87%, liquid limit w_L=90%, plastic limit w_p=48%, bulk unit weight γ=14.9 kN/m^3. Two different strain rates ($d\varepsilon/dt$) were performed with an order of first strain rate 3.3 x 10^{-6} s^{-1} until an axial strain of 12% then the strain rate was altered to 6.6 x 10^{-7} s^{-1} and kept until the vertical strain reached 15.5%. Subsequently, the strain rate was switched back to the initial strain rate 3.3 x 10^{-6} s^{-1} until the end of test.

Soil parameters λi, k, e_0 , μ, and υ_o were determined from the results of oedometer tests and were also reported by Rangeard [197]. The slope of the critical state line in compression was taken as 1.25 from triaxial tests [197]. The vertical pre-consolidation pressure was determined from the oedometer test as 52 kPa. Poisson ratio is taken as 0.3. There is no further rotation during a one-dimensional consolidation test so the actual value of parameter ω has no influence on the compression curve ε_v-σ'_v. Given that the clay is slightly structured, the degradation of inter-particle bonds can be ignored [197]. All soil parameters are summarised in Table 4.4.

Table 4.4: Model paramaters for St. Herblain clay

Model parameters		**Herblain clay**
Elasticity	κ	0.022
	ν	0.3
Critical state	M	1.25
	λ_i	0.41
Rotational hardening	α_0	0.46
	ω	-
	ω_d	-
Destructuration	x_0	-
	ξ	-
	ξ_d	-
Creep	μ	0.021

	$\dot{v}_0$ [s^{-1}]	1.42e-6
Initial state	p'_{m0} [kPa]	50
	e_0	2.26

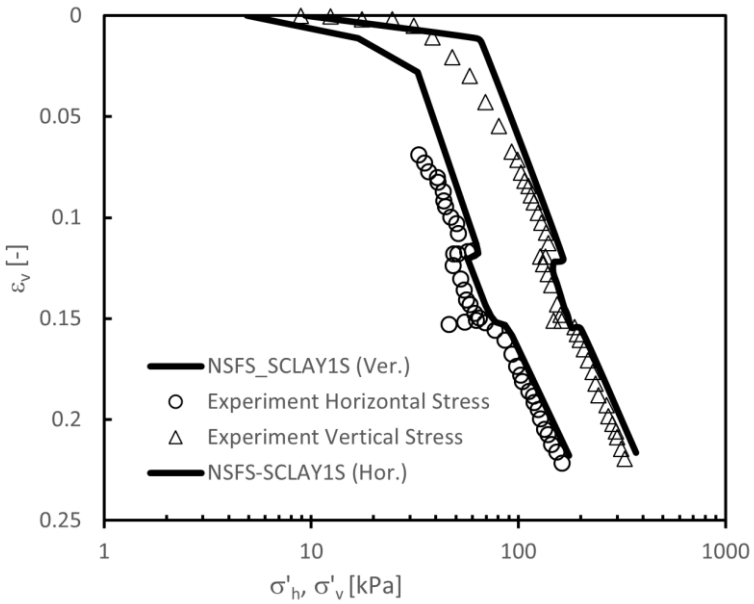

Figure 4.5: Simulation versus CSR oedometer tests on Saint-Herblain clays

The NSFS-SCLAY1S model is verified against the CSR oedometer tests on Sain-Herblain clays at different strain rates. The simulations against the experimental results are presented on Figure 4.5. It can be seen that the model predictions are in good agreement with the test results, particularly the reproduction of vertical stress. The model also captures very well the indentation due to the alteration of strain-rate during testing.

4.7.5 Undrained triaxial compression and extension tests on Kawasaki Clay

Nakase and Kamei [198] performed undrained triaxial compression and extension tests at various constant strain rates with the axial strain-rate varying from 0.7% to 0.007%/min to evaluate the strain-rate dependency of Kawasaki clays. The clay samples were reconstituted and anisotropically consolidated. The index properties of Kawasaki clay specimens were reported as plasticity index I_p=29.4, specific gravity G_s = 2.69, plastic limit w_P=25.9%, liquid limit w_L=55.3%, and clay content 22.3%. The clay samples were consolidated under a K_0 value of 0.42 until the vertical effective consolidation pressure of 392 kPa with a back pressure of 196 kPa. After the consolidation stage (assumed in one week), clay samples were subjected to undrained shearing in compression and extension.

The conventional soil parameters of Kawasaki clay , such as κ, λ_i, e_0, and M were reported by Kamei and Sakajo [199]. The critical stress ratio in triaxial compression and extension were determined as 1.65 and 1.24, respectively based on triaxial test data. The destructuration feature is not considered in this simulation since the clay samples were reconstituted which results in any initial bonding being destroyed during remoulding. The initial rotational angle is determined from the K_0 consolidation value and the absolute rate of yield surface rotation ω is determined from the triaxial extension with a typical range between 10/λi and 20/λI, taken as 77, similar to the value reported in Yin [200]. The relative rate of yield surface rotation ω_d is determined from M and K_0 as detailed in section 4.5. Creep parameters μ and υ_o are determined from compression index λ from the consolidation stage. All model parameters are summarised in Table 4.5.

Table 4.5: Model paramaters for Kawasaki clay

Model parameters		**Kawasaki clay**
Elasticity	κ	0.021
	ν	0.3
Critical state	M	1.65(M_c), 1.24 (M_e)
	λ_i	0.16
Rotational hardening	α_0	0.6
	ω	77
	ω_d	1.1
Destructuration	x_0	-
	ξ	-
	ξ_d	-
Creep	μ	0.031
	$\dot{v}_0$ [s^{-1}]	2.15e-6
Initial state	p'_{m0} [kPa]	86
	e_0	1.07

The simulations of NSFS-SCLAY1S of the undrained triaxial compression and extension tests against the laboratory tests results on Kawasaki clays are presented in Figure 4.6. The tests were simulated considering the consolidation stage. The numerical analysis of the NSFS-SCLAY1S model shows its response during triaxial

compression agrees very well with experimental results, while its predictions for the extension behaviour of soil are less accurate. This is a limitation of the model while describing the behaviour of soft clay inside the yield surface or elastic behaviour. Moreover, it could be in part due to adoption of an associated flow rule in the model formulation which was discussed in Taiebat [14]. It is noted that in triaxial compression tests, a better agreement between numerical results and experimental results is achieved at the higher strain rate as shown in Figure 4.6b. This is due to the structure of soil having less effect at high rate of shearing compared to the slow rate of shearing. Moreover, destructuration is excluded in this simulation since there is no initial bonding in reconstituted clay. However, in practice, some bonding has been gained during the consolidation stage that has some effects on very low shearing. This issue is discussed in the literature review, section 2.2.3 about rate effect. It is noticeable that it is likely no softening description in the lowest rate of shearing in compression.

The Figure 4.6a shows the relationship between the deviatoric stress against the axial strain. Although the numerical results capture very well the initial stiffness, ithey overestimate the shear strength in tension. This can result from the employment of an associated flow rule in this model as discussed above.

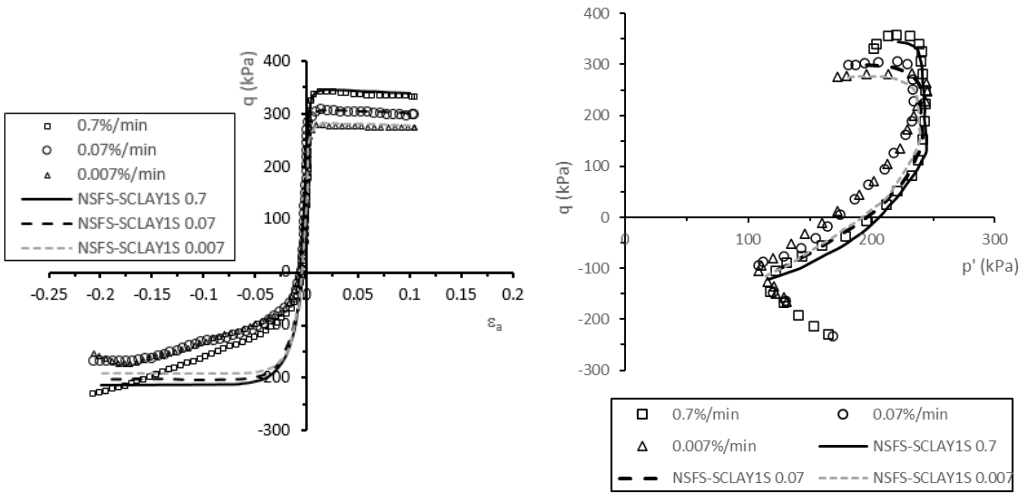

(a) Deviatoric stress versus axial strain

(b) Effective stress path

Figure 4.6: Verification of NSFS-SCLAY1S model against the undrained triaxial compression and extension tests on Kawasaki clays at different constant strain rates

4.7.6 Comparison of NSFS-SCLAY1S model with overstress based model

As discussed in the literature review, overstress theory based models have been reported with some limitations in describing the creep behaviour of soft soil, particularly the creep rupture ([153], [157], [158]). Although the destructuration feature in some advanced overstress based models can describe the creep behaviour [21], its accuracy needs to be investigated. Most overstress-based models in literature have not shown simulation to predict the creep behaviour, even the recently developed advanced model like EVP-SANICLAY [156]. A comparison between NSFS-SCLAY1S models using non-stationary flow surface and an overstress- based model EVP-SCLAY1S for a prediction of creep rupture on Haney clay is shown in Figure 4.7. It can be seen that the overstress-based model without destructuration feature (EVP-SCLAY1) is unable to capture the creep rupture on Haney clay as shown in Figure 4.7b. It is noticeable that EVP-SCLAY1S can capture very well creep rupture at the high constant deviatoric stress (329 kPa) but less accuracy with the lower deviatoric stress (267 kPa). In contrast, the NSFS-SCLAY1S model can capture very well the creep rupture on Haney Clay at both high and low constant deviatoric stress (Figure 4.7a). This proves the important role of a the time factor that is added in the yield surface formulation in the NSFS-SCLAY1S model thanks to the non-stationary flow surface theory. This enables the model to describe appropriately the creep behaviour of soft clay.

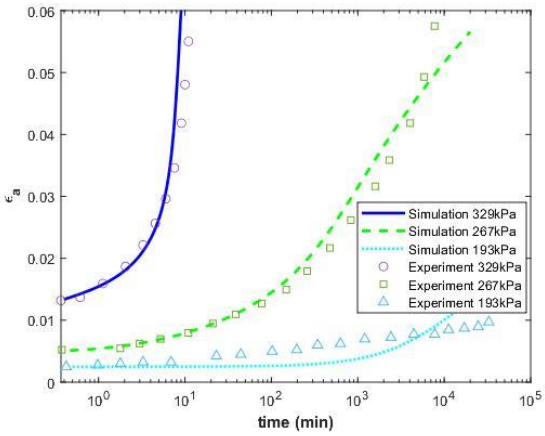

(a) Creep rupture prediction by NSFS-SCLAY1S

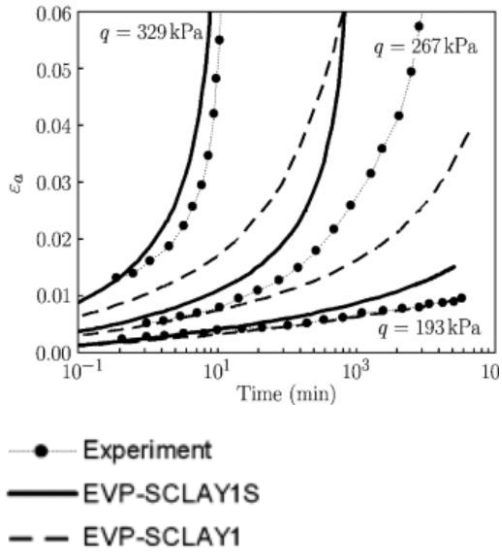

(b) Creep rupture prediction by EVP-SCLAY1S model [200]

Figure 4.7: Creep rupture prediction on Haney clay by (a) NSFS-SCLAY1S model and (b) EVP-SCLAY1S model.

Another important point on which the nonstationary flow surface theory based model (NSFS-SCLAY1S) is preferred to the overstress-based model is the capacity of describing the softening behaviour of soft clay over time. This feature was discussed in chapter 3 where NSFS-MCC (without destructuration feature) can describe the softening effect of soft clay thanks to the contribution of the time factor in NSFS-MCC formulation as discussed in section 3.7.1. The overstress-based model with destructuration feature can describe the softening behaviour of soft clay; however, this softening effect is only due to the degradation of structure on inter-particles, not including the softening due to time effect.

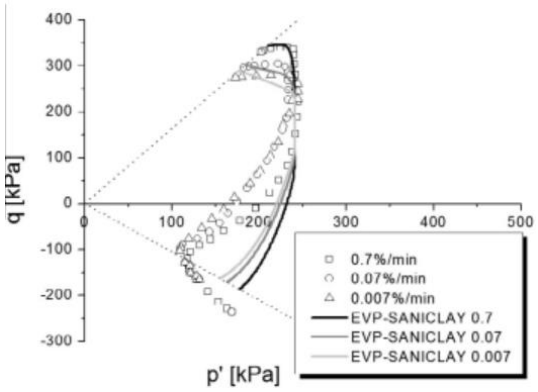

(a) EVP-SANICLAY

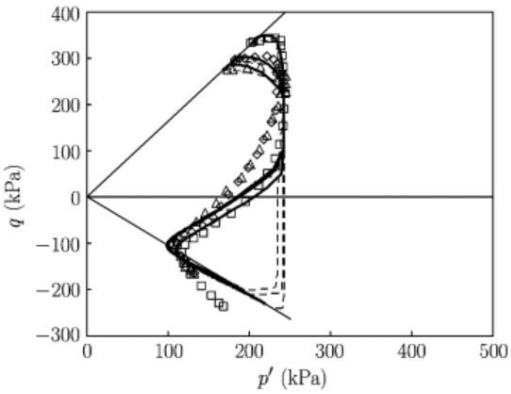

(b) EVP-SCLAY1S

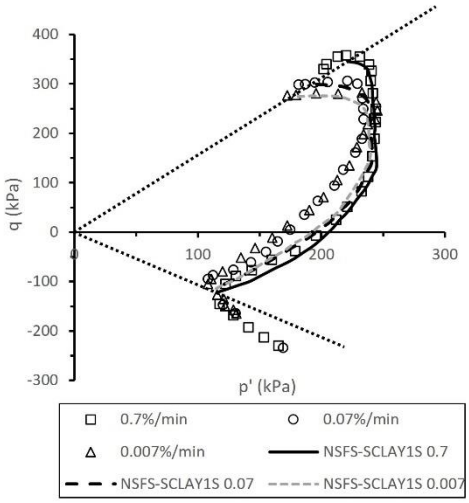

(c) NSFS-SCLAY1S

Figure 4.8: Simulations of triaxial undrained compression tests on Kawasaki

A comparison between the NSFS-SLAY1S model and two other overstress-based models EVP-SANICLAY [156] and EVP-SCLAY1S [200] on prediction of Kawasaki clay behaviour in compression is shown in Figure 4.8. Both models NSFS-SCLAY1S and EVP-SCLAY1S employ a similar destructuration law, while EVP-SANICLAY adopts a different destructuration law. The simulations by the three models on Kawasaki clay show that at high rate of compression, all models capture very well the experimental results; however the softening effect is not clear at this high rate in both simulation and experimental results since Kawasaki clay samples were reconstituted so only some extent of structure would develop from the consolidation stage. At lower rate of compression, experimental results show some extent of softening before failure, though EVP-SANICLAY (Figure 4.8a) shows no softening effect for both strain rate 0.07%/min and 0.007%/min and its predictions are less accurate. EVP-SCLAY1S (Figure 4.8b) shows better agreement with the experimental results on both lower strain rates compression tests; however, no sign of softening effect is described. Figure 4.8c shows that the simulations of NSFS-SCLAY1S not only agree with the experimental results, but it also describes some extent of softening effect at the low strain rates of compression. This iresultes from the time effect in the NSFS-SCLAY1S model.

4.8 Concluding points

In this chapter, an advanced time dependent constitutive model has been developed based on the nonstationary flow surface theory (NSFS) in combination with an advanced elasto-plastic model (SCLAY1S). This proposed model which is named as NSFS-SCLAY1S, is a further development of the isotropic time dependent constitutive NSFS-MCC model introduced in chapter 3. Limitations in the NSFS-MCC model are improved which enables the new model NSFS-SCLAY1S to describe two important advanced features of natural clay: fabric anisotropy and destructuration. With this improvement, NSFS-SCLAY1S is not only able to describe the time dependency feature of soft clay, but also describe successfully the fabric anisotropy and the degradation of inter-particle bonding of soil as well as the softening effect with time . This enables this model to provide a better prediction of the long-term behaviour of soft clay under different loading conditions. The simulations exhibit that the NSFS-SCLAY1S model is capable of describing the time and rate effects on the behaviour of natural clays. Validations against the results from some element level tests like undrained triaxial compression, extension tests, undrained triaxial creep test and CRS

oedometer tests showed that the predictions from NSFS-SCLAY1S for different soil tests agree well with the experimental data. This confirms the model being able to provide a promising solution for the simulation of the long-term creep deformations of soft ground. However, limitations of NSFS theory mean that there is purely elastic behaviour if the stress state is located inside the yield surface while in practice the creep behaviour of soil still occurs.

The proposed NSFS-SCLAY1S model has twelve parameters which can be determined straightforwardly from some standard tests in the laboratory such as triaxial test and oedometer test. The process of determining the model parameter is detailed in section 4.5.

The model NSFS-SCLAY1S shows some advantages compared to overstress-based models like describing the creep rupture, or softening effects. Particularly, the description of creep rupture is a limitation in overstress-based models due to its formulation that were discussed by many researchers. A comparison between the simulation s of NSFS-SCLAY1S model and two other overstress-based models was made to show the advantage of the proposed model in describing the creep behaviour of soft clay.

CHAPTER 5

CONCLUSION

5.1 Summary

The thesis presented an introduction and a comprehensive literature review in chapter 1 and chapter 2 about time dependent behaviour of soft clay. While chapter 1 provided a brief of the problems related to the time dependent behaviour of soft clay as well as the aims and objectives of this research, the chapter 2 reviewed the literature to provide insight into a scenario related to the research topic so that a gap in modelling the time dependent behaviour of soft clay is highlighted. Three key areas with respect to the advanced features of soft clay, the time-dependent behaviour and possible approaches to modelling this behaviour were discussed in chapter 2. The first area focused on the nature of soft soil which explains the establishment of the important features of soft clay regarding to the fabric anisotropy, destructuration and the time dependent behaviour. The following key section focused on time-related phenomena such as creep, stress relaxation and rate effect to provide insight into the mechanism of those phenomena and the importance of accounting for these behaviours. The last section explained the importance of the overstress and non-stationary flow surface theory on developing general time/rate dependent constitutive models. The advantages and limitations of each theory were discussed to finally offer an appropriate theory for developing time dependent constitutive models in this thesis, regarding NSFS-MCC model and NSFS-SCLAY1S model. The theory which was employed is Non stationary Flow Surface Theory which could overcome the limitation of overstress theory reported by mmany reserachers (e.g. [153], [157], [158]), arguing that it is unable to properly capture the creep behaviour of soil, in particular the acceleration creep process which leads to creep rupture. Among the time related manners, creep failure or creep rupture is an important issue requiring particular attention in geotechnical design. Therefore, the non-stationary flow surface (NSFS) has been employed as a mean of addressing this matter.

Before development of an advanced time dependent constitutive model which is capable of describing all significant features of soft clay such as fabric anisotropy, destructuration and time dependency, a preliminary time-dependent constitutive

model using non -stationary flow surface (NSFS) in combination with a well-known Modified Cam Clay (MCC) model was proposed in chapter 3. The model is named as NSFS-MCC. Its development is based on an assumption of isotropy that there is no fabric anisotropy or bonding in the nature of soil. Its focus is on development of the formula of a simple constitutive relationship, which can properly describe the time development of soft clay. The NSFS-MCC model exhibited the capacity of description of some related-time dependent phenomena of soft clay such as creep, time/rate dependent behaviour, creep rupture. The quantitative verification at elementary test level against the laboratory result of some natural clays such as Hanney clay, Batis can clay, HKMD clay shows it get along quite well. However, it requires an improvement to produce a better performance.

A further development of the isotropic time-dependent constitutive model NSFS-MCC to describe some advanced features of soft clay regarding fabric anisotropic and destructuration was presented in chaper 4. This advanced model is called as NSFS-SCLAY1S since this model is a combination of using NSFS theory with an advanced inviscous model, SCLAY1S. The determination of model parameters was discussed in this chapter. The model parameters are mostly determined from the result of standard laboratory except two parameters related to destructuration requires a calibration process. The model was experienced the qualitative and quantitative verification. The qualitative verification showed that the model can exhibit all time related dependent behaviour very well such as creep, time rate effect or creep rupture. The quantitative verification was carried out at elementary level test such as oedometer tests, undrained triaxial compression and extension tests, creep tests of five natural clays regarding Hanney clay, Batiscan clay, Saint Herblain clay and Kawasaki clay. It showed a signification improvement of NSFS-SCLAY1S model compared to NSFS-MCC model in reproduction of these tests results.

A comparison of NSFS-SCLAY1S model with two other overstress-based models EVP-SANICLAY and EVP-SCLAY1S was made to show the advantage of non-stationary flow surface based model NSFS-SCLAY1S in describing the creep behaviour and softening effect due to the time factor.

5.2 Conclusion

The time dependent behaviour of soft clay has remained an attractive research topic in geotechnical engineering over the last few decades. The prediction of the long-term settlement of soft ground is one of the key challenges in geotechnical design due to its complex response under the effect of many factors such as the history of soil

composition, environment effect, organic matters, structure of soft clay, loading condition. Therefore, an appropriate numerical solution is only achieved if some fundamental features of soft clay can be addressed such as fabric anisotropy, inter-particle bonding and time dependency. So, this research was attempted to develop a constitutive model which can describe those three features of soft clay so that an accurate prediction can be achieved.

Some related literature was reviewed to discover the approach for modelling and the gap in this field that needs to be filled. It is noticeable, most of the general time dependent constitutive models were developed based on the overstress theory thanks to its simplicity for discovering a formula. However, an important limitation for this approach is its lack of capacity of describing the creep behaviour of soft clay properly. Therefore, the current research employed a nonstationary flow surface to develop a time dependent constitutive model with a focus on fully describing the creep deformation and creep rupture. This was achieved through the model validation against the creep tests or the explanation of mechanism of the model response to creep or relaxation loading condition.

An isotropic time dependent constitutive model using nonstationary flow surface NSFS) was developed first to study the mechanism of NSFS theory on describing some time related phenomena. It is also a knowledge base to further development of an advanced time dependent model with inclusion of fabric anisotropy and destructuration features. Both isotropic and anisotropic time dependent models are verified qualitatively and quantitatively. The model was verified against various laboratory test types, such as undrained triaxial compression and extension tests at different strain rates, one dimensional compression tests on various constant strain rates, and undrained triaxial creep tests on different clay samples like Haney clay Kawasaki clay, Saint Herblain clay, and Batiscan clay. The result showed the models can capture the experimental results very well. With the inclusive fabric anisotropy and destructuration, it showed the superior improvement of the anistropic NSFS-SCLAY1S model compared to the isotropic NSFS-MCC model.

The NSFS-SCLAY1S was also compared with two other overstress-based models EVP-SANICLAY and EVP_SCLAY1S to evaluate the preference of using nonstationary flow surface in capturing the creep behaviour, in particular the creep rupture that the overstress-based model is unable to describe appropriately due to its mathematical formuation.

Although the developed model NSFS-SCLAY1S shows some advantages in simplicity and captures the creep behaviour of soft clay very well, there are still some limitations which need to be investigated further to improve the robustness of the proposed model. Some limitations of the proposed model are as follows:

- The model assumes no viscoplastic behaviour if the applied stress is less than the preconsolidation pressure or the stress state is located inside the yield surface. This is contradicted in practice where the creep behaviour is witnessed even when the applied stress is smaller than the pre-consolidation stress. This limitation is due to the assumption in formulations of non-stationary flow surface theory. Also, the model cannot describe the relaxation phenomenon from a stress state within the yield surface.
- The model employs the associated flow rule to unify the yield surface and potential surface for a simplicity in formulation. However, this limits the model applicability to normal or lightly consolidated soil. This results in less accurate prediction of extension tests as discussed in section 4.7.5.
- The model is limited to predict the contracted behaviour rather than dilated behaviour. So it is unable to be employed for predicting the behaviour of sand or heavily over consolidated clay.

5.3 Recommendation for future work

Along with this research topic, the following topics are worthy of further investigation.

- Natural clay exhibits both normally consolidated and overconsolidated states. The current proposed model is only adapted to normally consolidated or lightly overconsolidated clay. So, it demands further study to describe the dry side of overconsolidated clay.
- The current research ignores the creep existing inside the yield surface due to the limitation of the theory while there is an existence of creep deformation during the elastic stage. To capture the full creep behaviour, the model is required to be further developed to describe the creep behaviour inside the yield surface.
- The algorithm for the numerical analysis in this research is explicit algorithm for simplicity of numerical solution. However, to provide a better prediction and more robust simulation of a complex geotechnical problem, an improvement of algorithm is required.

- This research is based on an assumption that the coefficient of secondary compression is constant. However, this parameter is dependent on many factors, particularly the applied stress. Therefore, application of a non linear coefficient of secondary compression promises to provide more accurate prediction and reflect the reality.
- Initial volumetric strain rate $\dot{\upsilon}_0$ (the strain rate at the end of primary consolidation) is believed to have a clear physical meaning like the well-known coefficient of secondary compression, C_α. In this research the value of $\dot{\upsilon}_0$ is determined based on an expression proposed by Sekiguchi [57] relevant to C_α and time at the end of the primary consolidation. A further research to understand thoroughly this key parameter can facilitate the determination of creep parameter of this model and can support the model for better prediction of the rheological behaviour of soft natural clay.
- The current work assumes the flow surface to be circular shape in the deviatoric plane. This results in a model independent of the Lodge angle and parameter M is constant. However, the importance of Lodge angle dependency need to be considered so that more accuracy can be achieved in numerical analysis.

- The proposed model has been verified against various standard laboratory tests. To solve a practical geotechnical problem, the numerical solutions to the model are required to be further improved to enable the proposed model to integrate with the finite element analysis software to analyse practical geotechnical problems.

REFERENCES

[1] L. Bjerrum, “Engineering Geology of normally-consolidated Norwegian Marine Clays as related so settlement of buildings,” *Geotechnique*, vol. 17, pp. 81–118, 1967.

[2] S. Leroueil, M. Kabbaj, F. Tavenas, and R. Bouchard, “Stress–strain–strain rate relation for the compressibility of sensitive natural clays,” *Géotechnique*, vol. 35, no. 2, pp. 159–180, 1985.

[3] Y. Qiao, A. Ferrari, L. Laloui, and W. Ding, “Nonstationary flow surface theory for modeling the viscoplastic behaviors of soils,” *Comput. Geotech.*, vol. 76, pp. 105–119, 2016.

[4] W. Huang, S. Fityus, D. Bishop, D. Smith, and D. Sheng, “Finite-element parametric study of the consolidation behavior of a trial embankment on soft clay,” *Int. J. Geomech.*, vol. 6, no. 5, pp. 328–341, 2006.

[5] R. Genevois and M. Ghirotti, “The 1963 Vaiont Landslide,” *G. di Geol. Appl.*, vol. 1, pp. 41–52, 2005.

[6] A. S. Buisman, “Results of long duration settlement tests,” in *International Conference on Soil Mechanics and Foundation Engineering*, 1936, pp. 103–107.

[7] L. Suklje, “The analysis of the consolidation process by the isotaches method,” *Proceedings of the 4th International Conference on soil mechanics and foundation engineering*. pp. 201–206, 1957.

[8] P. Perzyna, “Fundamental problems in viscoplasticity,” *Adv. Appl. Mech.*, vol. 9, pp. 243–377, 1966.

[9] W. Olszak and P. Perzyna, “The constitutive equations of the flow theory for a non-stationary yield condition,” *Proceding Int. Congr. Appl. Mech. 11th*, vol. 11th, pp. 545–553, 1964.

[10] P. Olszak, W., and Perzyna, *Stationary and nonstationary viscoplasticity*. McGraw Hill Book Co., 1969.

[11] K. H. Roscoe and A. Schofield, “Mechanical behaviour of an idealized’wet’clay,” in *Proc. 3rd European Conference on Soil Mechanics and Foundation Engineering*, 1963, pp. 47–54.

[12] S. J. Wheeler, A. Näätänen, M. Karstunen, and M. Lojander, “An anisotropic elastoplastic model for soft clays,” *Can. Geotech. J.*, vol. 40, no. 2, pp. 403–418, Apr. 2003.

[13] M. Koskinen, M. Karstunen, and S. J. Wheeler, “Modelling destructuration and anisotropy of a natural soft clay,” in *European Conf. Numerical Methods in Geotechnical Engineering*, 2002, pp. 11–20.

[14] M. Taiebat, Y. F. Dafalias, and R. Peek, “A destructuration theory and its application to SANICLAY model,” *Int. J. Numer. Anal. Methods Geomech.*, vol. 34, no. 10, pp. 1009–1040, 2010.

[15] A. Singh and J. K. Mitchell, “CREEP POTENTIAL AND CREEP RUPTURE

OF SOILS," in *Soil Mech & Fdn Eng Conf Proc /Mexico/*, 1969, pp. 379–384.

[16] H. Sekiguchi, "Rheological characteristics of clays," in *Proc. of 9th International Conf. on Soil Mech. and Foundation Eng., Tokyo, 1977*, 1977, vol. 1, pp. 289–292.

[17] T. Adachi and F. Oka, "Constitutive equations for normally consolidated clay based on elasto-viscoplasticity," *Japanese Soc. Soil Mech. Found. Eng.*, vol. 22, no. 4, 1982.

[18] T. Matsui and N. Abe, "Elasto/viscoplastic constitutive equation of normally consolidated clays based on flow surface theory," *11th Int. Conf. Numer. methods Geomech.*, pp. 407–413, 1985.

[19] N. Sathialingam and B. L. Kutter, "Elastic-viscoplastic modelling of the rate-dependent behaviour of clays," *Géotechnique*, vol. 42, no. 3, pp. 427–441, 1992.

[20] J. Yin and J. Graham, "Elastic viscoplastic modelling of the time- dependent stress – strain behaviour of soils," vol. 745, pp. 736–745, 1999.

[21] Z. Y. Yin, C. S. Chang, M. Karstunen, and P. Y. Hicher, "An anisotropic elastic-viscoplastic model for soft clays," *Int. J. Solids Struct.*, vol. 47, no. 5, pp. 665–677, 2010.

[22] C. Zhou, J.-H. Yin, J.-G. Zhu, and C.-M. Cheng, "Elastic Anisotropic Viscoplastic Modeling of the Strain-Rate-Dependent Stress–Strain Behavior of -Consolidated Natural Marine Clays in Triaxial Shear Tests," *Int. J. Geomech.*, vol. 5, no. 3, pp. 218–232, 2005.

[23] J. B. Burland, "On the compressibility and shear strength of natural clays," *Géotechnique*, vol. 40, no. 3, pp. 329–378, 1990.

[24] S. Leroueil and P. R. Vaughan, "The general and congruent effects of structure in soils and weak rocks," *Geotechnique*, vol. 40, no. 3, pp. 467–488, 1990.

[25] E. W. Brand and R. P. Brenner, *Soft clay engineering*, vol. 20. Elsevier, 1981.

[26] B. B. Broms, "Stabilization of soft clay in Southeast Asia," in *5th Int. Geotech. Seminar on case histories of soft clay*, 1987, pp. 163–198.

[27] P. Vermeer and H. Neher, "A soft soil model that accounts for creep," *Proc. Int. …*, pp. 1–13, 1999.

[28] J. Feda, *Creep of Soils: and Related Phenomena*, vol. 68. Elsevier, 1992.

[29] J. K. Mitchell, K. Soga, and J. Wiley, *Fundamental of soil behaviour*. 2005.

[30] M. R. Coop, J. H. Atkinson, and T. R.N., "Strength, yielding and stiffness of structured and unstructured soils," *Proc. 11th ECSMFE, Copenhagen 1*, pp. 55–62, 1995.

[31] R. F. Craig, *Craig's soil mechanics*. CRC press, 2004.

[32] R. F. Craig, *Craig's Soil Mechanics, Seventh Edition*. 2004.

[33] N. Cruz, "Interactions of clay minerals and their effects on copper-gold flotation," 2016.

[34] Y. Wang, Y. Peng, T. Nicholson, and R. A. Lauten, "The role of cations in copper flotation in the presence of bentonite," *Miner. Eng.*, vol. 96, pp. 108–

112, 2016.

[35] H. H. Murray, “Applied clay mineralogy today and tomorrow,” *Clay Miner.*, vol. 34, no. 1, pp. 39–49, 1999.

[36] Z. Adamis and R. B. Williams, “Bentonite, kaolin and selected clay minerals,” 2005.

[37] J. Wilson, L. Wilson, and I. Patey, “The influence of individual clay minerals on formation damage of reservoir sandstones: A critical review with some new insights,” *Clay Miner.*, vol. 49, May 2014.

[38] R. E. Grim, R. H. Bray, and W. F. Bradley, “The mica in argillaceous sediments,” *Am. Mineral. J. Earth Planet. Mater.*, vol. 22, no. 7, pp. 813–829, 1937.

[39] H. E. Gaudette, J. L. Eades, and R. E. Grim, “The nature of illite,” *Clays Clay Miner.*, vol. 13, no. 1, pp. 33–48, 1964.

[40] V. N. S. Murthy, “Principles and practices of soil mechanics and foundation engineering,” *New York Marcek Decker INC*, 2002.

[41] A. F. Gualtieri *et al.*, “Structural characterization of the clay mineral illite-1M,” *J. Appl. Crystallogr.*, vol. 41, no. 2, pp. 402–415, 2008.

[42] R. E. Grim and F. L. Cuthbert, “The bonding action of clays. Part I: Clays in green molding sands,” *Rep. Investig. no. 102*, 1945.

[43] B. Menezes, W. Cortez-Vega, and C. Prentice, “Nanocomposites films obtained from protein isolates of mechanically deboned chicken meat added with montmorillonite,” *Polímeros*, vol. 27, pp. 75–82, Mar. 2017.

[44] G. Imai, “Settling behavior of clay suspension,” *Soils Found.*, vol. 20, no. 2, pp. 61–77, 1980.

[45] A. Sridharan and K. Prakash, “Settling behaviour and clay mineralogy,” *Soils Found.*, vol. 41, no. 2, pp. 105–109, 2001.

[46] R. H. Bennett and M. H. Hulbert, *Clay Microstructure*. International Human Resources Development Corporation, 1986.

[47] H. Cetin, “Soil-particle and pore orientations during consolidation of cohesive soils,” *Eng. Geol.*, vol. 73, no. 1–2, pp. 1–11, 2004.

[48] A. Prashant and D. Penumadu, “Effect of microfabric on mechanical behavior of kaolin clay using cubical true triaxial testing,” *J. Geotech. geoenvironmental Eng.*, vol. 133, no. 4, pp. 433–444, 2007.

[49] R. J. Pillai, R. G. Robinson, and A. Boominathan, “Effect of microfabric on undrained static and cyclic behavior of kaolin clay,” *J. Geotech. Geoenvironmental Eng.*, vol. 137, no. 4, pp. 421–429, 2010.

[50] A. Casagrande and N. Carillo, “Shear failure of anisotropic materials,” in *Boston scociety of Civil Engineering*, 1944, pp. 74–87.

[51] V. Jovičić and M. P. Coop, “The measurement of stiffness anisotropy in clays with bender element tests in the triaxial apparatus,” *Geotech. Test. J.*, vol. 21, no. 1, pp. 3–10, 1998.

[52] A. Udias and E. Buforn, *Principles of seismology*. Cambridge University Press,

2017.

[53] L. Zdravkovic and D. M. Potts, “Advances in modelling soil anisotropy,” in *Constitutive Modelling of Granular Materials*, 1999, pp. 491–521.

[54] S. J. Wheeler, A. Naatanen, M. Karstunen, and M. Lojander, “An anisotropic elastoplastic model for soft clays,” *Can. Geotech. J.*, vol. 40, no. 2, pp. 403–418, 2003.

[55] Y. F. Dafalias, “Anisotropic critical state soil,” *Mech. Res. Commun.*, vol. 13, no. 6, pp. 341–347, 1986.

[56] Y. F. Dafalias, M. T. Manzari, and A. G. Papadimitriou, “SANICLAY: Simple anisotropic clay plasticity model,” *Int. J. Numer. Anal. Methods Geomech.*, vol. 30, pp. 1231–1257, 2006.

[57] H. Sekiguchi and H. Ohta, “Induced anisotropy and time dependency in clays,” *Proc. 9th I.C.S.M.F.E. Spec. Sess. 9*, pp. 229–238, 1977.

[58] N. Sivasithamparam and M. Rezania, “The comparison of modelling inherent and evolving anisotropy on the behaviour of a full-scale embankment,” *Int. J. Geotech. Eng.*, vol. 11, no. 4, pp. 343–354, 2017.

[59] F. E. Wang, *Bonding theory for metals and alloys*. Elsevier, 2018.

[60] N. J. Pienta, “Chemistry: Molecules, Matter, and Change.” ACS Publications, 2001.

[61] M. Leroueil, S., Tavenas, F., Brucy, F., La Rochelle, P. & Roy, “Behaviour of destructured natural clays,” *J. Geotech. Eng. Div. ASCE*, vol. 105, no. 6, pp. 759–778, 1979.

[62] M. Taiebat, Y. F. Dafalias, and R. Peek, “A destructuration theory and its application to SANICLAY model,” *Int. J. Numer. Anal. Methods Geomech.*, vol. 34, no. 10, pp. 1009–1040, 2010.

[63] R. J. Mitchell, “On the yielding and mechanical strength of Leda clays,” *Can. Geotech. J.*, vol. 7, no. 3, pp. 297–312, 1970.

[64] L. Callisto and G. Calabresi, “Mechanical behaviour of a natural soft clay,” *Géotechnique*, vol. 48, no. 4, pp. 495–513, 1998.

[65] J. B. Burland, S. Rampello, V. N. Georgiannou, and G. Calabresi, “A laboratory study of the strength of four stiff clays,” *Géotechnique*, vol. 46, no. 3, pp. 491–514, 1996.

[66] S. Rampello, V. N. Georgiannou, and G. Viggiani, “Strength and dilatancy of natural and reconstituted Vallericca clay,” in *Proc. Int. Symp. on Hard Soils–Soft Rocks, Athens*, 1993, vol. 1, pp. 761–768.

[67] F. Cotecchia and R. J. Chandler, “A general framework for the mechanical behaviour of clays,” *Géotechnique*, vol. 50, no. 4, pp. 431–448, 2000.

[68] P. R. Smith, R. J. Jardine, and D. W. Hight, “The yielding of Bothkennar clay,” *Géotechnique*, vol. 42, no. 2, pp. 257–274, 1992.

[69] C. B. Crawford and K. I. Morrison, “Case histories illustrate the importance of secondary-type consolidation settlements in the Fraser River delta,” *Can. Geotech. J.*, vol. 33, no. 6, pp. 866–878, 1997.

[70] A. Komornik, G. Wiseman, and J. G. Zeitlen, “Building settlement on end-bearing driven piles,” in *Performance of Earth and Earth-Supported Structures*, 1972, p. 1135.

[71] G. Hannink, “Settlement of high-rise buildings in Rotterdam,” in *International conference on soil mechanics and foundation engineering*, 1994, pp. 441–444.

[72] C. F. Leung, F. H. Lee, and N. S. Yet, “The role of particle breakage in pile creep in sand,” *Can. Geotech. J.*, vol. 33, no. 6, pp. 888–898, 1997.

[73] B. Indraratna, C. Rujikiatkamjorn, R. Kelly, and H. Buys, “Soft soil foundation improved by vacuum and surcharge preloading at Ballina Bypass, Australia,” 2009.

[74] J. D. McIlquham, “GEOTECHNICAL DESIGN OF TRANSITION STRUCTURES FOR THE PORT BOTANY EXPANSION1.”

[75] J. Ameratunga, P. Boyle, C. De Bok, and C. Bamunawita, “Port of Brisbane (PoB) clay characteristics and use of wick drains to improve deep soft clay deposits,” in *Proceedings 17th Asian Geotechnical Conference, Taipei*, 2010, vol. 1, pp. 116–119.

[76] M. C. Ervin, “Engineering properties of Quaternary age sediments of the Yarra Delta,” in *Engineering geology of Melbourne*, Routledge, 2018, pp. 245–259.

[77] M. Ltifi, T. Abichou, and J. P. Tisot, “Effects of Soil Aging on Mechanical and Hydraulic Properties of a Silty Soil,” *Geotech. Geol. Eng.*, vol. 32, no. 4, pp. 1101–1108, 2014.

[78] J. K. Mitchell, “Fundamental aspects of thixotropy in soils,” *Trans. Am. Soc. Civ. Eng.*, vol. 126, no. 1, pp. 1586–1620, 1961.

[79] J. K. Mitchell, “Practical problems from surprising soil behaviour,” *J. Geotech. Engrg.*, vol. 112, no. 3, pp. 259–289, 1986.

[80] G. Leonards and B. Ramiah, “Time effects in the consolidation of clays,” in *Papers on Soils 1959 Meetings*, 1960.

[81] G. A. Leonards and A. G. Altschaeffl, “Compressibility of clay,” *J. Soil Mech. Found. Div.*, vol. 90, no. 5, pp. 133–156, 1964.

[82] L. Zeevaert, “An investigation of the engineering characteristics of the volcanic lacustrine clay deposits beneath Mexico City,” *Ph. D. thesis, Univ. Illinois Urbana-Champaign*, 1949.

[83] J. H. Schmertmann, “A simple question about consolidation,” *J. Geotech. Eng.*, vol. 109, no. 1, pp. 119–122, 1983.

[84] J. H. Schmertmann, “Discussion of ‘Time-dependent strength gain in freshly deposited or densified sand’ by James K. Mitchell and Zoltan V. Solymar (November, 1984),” *J. Geotech. Eng.*, vol. 113, no. 2, pp. 173–175, 1987.

[85] J. H. Schmertmann, “The mechanical aging of soils,” *J. Geotech. Eng.*, vol. 117, no. 9, pp. 1288–1330, 1991.

[86] J. H. Schmertmann, “Update on the mechanical aging of soils,” in *for the symposium “Sobre Envejecimiento de Suelos,” The Mexican Society of Soil Mechanics, Mexico City*, 1993.

[87] R. C. Graham and S. W. Buol, “Soil-geomorphic relations on the Blue Ridge

Front: II. Soil characteristics and pedogenesis," *Soil Sci. Soc. Am. J.*, vol. 54, no. 5, pp. 1367–1377, 1990.

[88] D. F. T. Nash, J. J. M. Powell, and I. M. Llyod, "Discussion: Initial investigation of the soft clay test site at Bothkennar," *Géotechnique*, vol. 43, no. 3, pp. 503–504, 1993.

[89] R. J. Dunn and J. K. Mitchell, "Fluid conductivity testing of fine-grained soils," *J. Geotech. Eng.*, vol. 110, no. 11, pp. 1648–1665, 1984.

[90] J. K. Mitchell, D. R. Hooper, and R. G. Campenella, "Permeability of compacted clay," *J. Soil Mech. Found. Div.*, vol. 91, no. 4, pp. 41–66, 1965.

[91] S. Leroueil, M. Kabbaj, F. Tavenas, and R. Bouchard, "Stress–strain–strain-rate relation for thecompressibility of sensitive natural clays," *Geotechnique*, vol. 35, no. 2, pp. 159–180, 1985.

[92] S. Leroueil, M. Kabbaj, R. Bouchard, and F. Tavenas, "Discussion: Stress—strain—strain rate relation for the compressibility of sensitive natural clays," *Géotechnique*, vol. 36, no. 2, pp. 283–290, 1986.

[93] R. Jia, J.-C. Chai, T. Hino, and Z.-S. Hong, "Strain-rate effect on consolidation behaviour of Ariake clay," *Proc. Inst. Civ. Eng. Eng.*, vol. 163, no. 5, pp. 267–277, 2010.

[94] Y. P. Vaid and R. G. Campanella, "Time-dependent behaviour of undisturbed clay," *J. Geotech. Eng.*, vol. 103, no. 7, pp. 693–709, 1977.

[95] D. W. Armour and V. P. Drnevich, "Improved techniques for the constant-rate-of-strain consolidation test," in *Consolidation of Soils: Testing and Evaluation*, ASTM International, 1986.

[96] C. B. Crawford, "Interpretation of the consolidation test," *J. Soil Mech. Found. Div*, vol. 90, no. Proceeding Paper Pt 1, 1964.

[97] C. T. Gorman, T. C. Hopkins, R. C. Deen, and V. P. Drnevich, "Constant-rate-of-strain and controlled-gradient consolidation testing," *Geotech. Test. J.*, vol. 1, no. 1, pp. 3–15, 1978.

[98] R. E. Smith and H. E. Wahls, "Consolidation under constant rates of strain," *J. Soil Mech. Found. Div*, 1969.

[99] G. Mesri and T.-W. Feng, "Constant rate of strain consolidation testing of soft clays and fibrous peats," *Can. Geotech. J.*, vol. 56, no. 10, pp. 1526–1533, 2018.

[100] G. Sandbaekken, T. Berre, and S. Lacasse, "Oedometer testing at the Norwegian Geotechnical Institute," in *Consolidation of soils: Testing and evaluation*, ASTM International, 1986.

[101] S. Leroueil, "The isotache approach. Where are we 50 years after its development by Professor Šuklje? (2006 Prof. Šuklje's Memorial Lecture)," in *Ljubljana Slovenia*, 2006, pp. 55–88.

[102] A. M. Richardson and R. V. Whitman, "Effect of the strain rate upon undrained shear resistence of a saturated remoulded fat clay," *Geotechnique*, vol. 13, no. 3, pp. 310–324, 1963.

[103] K. Y. Lo and J. P. Morin, "Strength anisotropy and time effects of two sensitive clays," *Can. Geotech. J.*, vol. 9, no. 3, pp. 261–277, 1972.

[104] O. B. Andersland and A. G. Douglas, “Soil deformation rates and activation energies,” *Geotechnique*, vol. 20, no. 1, pp. 1–16, 1970.

[105] D. W. Taylor and W. Merchant, “A theory of clay consolidation accounting for secondary compression,” *J. Math. Phys.*, vol. 19, no. 1–4, pp. 167–185, 1940.

[106] G. Mesri, “Coefficient of secondary compression.,” *ASCE J Soil Mech Found Div-v 99*, no. SM1, pp. 123–137, 1973.

[107] T. M. Le, B. Fatahi, and H. Khabbaz, “Viscous behaviour of soft clay and inducing factors,” *Geotech. Geol. Eng.*, vol. 30, no. 5, pp. 1069–1083, 2012.

[108] Mesri G, “Coefficient of secondary compression,” *J. Soil. Mech. Div. ASCE*, 1973.

[109] K. Terzaghi, *Undisturbed clay samples and undisturbed clays*. Harvard University, 1941.

[110] S. Murayama and T. Shibata, “Rheological properties of clays,” in *Proceedings*, 1961, pp. 269–273.

[111] R. W. Christensen and T. H. Wu, “Analysis of clay deformation as a rate process,” *J. Soil Mech. Found. Div.*, vol. 90, no. 6, pp. 125–160, 1964.

[112] J. K. Mitchell, “Shearing resistance of soils as a rate process,” *J. Soil Mech. Found. Div*, vol. 90, no. Proc. Paper 3773, 1964.

[113] C.-Y. Kwok and M. D. Bolton, “DEM simulations of thermally activated creep in soils,” *Géotechnique*, vol. 60, no. 6, pp. 425–433, 2010.

[114] M. R. Kuhn and J. K. Mitchell, “New perspectives on soil creep,” *J. Geotech. Eng.*, vol. 119, no. 3, pp. 507–524, 1993.

[115] P. F. Low, “Influence of adsorbed water on exchangeable ion movement,” *Clays Clay Miner.*, vol. 9, no. 1, pp. 219–228, 1960.

[116] J. K. Mitchell, R. G. Campanella, and A. Singh, “Soil creep as a rate process,” *J. Soil Mech. Found. Div*, 1968.

[117] R. E. Grim, “Applied clay mineralogy,” 1962.

[118] P. L. Berry and T. J. Poskitt, “The consolidation of peat,” *Geotechnique*, vol. 22, no. 1, pp. 27–52, 1972.

[119] V. Navarro and E. E. Alonso, “Secondary compression of clays as a local dehydration process,” *Géotechnique*, vol. 51, no. 10, pp. 859–869, 2001.

[120] Y. H. Wang and D. Xu, “Dual porosity and secondary consolidation,” *J. Geotech. geoenvironmental Eng.*, vol. 133, no. 7, pp. 793–801, 2007.

[121] L. Zeevaert, “Consolidation in the intergranular viscosity of highly compressible soils,” in *Consolidation of soils: testing and evaluation*, ASTM International, 1986.

[122] H. Akagi, “A physico-chemical approach to the consolidation mechanism of soft clays,” *Soils Found.*, vol. 34, no. 4, pp. 43–50, 1994.

[123] L. Barden, “Time dependent deformation of normally consolidated clays and peats,” *J. Soil Mech. Found. Div*, 1969.

[124] L. Bjerrum, “Engineering geology of norwegian normally consolidated marine clays as related to settlements of buildings,” *Geotechnique*, vol. 17, no. 2, pp.

81–118, 1967.

[125] I. F. Christie, “Developments in the time lines theory of consolidation,” in *Proc. 11th Int. Conf. SMFE*, 1985, vol. 2, pp. 423–426.

[126] J.-H. Yin, J.-G. Zhu, and J. Graham, “A new elastic viscoplastic model for time-dependent behaviour of normally and overconsolidated clays: theory and verification,” *Can. Geotech. J.*, vol. 39, no. 1, pp. 157–173, 2002.

[127] J. E. Garlanger, “The consolidation of soils exhibiting creep under constant effective stress,” *Geotechnique*, vol. 22, no. 1, pp. 71–78, 1972.

[128] N. Guven, “Molecular aspects of clay-water interactions,” *Clay-water interface its Rheol. Implic.*, pp. 2–79, 1992.

[129] H. F. Winterkorn, “The condition of water in porous systems,” *Soil Sci.*, vol. 56, no. 2, pp. 109–116, 1943.

[130] J. H. Yin, “Calculation of settlements of foundation soils considering creep,” in *soft ground engineering in coastal areas: proceedings of The Nakase memorial symposium*, 2003, pp. 205–211.

[131] N. Abe, “Elasto-viscoplastic model of clays including creep rupture criteria,” *Proc. 8th ARC*, vol. 1, pp. 1–4, 1987.

[132] H. Sekiguchi, “Theory of Undranied Creep rupture of nomarlly consolidated clay based on Elasto Viscoplasticity,” *Japanese Soc. Soil Mech. Found. Eng.*, vol. 24, no. 1, pp. 129–147, 1984.

[133] W. D. L. Finn, “Creep and creep rupture of undisturbed sensitive clay,” in *Proceedings of the 8th ICSMFE*, 1973, vol. 1, pp. 135–142.

[134] A. Singh and J. K. Mitchell, “CLOSURE OF GENERAL STRESS-STRAIN-TIME FUNCTION FOR SOILS,” *J. Soil Mech. Found. Div*, 1969.

[135] M. Saito, “Failure of soil due to creep,” in *Proc. 5th Int. Conf. on SMFE*, 1961, pp. 315–318.

[136] M. Saito, “Forecasting the time of occurrence of a slope failure.,” in *Proc. 6 th Int. Conf. Soil Mechanics and Foundation Eng.*, 1965, pp. 537–541.

[137] M. Saito, “Forecasting time of slope failure by tertiary creep,” in *Proc. 7th Int. Conf on Soil Mechanics and Foundation Engineering, Mexico City*, 1969, vol. 2, pp. 677–683.

[138] D. W. Taylor, *Fundamental of soil mechanics*. 1948.

[139] L. Šuklje, “The analysis of the consolidation process by the isotache method,” in *Proceedings of the 4th International Conference on Soil Mechanics and Foundation Engineering, London*, 1957, vol. 1, pp. 200–206.

[140] J.-H. Yin, “Non-linear creep of soils in oedometer tests,” *Géotechnique*, vol. 49, no. 5, pp. 699–707, 1999.

[141] M. R. Karim, “Modeling the long term behaviour of soft soils,” *Sch. Eng. Inf. Technol.*, vol. PhD, 2011.

[142] G. Mesri and P. M. Godlewski, “Time and stress-compressibility interre-lationship,” *Porc. ASCE*, no. 103, pp. 417–430, 1977.

[143] M. Liingaard, A. Augustesen, and P. V. Lade, “Characterization of Models for

Time-Dependent Behavior of Soils," *Int. J. Geomech.*, vol. 4, no. September, pp. 157–177, 2004.

[144] S. D. Hinchberger and R. K. Rowe, "Evaluation of the predictive ability of two elastic-viscoplastic constitutive models," *Can. Geotech. J.*, vol. 42, no. 6, pp. 1675–1694, 2005.

[145] T. ADACHI and M. OKANO, "A constitutive equation for normally consolidated clay," *Soils Found.*, vol. 14, no. 4, pp. 55–73, 1974.

[146] A. Fodil, W. Aloulou, and P. Y. Hicher, "Viscoplastic behaviour of soft clay," *Géotechnique*, vol. 47, no. 3, pp. 581–591, 1997.

[147] J.-H. Yin and J. Graham, "Viscous–elastic–plastic modelling of one-dimensional time-dependent behaviour of clays," *Can. Geotech. J.*, vol. 26, no. 2, pp. 199–209, 1989.

[148] M. Leoni *et al.*, "Anisotropic creep model for soft soils," *Geotech. 58*, no. 3, pp. 215–226, 2008.

[149] F. Oka, "Prediction of time dependent behavior of clay," in *Proc. 10th Int. Conf. on SMFE, Stockholm*, 1981, vol. 1, pp. 215–218.

[150] T. ADACHI and F. OKA, "Constitutive equations for normally consolidated clay based on elasto-viscoplasticity," *Soils Found.*, vol. 22, no. 4, pp. 57–70, 1982.

[151] T. ADACHI, F. Oka, and M. Mimura, "Mathematical structure of an overstress elasto-viscoplastic model for clay," *Soils Found.*, vol. 27, no. 3, pp. 31–42, 1987.

[152] T. Adachi, "Modelling aspects associated with time dependent behavior of soils," *Meas. Model. Time Depend. Soil Behav. ASCE STP*, vol. 61, pp. 61–95, 1997.

[153] M. G. Katona, "Evaluation of Viscoplastic Cap Model," *J. Geotech. Eng.*, vol. 110, no. 8, pp. 1106–1125, 1984.

[154] M. G. Katona and M. A. Mulert, *A viscoplastic cap model for soils and rock*. Wiley, 1984.

[155] Z. Y. Yin and M. Karstunen, "Modelling strain-rate-dependency of natural soft clays combined with anisotropy and destructuration," *Acta Mech. Solida Sin.*, vol. 24, no. 3, pp. 216–230, 2011.

[156] M. Rezania, M. Taiebat, and E. Poletti, "A viscoplastic SANICLAY model for natural soft soils," *Comput. Geotech.*, vol. 73, pp. 128–141, 2016.

[157] F. Oka, "Elasto/viscoplastic constitutive equations with memory and internal variables," *Comput. Geotech.*, vol. 1, no. 1, pp. 59–69, 1985.

[158] M. Mimura and H. Sekiguchi, "A review of existing viscoplastic constitutive models regarding the performance of creep rupture prediction," in *Proc., 40th Japan Nat. Conf., JSCE*, 1985, pp. 1097–1100.

[159] T. Adachi, "An elasto-viscoplastic theory for clay failure," in *Proc. 8th Asian Regional Conf., SMFE, 1987*, 1987, vol. 1, pp. 5–8.

[160] M. Rezania, H. Nguyen, H. Zanganeh, and M. Taiebat, "Numerical analysis of Ballina test embankment on a soft structured clay foundation," *Comput.*

Geotech., vol. 93, pp. 61–74, 2018.

[161] H. Sekiguchi and H. Ohta, "Induced Anisotropy and time dependancy in clays," *9th ICSMFE*, pp. 163–175, 1977.

[162] Y. F. Dafalias and M. Taiebat, "Anatomy of rotational hardening in clay plasticity," *Geotechnique*, vol. 63, no. 16, pp. 1406–1418, 2013.

[163] S. A. Naghdi, P. M., and Mursh, "On the mechanical behaviour of viscoelastic/plastic solids," *J. Appl. Meteoroly*, vol. 30, pp. 321–328, 1963.

[164] O. M. Heeres, A. S. J. Suiker, and R. de Borst, "A comparison between the Perzyna viscoplastic model and the consistency viscoplastic model," *Eur. J. Mech.*, vol. 21, no. 1, pp. 1–12, 2002.

[165] W. M. Wang, L. J. Sluys, and R. De Borst, "Viscoplasticity for instabilities due to strain softening and strain-rate softening," *Int. J. Numer. Methods Eng.*, vol. 40, no. 20, pp. 3839–3864, 1997.

[166] H. Sekiguchi, "Macrometric Approaches Static Intrinsically Time Dependent," *Proc. Discussion Session ,11th ICSMFE, San Francisco , USA*, 1985. [Online]. Available: https://getinfo.de/app/Macrometric-Approaches-Static-Intrinsically-Time/id/BLCP%3ACN016929500. [Accessed: 19-Mar-2015].

[167] A. Gens and R. Nova, "Conceptual bases for a constitutive model for bonded soils and weak rocks," *Geotech. Eng. hard soils-soft rocks*, vol. 1, no. 1, pp. 485–494, 1993.

[168] K. McGinthy, M. Karstunen, and S. J. Wheeler, "Modelling destructuration and anisotropy of bothkennar clay," *Geotech. Soft Soils*, pp. 263–268, 2008.

[169] F. Tavenas, S. Leroueil, P. L. Rochelle, and M. Roy, "Creep behaviour of an undisturbed lightly overconsolidated clay," *Can. Geotech. J.*, vol. 15, no. 3, pp. 402–423, 1978.

[170] Z. Y. Yin and M. Karstunen, "Influence of anisotropy, destructuration and viscosity on the behavior of an embankment on soft clay," in *Proc., 12th Int. Conf. of Int. Association for Computer Methods and Advances in Geomechanics (IACMAG)*, 2008, pp. 4728–4735.

[171] W. Olszak and P. Perzyna, "Olszak-Perzyna 1964 - Constitutive equation of the flow theory for Non-stationary Yiel Condition.pdf," in *Proceedings of the international congress for applied mechanics*, 1964, pp. 545–553.

[172] K. Roscoe and J. B. Burland, "On the generalized stress-strain behaviour of wet clay," 1968.

[173] D. M. Wood, *Soil behaviour and critical state soil mechanics / David Muir Wood*. Cambridge: Cambridge : Cambridge University Press, 1990.

[174] D. C. Drucker, "A more fundamental approach to plastic stress-strain relations," *1st U.S National Congress on Applied Mechanics*. pp. 487–491, 1951.

[175] W. Olszak and P. Perzyna, "Stationary and nonstationary viscoplasticity," *Inelast. Behav. Solids*, pp. 53–75, 1970.

[176] G. Mesri and P. M. Godlewski, "Time and stress-compressibility interrelationship," *ASCE J Geotech Eng Div*, vol. 103, no. 5, pp. 417–430, 1977.

[177] R. I. Borja and E. Kavaznjian, "A constitutive model for the σ-ε-t behaviour of

wet clays," *Geotechnique*, vol. 35, pp. 283–298, 1985.

[178] P. Vermeer and H. Neher, "A soft soil model that accounts for creep," *Proc. Int. ...*, pp. 1–13, 1999.

[179] J. Graham, M. L. Noonan, and K. V Lew, "Yield states and stress–strain relationships in a natural plastic clay," *Can. Geotech. J.*, vol. 20, no. 3, pp. 502–516, 1983.

[180] K.-H. Korhonen and M. Lojander, "Yielding of Perno clay," in *International Conference on Constitu- tive Laws for Engineering Materials*, 1987, pp. 1249–1255.

[181] M. C. R. Davies and T. A. Newson, "A critical state constitutive model for anisotropic soil," in *Predictive soil mechanics: Proceedings of the Wroth Memorial Symposium held at St Catherine's College, Oxford, 27-29 July 1992*, 1992, pp. 219–229.

[182] A. J. Whittle and M. J. Kavvadas, "Formulation of MIT-E3 constitutive model for overconsolidated clays," *J. Geotech. Eng.*, vol. 120, no. 1, pp. 173–198, 1994.

[183] D. W. Taylor, *Fundamentals of soil mechanics*, vol. 66, no. 2. LWW, 1948.

[184] S. W. Sloan, "Substepping schemes for the numerical integration of elasto-plastic stress-strain relations," *Int. J. Numer. Methods Eng.*, vol. 24, no. 5, pp. 893–911, 1987.

[185] W. S. Sloan, J. A. Abbo, and D. Sheng, "Refined explicit integration of elastoplastic models with automatic error control," *Eng. Comput.*, vol. 18, no. 1, pp. 121–154, 2001.

[186] R. Brinkgreve, W. Broere, and D. Waterman, *PLAXIS Finite Element Code for Soil and Rock Analysis- 2D Version 9*. 2008.

[187] G. Rocchi, M. Fontana, and M. Da Prat, "Modelling of natural soft clay destruction processes using viscoplasticity theory," *Géotechnique*, vol. 53, no. 8, pp. 729–745, 2003.

[188] S. J. Wheeler, M. Cudny, H. P. Neher, and C. Wiltafsky, "Some developments in constitutive modelling of soft clays," in *Proceedings of the International Workshop on Geotechnics of Soft Soils-Theory and Practice, Noordwijkerhoud, the Netherlands*, 2003, pp. 17–19.

[189] S. D. Hinchberger and G. Qu, "Constitutive approach for rate-sensitive structured clays," *Can. Geotech. J.*, vol. 46, no. 6, pp. 609–626, 2009.

[190] S. Kimoto, F. Oka, and Y. Higo, "Strain localization analysis of elasto-viscoplastic soil considering structural degradation," *Comput. Methods Appl. Mech. Eng.*, vol. 193, no. 27–29, pp. 2845–2866, 2004.

[191] Z.-Y. Yin, M. Karstunen, C. S. Chang, M. Koskinen, and M. Lojander, "Modeling Time-Dependent Behavior of Soft Sensitive Clay," *J. Geotech. Geoenvironmental Eng.*, vol. 137, no. November, pp. 1103–1113, 2011.

[192] M. Karstunen and Z.-Y. Yin, "Modelling time-dependent behaviour of Murro test embankment," no. 10, pp. 735–749, 2010.

[193] H. F. Schweiger, F. Scharinger, C. Wiltafsky, and V. Galavi, "A multilaminate

framework for modelling induced and inherent anisotropy of soils," *Géotechnique*, vol. 59, no. 2, pp. 87–101, 2009.

[194] M. Karstunen, H. Krenn, S. J. Wheeler, M. Koskinen, and R. Zentar, "Effect of Anisotropy and Destructuration on the Behavior of Murro Test Embankment," *Int. J. Geomech.*, vol. 5, no. 2, pp. 87–97, Jun. 2005.

[195] R. Zentar, M. Karstunen, C. Wiltafsky, and H. F. Schweiger, "Comparison of two approaches for modelling anisotropy of soft clays," in *8th Interna- tional Symposium on Numerical Models in Geomechanics*, 2002, pp. 115–121.

[196] R. Zentar, M. Karstunen, and S. J. Wheeler, "Influence of anisotropy and destructuration on undrained shearing of natural clays," in *Proceedings of the 5th European Conference on Numerical Methods in Geotechnical Engineering*, 2002, pp. 21–26.

[197] Rangeard, D., 2002. *Identification des caractéristiques hydro-mécaniques d'une argile par analyse inverse d'essais pressiométriques* (Doctoral dissertation, Nantes).

[198] Nakase, Akio, and Takeshi Kamei. "Influence of strain rate on undrained shear characteristics of K0-consolidated cohesive soils." *Soils and Foundations* 26, no. 1 (1986): 85-95.

[199] Kamei T, Sakajo S. Evaluation of undrained shear behaviour of K0-consolidated cohesive soils using elasto-viscoplastic model. Computers and Geotechnics. 1995 Jan 1;17(3):397-417.

[200] Yin ZY, Karstunen M. Modelling strain-rate-dependency of natural soft clays combined with anisotropy and destructuration. Acta Mechanica Solida Sinica. 2011 Jun;24(3):216-30.

APPENDIX 1: NSFS-MCC model formulation in the general stress space

NSFS-MCC model is extended from the triaxial stress to the general stress space to address the general practical geotechnical problem. The formulation to the NSFS-MCC model in the general stress space is presented in the following sections.

- **Definition in general stress space**

The formulation to the NSFS-MCC model described in the triaxial stress space can be extended to the general stress space by using the following definitions:

$$\text{Stress vector } \bar{\sigma}'_{ij} \text{ is defined as } \bar{\sigma}'_{ij} = \begin{Bmatrix} \sigma'_{xx} \\ \sigma'_{yy} \\ \sigma'_{zz} \\ \tau'_{xy} \\ \tau'_{yz} \\ \tau'_{zx} \end{Bmatrix}$$

$$\text{Mean effective stress is defined as } p' = \frac{1}{3}\left(\sigma'_{xx} + \sigma'_{yy} + \sigma'_{zz}\right)$$

Deviatoric stress vector $\bar{\sigma}_d$ is defined as:

$$\bar{\sigma}_d = \begin{Bmatrix} \sigma'_{xx} - p' \\ \sigma'_{yy} - p' \\ \sigma'_{zz} - p' \\ \sqrt{2}.\tau'_{xy} \\ \sqrt{2}.\tau'_{yz} \\ \sqrt{2}.\tau'_{zx} \end{Bmatrix} = \begin{Bmatrix} \frac{1}{3}(2\sigma'_{xx} - \sigma'_{yy} - \sigma'_{zz}) \\ \frac{1}{3}(-\sigma'_{xx} + 2\sigma'_{yy} - \sigma'_{zz}) \\ \frac{1}{3}(-\sigma'_{xx} - \sigma'_{yy} + 2\sigma'_{zz} \\ \sqrt{2}.\tau'_{xy} \\ \sqrt{2}.\tau'_{yz} \\ \sqrt{2}.\tau'_{zx} \end{Bmatrix}$$

The scalar value of deviatoric stress q (used in the simplified version of the model for triaxial stress space) is defined by:

$$q^2 = \frac{3}{2}\{\bar{\sigma}_d\}^T\{\bar{\sigma}_d\}$$

$$\text{Strain vector } \bar{\varepsilon}_{ij} \text{ is defined as } \bar{\varepsilon}_{ij} = \begin{Bmatrix} \varepsilon_{xx} \\ \varepsilon_{yy} \\ \varepsilon_{zz} \\ \varepsilon_{xy} \\ \varepsilon_{yz} \\ \varepsilon_{zx} \end{Bmatrix}$$

Deviatoric strain increment vector $d\bar{\varepsilon}_d$ is defined as,

$$d\bar{\varepsilon}_d = \begin{Bmatrix} \frac{1}{3}(2d\varepsilon_{xx} - d\varepsilon_{yy} - d\varepsilon_{zz}) \\ \frac{1}{3}(-d\varepsilon_{xx} + 2d\varepsilon_{yy} - d\varepsilon_{zz}) \\ \frac{1}{3}(-d\varepsilon_{xx} - d\varepsilon_{yy} + 2d\varepsilon_{zz} \\ \sqrt{2}.d\varepsilon_{xy} \\ \sqrt{2}.d\varepsilon_{yz} \\ \sqrt{2}.d\varepsilon_{zx} \end{Bmatrix}$$

Volumetric strain increment $d\varepsilon_v$ is defined as:

$$d\varepsilon_v = d\varepsilon_{xx} + d\varepsilon_{yy} + d\varepsilon_{zz}$$

The scalar value of deviatoric strain increment $d\varepsilon_d^2$ is defined by:

$$d\varepsilon_d^2 = \frac{2}{3}\{d\bar{\varepsilon}_d\}^T\{d\bar{\varepsilon}_d\}$$

- **Elastic part of the model**

According to NSFS theory [9], when the flow surface F has a negative value (F<0) the predicted behaviour of soil is purely elastic. The elastic bulk modulus K' and elastic shear modulus G have the same definition as those of the MCC model:

$$K' = \frac{(1+e)p'}{\kappa}$$

$$G = \frac{3(1+e)p'}{2\kappa}\frac{1-2\nu}{1+\nu}$$

The elastic stiffness matrix can be expressed in terms of the elastic bulk modulus K' and elastic shear modulus G as follows (after [53], [173]),

$$[D^e] = \begin{bmatrix} 2G\frac{1-\nu'}{1-2\nu'} & 2G\frac{\nu'}{1-2\nu'} & 2G\frac{\nu'}{1-2\nu'} & 0 & 0 & 0 \\ 2G\frac{\nu'}{1-2\nu'} & 2G\frac{1-\nu'}{1-2\nu'} & 2G\frac{\nu'}{1-2\nu'} & 0 & 0 & 0 \\ 2G\frac{\nu'}{1-2\nu'} & 2G\frac{\nu'}{1-2\nu'} & 2G\frac{1-\nu'}{1-2\nu'} & 0 & 0 & 0 \\ 0 & 0 & 0 & G & 0 & 0 \\ 0 & 0 & 0 & 0 & G & 0 \\ 0 & 0 & 0 & 0 & 0 & G \end{bmatrix}$$

- **Flow surface**

The process for defining the proposed flow surface in general stress space is similar to that in the triaxial space. However, the equation of the flow surface is expressed in the form associated with the general stress. The flow surface in NSFS-MCC model in the general stress space is proposed as:

$$F(\bar{\sigma}'_{ij}, \bar{\varepsilon}'_{ij}, t) = \mu ln\left(\frac{\dot{v}_0 t}{\mu} e^{\left(\frac{f}{\mu}\right)} + 1\right) - \varepsilon_v = 0 \qquad [A1.1]$$

where f is a scaler function of stress state defined as:

$$f = \frac{\lambda - \kappa}{1 + e_0} ln\left(\frac{p'}{p'_0}\right) + \frac{\lambda - \kappa}{1 + e_0} ln\left(1 + \frac{{}^{3}/_{2}\{\bar{\sigma}_d\}^T\{\bar{\sigma}_d\}}{M^2 p'^2}\right)$$

The flow surface is assumed as a circular shape in the deviatoric plane. This results in the independence of the Lodge angle and parameter M is constant.

- **Flow rule**

An associated flow rule is assumed for the NSFS-MCC model in the general stress space, leading to the plastic potential (G) and non-stationary yield surface (F) which are identical. The flow rule is mathematically expressed as follows:

$$\dot{\varepsilon}_{ij}^{vp} = \langle\dot{\lambda}\rangle \frac{\partial G}{\partial \bar{\sigma}'_{ij}} = \langle\dot{\lambda}\rangle \frac{\partial F}{\partial \bar{\sigma}'_{ij}} \; or \; d\bar{\varepsilon}_{ij}^{vp} = \langle d\lambda\rangle \frac{\partial F}{\partial \bar{\sigma}'_{ij}} \qquad [A1.2]$$

where $\langle d\lambda\rangle$ is a non-negative viscoplastic multiplier, if $d\lambda$ is negative, $\langle d\lambda\rangle$ is taken as zero.

- **Stress-strain-time relation**

Following the NSFS theory, when the stress state reaches the yield surface, the viscoplastic behaviour is initiated and is continuous. The stress state is not allowed to be located outside of the yield surface in order to satisfy the consistency condition. This is expressed in formulation as,

$$F = F + \frac{\partial F}{\partial t} dt = 0 \qquad [A1.3]$$

$$or \; \frac{\partial F}{\partial \bar{\sigma}'_{ij}} \dot{\sigma}'_{ij} dt + \frac{\partial F}{\partial \bar{\varepsilon}_{ij}^{vp}} \dot{\varepsilon}'_{ij} dt + \frac{\partial F}{\partial t} dt = 0$$

$$\Leftrightarrow \frac{\partial F}{\partial \bar{\sigma}'_{ij}} d\bar{\sigma}_{ij} + \frac{\partial F}{\partial \bar{\varepsilon}_{ij}^{vp}} d\bar{\varepsilon}_{ij} + \frac{\partial F}{\partial t} dt = 0 \qquad [A1.4]$$

where $d\bar{\sigma}_{ij}$ and $d\bar{\varepsilon}_{ij}$ are the stress increment vector and strain increment vector respectively.

Subtituting [] into [], the viscoplastic multiplier can be derived in relation to the stress increment as:

$$\langle d\lambda \rangle = -\frac{\frac{\partial F}{\partial \bar{\sigma}'_{ij}} d\bar{\sigma}'_{ij} + \frac{\partial F}{\partial t} dt}{\frac{\partial F}{\partial \bar{\varepsilon}^{vp}_{ij}} \frac{\partial F}{\partial \bar{\sigma}'_{ij}}} \qquad [A1.5]$$

To find the viscoplastic multiplier in relation to the strain increment, subtituting $d\bar{\sigma}'_{ij} = [D^e](d\bar{\varepsilon}_{ij} - d\bar{\varepsilon}^{vp}_{ij})$ into [] and doing some manipulations, it yields the definition of the viscoplastic multiplier in relation to the strain increment as,

$$\langle d\lambda \rangle = -\frac{\frac{\partial F}{\partial \bar{\sigma}'_{ij}} \left[D^e_{ijkl}\right] d\bar{\varepsilon} + \frac{\partial F}{\partial t} dt}{-\frac{\partial F}{\partial \bar{\varepsilon}^{vp}_{ij}} \left[D^e_{ijkl}\right] \frac{\partial F}{\partial \bar{\sigma}'_{ij}} + \frac{\partial F}{\partial \bar{\varepsilon}^{vp}_{ij}} \frac{\partial F}{\partial \bar{\sigma}'_{ij}}} \qquad [A1.6]$$

with F the nonstationary flow surface as shown in [],

$$F = ln\left(\frac{\dot{v}_0 e^{\frac{f}{\mu}t}}{\mu} + 1\right) - \varepsilon_v = 0,$$

and f is a scalar function of stress state expressed as:

$$f = \frac{\lambda - \kappa}{1 + e_0} ln\left(\frac{p'}{p'_0}\right) + \frac{\lambda - \kappa}{1 + e_0} ln\left(1 + \frac{{}^3\!/_2 \{\bar{\sigma}_d\}^T \{\bar{\sigma}_d\}}{M^2 p'^2}\right)$$

Some auxiliary derivatives in [] can be defined as follows:

$$\frac{\partial F}{\partial \bar{\sigma}'_{ij}} = \left(1 - exp\left(-\frac{\varepsilon^{vp}_v}{\mu}\right)\right) \frac{\partial f}{\partial \bar{\sigma}'_{ij}} \qquad [A1.7]$$

$$\frac{\partial F}{\partial t} = \dot{v}_0 exp\left(\frac{f - \varepsilon^{vp}_v}{\mu}\right) \qquad [A1.8]$$

$$\frac{\partial F}{\partial \bar{\varepsilon}^{vp}_{ij}} = \frac{\partial F}{\partial \varepsilon^{vp}_v} = -1 \qquad [A1.9]$$

Following the equation [] and [], the viscoplastic multiplier is dependent on stress (strain) increment and time increment. This implies that the viscoplastic strain increment occurs even when the stress or strain is sustained. Hence the NSFS-MCC

model is capable of properly describing the creep behaviour and stress relaxation which are the time related phenomena of natural clays.

Combining [], [] and the conventional stress-strain increment relationship, $d\bar{\sigma}'_{ij} = [D^e](d\bar{\varepsilon}_{ij} - d\bar{\varepsilon}^{vp}_{ij})$, the complete constitutive stress-strain-time relationship in NSFS-MCC model is defined as follows:

$$d\bar{\sigma}'_{ij} = \left[D^e_{ijkl}\right]d\bar{\varepsilon}_{ij} - \left[D^e_{ijkl}\right]\left[-\frac{\frac{\partial F}{\partial \bar{\sigma}'_{ij}}\left[D^e_{ijkl}\right]d\bar{\varepsilon}_{ij} + \frac{\partial F}{\partial t}dt}{-\frac{\partial F}{\partial \bar{\varepsilon}^{vp}_{ij}}\left[D^e_{ijkl}\right]\frac{\partial F}{\partial \bar{\sigma}'_{ij}} + \frac{\partial F}{\partial \bar{\varepsilon}^{vp}_{ij}}\frac{\partial F}{\partial \bar{\sigma}'_{ij}}}\right]\frac{\partial F}{\partial \sigma'_{ij}} \qquad \text{[A1.10]}$$

- **Hardening law**

The hardening law in generalised space is similar to that in the triaxial stress space:

$$dp'_m = p'_0\frac{1+e_0}{\lambda-\kappa}d\varepsilon^{vp}_v \qquad \text{[A1.11]}$$

APPENDIX 2: Derivatives in NSFS-SCLAY1S

The flow surface in NSFS-SCLAY1S model is expressed in general space:

$$F(\bar{\sigma}'_{ij}, \bar{\varepsilon}'_{ij}, t) = \mu ln\left(\frac{\dot{v}_0 t}{\mu} e^{\left(\frac{f}{\mu}\right)} + 1\right) - \varepsilon_v = 0 \qquad [0.1]$$

where f is a scalar function defined as

$$f = \frac{\lambda_i - \kappa}{1 + e_0} ln\left(\frac{p'}{p'_0}\right) + \frac{\lambda_i - \kappa}{1 + e_0} ln\left(1 + \frac{3}{2}\frac{\{\bar{\sigma}'_d - \overline{\alpha_d} p'\}^T \{\bar{\sigma}'_d - \overline{\alpha_d} p'\}}{(M^2 - \alpha^2) p'^2}\right) + \frac{\lambda_i - \kappa}{1 + e_0} ln\left(\frac{1 + x_0}{1 + x}\right)$$

$$\bar{\sigma}_d = \begin{Bmatrix} \sigma'_{xx} - p' \\ \sigma'_{yy} - p' \\ \sigma'_{zz} - p' \\ \sqrt{2}.\tau'_{xy} \\ \sqrt{2}.\tau'_{yz} \\ \sqrt{2}.\tau'_{zx} \end{Bmatrix} = \begin{Bmatrix} \frac{1}{3}(2\sigma'_{xx} - \sigma'_{yy} - \sigma'_{zz}) \\ \frac{1}{3}(-\sigma'_{xx} + 2\sigma'_{yy} - \sigma'_{zz}) \\ \frac{1}{3}(-\sigma'_{xx} - \sigma'_{yy} + 2\sigma'_{zz}) \\ \sqrt{2}.\tau'_{xy} \\ \sqrt{2}.\tau'_{yz} \\ \sqrt{2}.\tau'_{zx} \end{Bmatrix}$$

$$p' = \tfrac{1}{3}(\sigma'_{xx} + \sigma'_{yy} + \sigma'_{zz})$$

$$\alpha^2 = \frac{3}{2}\{\alpha_d\}^T\{\alpha_d\}$$

$$\alpha_d = \begin{Bmatrix} \alpha_{xx} - 1 \\ \alpha_{yy} - 1 \\ \alpha_{zz} - 1 \\ \sqrt{2}.\alpha_{xy} \\ \sqrt{2}.\alpha_{yz} \\ \sqrt{2}.\alpha_{zx} \end{Bmatrix}$$

Viscoplastic multiplier:

$$\langle d\lambda \rangle = -\frac{\frac{\partial F}{\partial \bar{\sigma}'_{ij}}\left[D^e_{ijkl}\right] d\bar{\varepsilon} + \frac{\partial F}{\partial t} dt}{-\frac{\partial F}{\partial \bar{\sigma}'_{ij}}\left[D^e_{ijkl}\right]\frac{\partial F}{\partial \bar{\sigma}'_{ij}} + \frac{\partial F}{\partial \bar{\varepsilon}^{vp}_{ij}}\frac{\partial F}{\partial \bar{\sigma}'_{ij}}}$$

$$\frac{\partial F}{\partial \bar{\sigma}'_{ij}} = \left(1 - exp\left(-\frac{\varepsilon_v^{vp}}{\mu}\right)\right)\frac{\partial f}{\partial \bar{\sigma}'_{ij}}$$

$$\frac{\partial F}{\partial t} = \dot{v}_0 exp\left(\frac{f - \varepsilon_v^{vp}}{\mu}\right)$$

$$\frac{\partial F}{\partial \bar{\varepsilon}_{ij}^{vp}}\frac{\partial F}{\partial \bar{\sigma}'_{ij}} = -\frac{\partial F}{\partial p'} + \frac{\partial F}{\partial \alpha_d}\left(\frac{\partial \alpha_d}{\partial \varepsilon_v^{vp}}\frac{\partial F}{\partial p'} + \frac{\partial \alpha_d}{\partial \varepsilon_d^{vp}}\frac{\partial F}{\partial \sigma_d}\right) + \frac{\partial F}{\partial x}\left(\frac{\partial x}{\partial \varepsilon_v^{vp}}\frac{\partial F}{\partial p'} + \frac{\partial x}{\partial \varepsilon_d^{vp}}\frac{\partial F}{\partial \sigma_d}\right)$$

$$\frac{\partial F}{\partial \alpha_d} = \left(1 - exp\left(-\frac{\varepsilon_v^{vp}}{\mu}\right)\right)\frac{\partial f}{\partial \alpha_d}$$

$$\frac{\partial F}{\partial \sigma_d} = \left(1 - exp\left(-\frac{\varepsilon_v^{vp}}{\mu}\right)\right)\frac{\partial f}{\partial \sigma_d}$$

$$\frac{\partial F}{\partial x} = \left(1 - exp\left(-\frac{\varepsilon_v^{vp}}{\mu}\right)\right)\frac{\partial f}{\partial x}$$

Derivatives in detail

$$\frac{\partial f}{\partial \bar{\sigma}'_{ij}} = \left\{\frac{\partial f}{\partial \sigma'_{xx}}; \frac{\partial f}{\partial \sigma'_{yy}}; \frac{\partial f}{\partial \sigma'_{zz}}; \frac{\partial f}{\partial \tau_{xy}}; \frac{\partial f}{\partial \tau_{yz}}; \frac{\partial f}{\partial \tau_{xz}}\right\}$$

$$\frac{\partial f}{\partial \alpha_d} = \left\{\frac{\partial f}{\partial \alpha_{d1}}; \frac{\partial f}{\partial \alpha_{d2}}; \frac{\partial f}{\partial \alpha_{d3}}; \frac{\partial f}{\partial \alpha_{d4}}; \frac{\partial f}{\partial \alpha_{d5}}; \frac{\partial f}{\partial \alpha_{d6}}\right\}$$

$$\frac{\partial f}{\partial \sigma_d} = \left\{\frac{\partial f}{\partial \sigma_{d1}}; \frac{\partial f}{\partial \sigma_{d2}}; \frac{\partial f}{\partial \alpha_{d3}}; \frac{\partial f}{\partial \sigma_{d4}}; \frac{\partial f}{\partial \sigma_{d5}}; \frac{\partial f}{\partial \sigma_{d6}}\right\}$$

$$\frac{\partial F}{\partial p'} = \frac{\partial F}{\partial \sigma'_{xx}} + \frac{\partial F}{\partial \sigma'_{yy}} + \frac{\partial F}{\partial \sigma'_{zz}}$$

Set s1 = σ'_{xx} ; s2 = σ'_{yy} ; s3 = σ'_{zz} ; s4 = τ_{xy} ; s5 = τ_{yz} ; s6 = τ_{xz} ;
sd1= σ_{d1} ; sd2= σ_{d2} ; sd 3= σ_{d3} ; sd 4= σ_{d4} ; sd 5= σ_{d5} ; sd 6= σ_{d6} ;
a1= α_{xx} ; a2= α_{yy} ; a3= α_{zz} ; a4= α_{xy} ; a5= α_{yz} ; a6= α_{xz} ;
ad1= α_{d1} ; a2= α_{d2} ; a3= α_{d3} ; a4= α_{d4} ; a5= α_{d5} ; a6= α_{d6} ;

$$\frac{\partial f}{\partial \sigma_{xx}} =$$

```
(λi-κ)/(1+e₀)*(((-9 + 6*a1 - 3*a2 - 3*a3 - M^2)*s1^2 + (18 +
6*a1 - 3*a2 - 3*a3 - M^2)*s2^2 + (9 + 12*a1 - 6*a2 - 6*a3 -
2*M^2)*s2*s3 + 18*s3^2 + 6*a1*s3^2 - 3*a2*s3^2 - 3*a3*s3^2
- M^2*s3^2 + 2*(-9 + 6*a1 - 3*a2 - 3*a3 - M^2)*s1*(s2 + s3)
+ 27*s4^2 + 27*s5^2 + 27*s6^2)/                ((s1 + s2 +
s3)*((-9 + 6*a1 - 3*a2 - 3*a3 - M^2)*s1^2 - (9 + 3*a1 -
6*a2 + 3*a3 + M^2)*s2^2 + (9 - 6*a1 + 3*a2 + 3*a3 -
2*M^2)*s2*s3 - 9*s3^2 - 3*a1*s3^2 - 3*a2*s3^2 + 6*a3*s3^2 -
M^2*s3^2 + 18*a4*s3*s4 - 27*s4^2 + 18*a5*s3*s5 - 27*s5^2 +
```

```
18*a6*s3*s6 - 27*s6^2 + 18*s2*(a4*s4 + a5*s5 + a6*s6) +
s1*((9 + 3*a1 + 3*a2 - 6*a3 - 2*M^2)*s2 + (9 + 3*a1 - 6*a2
+ 3*a3 - 2*M^2)*s3 + 18*(a4*s4 + a5*s5 + a6*s6)))))
```

$$\frac{\partial f}{\partial \sigma_{yy}} =$$

```
(λi-κ)/(1+e0)*(-(((-18 + 3*a1 - 6*a2 + 3*a3 + M^2)*s1^2 +
2*(9 + 3*a1 - 6*a2 + 3*a3 + M^2)*s1*s2 +(9 + 3*a1 - 6*a2 +
3*a3 + M^2)*s2^2 + (-9 + 6*a1 - 12*a2 + 6*a3 + 2*M^2)*s1*s3
+                  2*(9 + 3*a1 - 6*a2 + 3*a3 + M^2)*s2*s3 -
18*s3^2 + 3*a1*s3^2 - 6*a2*s3^2 + 3*a3*s3^2 + M^2*s3^2 -
27*s4^2 - 27*s5^2 - 27*s6^2)/((s1 + s2 + s3)*((-9 + 6*a1 -
3*a2 - 3*a3 - M^2)*s1^2 - (9 + 3*a1 - 6*a2 + 3*a3 +
M^2)*s2^2 +                (9 - 6*a1 + 3*a2 + 3*a3 -
2*M^2)*s2*s3 - 9*s3^2 - 3*a1*s3^2 - 3*a2*s3^2 + 6*a3*s3^2 -
M^2*s3^2 + 18*a4*s3*s4 - 27*s4^2 + 18*a5*s3*s5 - 27*s5^2 +
18*a6*s3*s6 - 27*s6^2 + 18*s2*(a4*s4 + a5*s5 + a6*s6) +
s1*((9 + 3*a1 + 3*a2 - 6*a3 - 2*M^2)*s2 + (9 + 3*a1 - 6*a2
+ 3*a3 - 2*M^2)*s3 + 18*(a4*s4 + a5*s5 + a6*s6))))));
```

$$\frac{\partial f}{\partial \sigma_{zz}} =$$

```
(λi-κ)/(1+e0)*(-(((-18 + 3*a1 + 3*a2 - 6*a3 + M^2)*s1^2 + (-
9 + 6*a1 + 6*a2 - 12*a3 + 2*M^2)*s1*s2 + (-18 + 3*a1 + 3*a2
- 6*a3 + M^2)*s2^2 + 2*(9 + 3*a1 + 3*a2 - 6*a3 + M^2)*s1*s3
+ 2*(9 + 3*a1 + 3*a2 - 6*a3 + M^2)*s2*s3 + 9*s3^2 +
3*a1*s3^2 + 3*a2*s3^2 - 6*a3*s3^2 + M^2*s3^2 - 27*s4^2 -
27*s5^2 - 27*s6^2)/((s1 + s2 + s3)*((-9 + 6*a1 - 3*a2 -
3*a3 - M^2)*s1^2 - (9 + 3*a1 - 6*a2 + 3*a3 + M^2)*s2^2 +(9
- 6*a1 + 3*a2 + 3*a3 - 2*M^2)*s2*s3 - 9*s3^2 - 3*a1*s3^2 -
3*a2*s3^2 + 6*a3*s3^2 - M^2*s3^2 + 18*a4*s3*s4 - 27*s4^2 +
18*a5*s3*s5 - 27*s5^2 + 18*a6*s3*s6 - 27*s6^2 +
18*s2*(a4*s4 + a5*s5 + a6*s6) +                  s1*((9 +
3*a1 + 3*a2 - 6*a3 - 2*M^2)*s2 + (9 + 3*a1 - 6*a2 + 3*a3 -
2*M^2)*s3 + 18*(a4*s4 + a5*s5 + a6*s6))))));
```

$$\frac{\partial f}{\partial \tau_{xy}} =$$

```
(λi-κ)/(1+e0)*((-18*(a4*(s1 + s2 + s3) - 3*s4))/
 (((-3*((-1 + a1)^2 + (-1 + a2)^2 + (-1 + a3)^2 + 2*a4^2 +
2*a5^2 + 2*a6^2))/2. + M^2)*(s1 + s2 + s3)^2*(1 + (3*(((-3
+ a1)*s1 + a1*(s2 + s3))^2 + (-3*s2 + a2*(s1 + s2 + s3))^2
+(-3*s3 + a3*(s1 + s2 + s3))^2 + 2*(a4*(s1 + s2 + s3) -
3*s4)^2 +2*(a5*(s1 + s2 + s3) - 3*s5)^2 + 2*(a6*(s1 + s2 +
s3) - 3*s6)^2))/(2.*((-3*((-1 + a1)^2 + (-1 + a2)^2 + (-1
+ a3)^2 + 2*a4^2 + 2*a5^2 + 2*a6^2))/2. + M^2)*(s1 + s2 +
s3)^2))));
```

$$\frac{\partial f}{\partial \tau_{yz}} =$$

```
(λi-κ)/(1+e0)*((-18*(a5*(s1 + s2 + s3) - 3*s5))/(((-3*((-1
+ a1)^2 + (-1 + a2)^2 + (-1 + a3)^2 + 2*a4^2 + 2*a5^2 +
2*a6^2))/2. + M^2)*(s1 + s2 + s3)^2*(1 + (3*(((-3 + a1)*s1
+ a1*(s2 + s3))^2 + (-3*s2 + a2*(s1 + s2 + s3))^2 +(-3*s3
+ a3*(s1 + s2 + s3))^2 + 2*(a4*(s1 + s2 + s3) - 3*s4)^2 +
2*(a5*(s1 + s2 + s3) - 3*s5)^2 + 2*(a6*(s1 + s2 + s3) -
3*s6)^2))/(2.*((-3*((-1 + a1)^2 + (-1 + a2)^2 + (-1 +
a3)^2 + 2*a4^2 + 2*a5^2 + 2*a6^2))/2. + M^2)*
(s1 + s2 + s3)^2))));
```

$$\frac{\partial f}{\partial \tau_{xz}} =$$

```
(λi-κ)/(1+e0)*(  (-18*(a6*(s1 + s2 + s3) - 3*s6))/
(((-3*((-1 + a1)^2 + (-1 + a2)^2 + (-1 + a3)^2 + 2*a4^2 +
2*a5^2 + 2*a6^2))/2. + M^2)*(s1 + s2 + s3)^2*(1 + (3*(((-3
+ a1)*s1 + a1*(s2 + s3))^2 + (-3*s2 + a2*(s1 + s2 + s3))^2
+ (-3*s3 + a3*(s1 + s2 + s3))^2 + 2*(a4*(s1 + s2 + s3) -
3*s4)^2 + 2*(a5*(s1 + s2 + s3) - 3*s5)^2 + 2*(a6*(s1 + s2
+ s3) - 3*s6)^2))/(2.*((-3*((-1 + a1)^2 + (-1 + a2)^2 + (-
1 + a3)^2 + 2*a4^2 + 2*a5^2 + 2*a6^2))/2. + M^2)*(s1 + s2
+ s3)^2))));
```

$$\frac{\partial f}{\partial \alpha_{d1}} =$$

```
(λi-κ)/(1+e0)* ((3*(2*((-3*(ad1^2 + ad2^2 + ad3^2 + ad4^2 +
ad5^2 + ad6^2))/2. + M^2)*(s1 + s2 + s3)*((-2 + ad1)*s1 +
(1 + ad1)*(s2 + s3)) + 3*ad1*((s1 + ad2*s1 - 2*s2 + ad2*s2
+ s3 + ad2*s3)^2 + s1 + ad3*s1 + s2 + ad3*s2 - 2*s3 +
ad3*s3)^2 + ((-2 + ad1)*s1 + (1 + ad1)*(s2 + s3))^2 +
(ad4*(s1 + s2 + s3) - 3*sqrt(2)*s4)^2 + (ad5*(s1 + s2 +
s3) - 3*sqrt(2)*s5)^2 + ad6*(s1 + s2 + s3) -
3*sqrt(2)*s6)^2)))/(2.*((-3*(ad1^2 + ad2^2 + ad3^2 + ad4^2
+ ad5^2 + ad6^2))/2. + M^2)^2*(s1 + s2 + s3)^2*(1 +
(3*((s1 + ad2*s1 - 2*s2 + ad2*s2 + s3 + ad2*s3)^2 +
(s1 + ad3*s1 + s2 + ad3*s2 - 2*s3 + ad3*s3)^2 + ((-2 +
ad1)*s1 + (1 + ad1)*(s2 + s3))^2 + (ad4*(s1 + s2 + s3) -
3*sqrt(2)*s4)^2 + (ad5*(s1 + s2 + s3) - 3*sqrt(2)*s5)^2 +
(ad6*(s1 + s2 + s3) - 3*sqrt(2)*s6)^2))/(2.*((-3*(ad1^2 +
ad2^2 + ad3^2 + ad4^2 + ad5^2 + ad6^2))/2. + M^2)*(s1 + s2
+ s3)^2))));
```

$$\frac{\partial f}{\partial \alpha_{d2}} =$$

```
(λi-κ)/(1+e0)* ((3*(2*((-3*(ad1^2 + ad2^2 + ad3^2 + ad4^2 +
ad5^2 + ad6^2))/2. + M^2)*(s1 + s2 + s3)*(s1 + ad2*s1 -
2*s2 + ad2*s2 + s3 + ad2*s3) + 3*ad2*((s1 + ad2*s1 - 2*s2
+ ad2*s2 + s3 + ad2*s3)^2 +(s1 + ad3*s1 + s2 + ad3*s2 -
2*s3 + ad3*s3)^2 + ((-2 + ad1)*s1 + (1 + ad1)*(s2 + s3))^2
+ (ad4*(s1 + s2 + s3) - 3*sqrt(2)*s4)^2 + (ad5*(s1 + s2 +
s3) - 3*sqrt(2)*s5)^2 + (ad6*(s1 + s2 + s3) -
3*sqrt(2)*s6)^2)))/(2.*((-3*(ad1^2 + ad2^2 + ad3^2 + ad4^2
+ ad5^2 + ad6^2))/2. + M^2)^2*(s1 + s2 + s3)^2*(1 +
(3*((s1 + ad2*s1 - 2*s2 + ad2*s2 + s3 + ad2*s3)^2 +
(s1 + ad3*s1 + s2 + ad3*s2 - 2*s3 + ad3*s3)^2 + ((-2 +
ad1)*s1 + (1 + ad1)*(s2 + s3))^2 + (ad4*(s1 + s2 + s3) -
3*sqrt(2)*s4)^2 + (ad5*(s1 + s2 + s3) - 3*sqrt(2)*s5)^2 +
(ad6*(s1 + s2 + s3) - 3*sqrt(2)*s6)^2))/(2.*((-3*(ad1^2 +
ad2^2 + ad3^2 + ad4^2 + ad5^2 + ad6^2))/2. + M^2)*(s1 + s2
+ s3)^2))));
```

$$\frac{\partial f}{\partial \alpha_{d3}} =$$

```
(λi-κ)/(1+e0)* ((3*(2*((-3*(ad1^2 + ad2^2 + ad3^2 + ad4^2 +
ad5^2 + ad6^2))/2. + M^2)*(s1 + s2 + s3)*(s1 + ad3*s1 + s2
+ ad3*s2 - 2*s3 + ad3*s3) + 3*ad3*((s1 + ad2*s1 - 2*s2 +
ad2*s2 + s3 + ad2*s3)^2 + (s1 + ad3*s1 + s2 + ad3*s2 -
2*s3 + ad3*s3)^2 + ((-2 + ad1)*s1 + (1 + ad1)*(s2 + s3))^2
+ (ad4*(s1 + s2 + s3) - 3*sqrt(2)*s4)^2 + (ad5*(s1 + s2 +
s3) - 3*sqrt(2)*s5)^2 + (ad6*(s1 + s2 + s3) -
3*sqrt(2)*s6)^2)))/(2.*((-3*(ad1^2 + ad2^2 + ad3^2 + ad4^2
+ ad5^2 + ad6^2))/2. + M^2)^2*(s1 + s2 + s3)^2*(1 +
(3*((s1 + ad2*s1 - 2*s2 + ad2*s2 + s3 + ad2*s3)^2 + (s1 +
ad3*s1 + s2 + ad3*s2 - 2*s3 + ad3*s3)^2 + ((-2 + ad1)*s1 +
(1 + ad1)*(s2 + s3))^2 + (ad4*(s1 + s2 + s3) -
3*sqrt(2)*s4)^2 + (ad5*(s1 + s2 + s3) - 3*sqrt(2)*s5)^2 +
(ad6*(s1 + s2 + s3) - 3*sqrt(2)*s6)^2))/(2.*((-3*(ad1^2 +
ad2^2 + ad3^2 + ad4^2 + ad5^2 + ad6^2))/2. + M^2)*(s1 + s2
+ s3)^2))));
```

$$\frac{\partial f}{\partial \alpha_{d4}} =$$

```
(λi-κ)/(1+e0)* ((3*(2*((-3*(ad1^2 + ad2^2 + ad3^2 + ad4^2
+ ad5^2 + ad6^2))/2. + M^2)*(s1 + s2 + s3)*(ad4*(s1 + s2
+ s3) - 3*sqrt(2)*s4) + 3*ad4*((s1 + ad2*s1 - 2*s2 +
```

```
ad2*s2 + s3 + ad2*s3)^2 + (s1 + ad3*s1 + s2 + ad3*s2 -
2*s3 + ad3*s3)^2 + ((-2 + ad1)*s1 + (1 + ad1)*(s2 +
s3))^2 + (ad4*(s1 + s2 + s3) - 3*sqrt(2)*s4)^2 + (ad5*(s1
+ s2 + s3) - 3*sqrt(2)*s5)^2 + (ad6*(s1 + s2 + s3) -
3*sqrt(2)*s6)^2)))/(2.*((-3*(ad1^2 + ad2^2 + ad3^2 +
ad4^2 + ad5^2 + ad6^2))/2. + M^2)^2*(s1 + s2 + s3)^2*
(1 + (3*((s1 + ad2*s1 - 2*s2 + ad2*s2 + s3 + ad2*s3)^2 +
(s1 + ad3*s1 + s2 + ad3*s2 - 2*s3 + ad3*s3)^2 + ((-2 +
ad1)*s1 + (1 + ad1)*(s2 + s3))^2 + (ad4*(s1 + s2 + s3) -
3*sqrt(2)*s4)^2 + (ad5*(s1 + s2 + s3) - 3*sqrt(2)*s5)^2 +
(ad6*(s1 + s2 + s3) - 3*sqrt(2)*s6)^2))/(2.*((-3*(ad1^2 +
ad2^2 + ad3^2 + ad4^2 + ad5^2 + ad6^2))/2. + M^2)*(s1 +
s2 + s3)^2))));
```

$$\frac{\partial f}{\partial \alpha_{d5}} =$$

```
(λi-κ)/(1+e0)* ((3*(2*((-3*(ad1^2 + ad2^2 + ad3^2 + ad4^2
+ ad5^2 + ad6^2))/2. + M^2)*(s1 + s2 + s3)*(ad5*(s1 + s2
+ s3) - 3*sqrt(2)*s5) + 3*ad5*((s1 + ad2*s1 - 2*s2 +
ad2*s2 + s3 + ad2*s3)^2 + (s1 + ad3*s1 + s2 + ad3*s2 -
2*s3 + ad3*s3)^2 + ((-2 + ad1)*s1 + (1 + ad1)*(s2 +
s3))^2 + (ad4*(s1 + s2 + s3) - 3*sqrt(2)*s4)^2 + (ad5*(s1
+ s2 + s3) - 3*sqrt(2)*s5)^2 + (ad6*(s1 + s2 + s3) -
3*sqrt(2)*s6)^2)))/(2.*((-3*(ad1^2 + ad2^2 + ad3^2 +
ad4^2 + ad5^2 + ad6^2))/2. + M^2)^2*(s1 + s2 + s3)^2*
(1 + (3*((s1 + ad2*s1 - 2*s2 + ad2*s2 + s3 + ad2*s3)^2 +
(s1 + ad3*s1 + s2 + ad3*s2 - 2*s3 + ad3*s3)^2 + ((-2 +
ad1)*s1 + (1 + ad1)*(s2 + s3))^2 + (ad4*(s1 + s2 + s3) -
3*sqrt(2)*s4)^2 + (ad5*(s1 + s2 + s3) - 3*sqrt(2)*s5)^2 +
(ad6*(s1 + s2 + s3) - 3*sqrt(2)*s6)^2))/(2.*((-3*(ad1^2 +
ad2^2 + ad3^2 + ad4^2 + ad5^2 + ad6^2))/2. + M^2)*(s1 +
s2 + s3)^2))));
```

$$\frac{\partial f}{\partial \alpha_{d6}} =$$

```
(λi-κ)/(1+e0)* ((3*(2*((-3*(ad1^2 + ad2^2 + ad3^2 + ad4^2
+ ad5^2 + ad6^2))/2. + M^2)*(s1 + s2 + s3)*(ad6*(s1 + s2
+ s3) - 3*sqrt(2)*s6) + 3*ad6*((s1 + ad2*s1 - 2*s2 +
ad2*s2 + s3 + ad2*s3)^2 + (s1 + ad3*s1 + s2 + ad3*s2 -
2*s3 + ad3*s3)^2 + ((-2 + ad1)*s1 + (1 + ad1)*(s2 +
s3))^2 + (ad4*(s1 + s2 + s3) - 3*sqrt(2)*s4)^2 + (ad5*(s1
+ s2 + s3) - 3*sqrt(2)*s5)^2 + (ad6*(s1 + s2 + s3) -
3*sqrt(2)*s6)^2)))/(2.*((-3*(ad1^2 + ad2^2 + ad3^2 +
ad4^2 + ad5^2 + ad6^2))/2. + M^2)^2*(s1 + s2 + s3)^2*
(1 + (3*((s1 + ad2*s1 - 2*s2 + ad2*s2 + s3 + ad2*s3)^2 +
(s1 + ad3*s1 + s2 + ad3*s2 - 2*s3 + ad3*s3)^2 + ((-2 +
ad1)*s1 + (1 + ad1)*(s2 + s3))^2 + (ad4*(s1 + s2 + s3) -
3*sqrt(2)*s4)^2 + (ad5*(s1 + s2 + s3) - 3*sqrt(2)*s5)^2 +
(ad6*(s1 + s2 + s3) - 3*sqrt(2)*s6)^2))/(2.*((-3*(ad1^2 +
ad2^2 + ad3^2 + ad4^2 + ad5^2 + ad6^2))/2. + M^2)*(s1 +
s2 + s3)^2))));
```

$$\frac{\partial f}{\partial \sigma_{d1}} =$$

```
(λi-κ)/(1+e0)* ((6*ad1*pdash - 6*sd1)/(-2*M^2*pdash^2 +
6*ad1*pdash*sd1 - 3*(sd1^2 - 2*ad2*pdash*sd2 + sd2^2 -
2*ad3*pdash*sd3 + sd3^2 - 2*ad4*pdash*sd4 + sd4^2 -
2*ad5*pdash*sd5 + sd5^2 - 2*ad6*pdash*sd6 + sd6^2)));
```

$$\frac{\partial f}{\partial \sigma_{d2}} =$$ `(λi-κ)/(1+e0)* ((6*ad2*pdash - 6*sd2)/(-2*M^2*pdash^2 + 6*ad1*pdash*sd1 - 3*(sd1^2 - 2*ad2*pdash*sd2 + sd2^2 - 2*ad3*pdash*sd3 + sd3^2 - 2*ad4*pdash*sd4 + sd4^2 - 2*ad5*pdash*sd5 + sd5^2 - 2*ad6*pdash*sd6 + sd6^2)));`

$$\frac{\partial f}{\partial \sigma_{d3}} =$$ `(λi-κ)/(1+e0)* ((6*ad3*pdash - 6*sd3)/(-2*M^2*pdash^2 + 6*ad1*pdash*sd1 - 3*(sd1^2 - 2*ad2*pdash*sd2 + sd2^2 - 2*ad3*pdash*sd3 + sd3^2 - 2*ad4*pdash*sd4 + sd4^2 - 2*ad5*pdash*sd5 + sd5^2 - 2*ad6*pdash*sd6 + sd6^2)));`

$$\frac{\partial f}{\partial \sigma_{d4}} =$$ `(λi-κ)/(1+e0)* ((6*ad4*pdash - 6*sd4)/(-2*M^2*pdash^2 + 6*ad1*pdash*sd1 - 3*(sd1^2 - 2*ad2*pdash*sd2 + sd2^2 - 2*ad3*pdash*sd3 + sd3^2 - 2*ad4*pdash*sd4 + sd4^2 - 2*ad5*pdash*sd5 + sd5^2 - 2*ad6*pdash*sd6 + sd6^2)));`

$$\frac{\partial f}{\partial \sigma_{d5}} =$$ `(λi-κ)/(1+e0)* ((6*ad5*pdash - 6*sd5)/(-2*M^2*pdash^2 + 6*ad1*pdash*sd1 - 3*(sd1^2 - 2*ad2*pdash*sd2 + sd2^2 - 2*ad3*pdash*sd3 + sd3^2 - 2*ad4*pdash*sd4 + sd4^2 - 2*ad5*pdash*sd5 + sd5^2 - 2*ad6*pdash*sd6 + sd6^2)));`

$$\frac{\partial f}{\partial \sigma_{d6}} =$$ `(λi-κ)/(1+e0)* ((6*ad6*pdash - 6*sd6)/(-2*M^2*pdash^2 + 6*ad1*pdash*sd1 - 3*(sd1^2 - 2*ad2*pdash*sd2 + sd2^2 - 2*ad3*pdash*sd3 + sd3^2 - 2*ad4*pdash*sd4 + sd4^2 - 2*ad5*pdash*sd5 + sd5^2 - 2*ad6*pdash*sd6 + sd6^2)));`

$$\frac{\partial \alpha_{d(1)}}{\partial \varepsilon_v^{vp}} =$$ `ω*(1-a1+(9*(s1+1/3*(-s1-s2-s3)))/(4*(s1+s2+s3)));`

$$\frac{\partial \alpha_{d(2)}}{\partial \varepsilon_v^{vp}} =$$ `ω*(1-a2+(9*(s2+1/3*(-s1-s2-s3)))/(4*(s1+s2+s3)));`

$$\frac{\partial \alpha_{d(3)}}{\partial \varepsilon_v^{vp}} =$$ `ω*(1-a3+(9*(s3+1/3*(-s1-s2-s3)))/(4*(s1+s2+s3)));`

$$\frac{\partial \alpha_{d(4)}}{\partial \varepsilon_v^{vp}} =$$ `ω*(-sqrt(2)*a4+(9*s4/(2*sqrt(2)*(s1+s2+s3))));`

$$\frac{\partial \alpha_{d(5)}}{\partial \varepsilon_v^{vp}} =$$ `ω*(-sqrt(2)*a5+(9*s5/(2*sqrt(2)*(s1+s2+s3))));`

$$\frac{\partial \alpha_{d(6)}}{\partial \varepsilon_v^{vp}} =$$ `ω*(-sqrt(2)*a6+(9*s6/(2*sqrt(2)*(s1+s2+s3))));`

$$\frac{\partial \alpha_{d(1)}}{\partial \varepsilon_d^{vp}} =$$ ω*ω_d*(-ad1+(s1+1/3*(-s1-s2-s3))/(s1+s2+s3));

$$\frac{\partial \alpha_{d(2)}}{\partial \varepsilon_d^{vp}} =$$ ω*ω_d*(-ad2+(s2+1/3*(-s1-s2-s3))/(s1+s2+s3));

$$\frac{\partial \alpha_{d(3)}}{\partial \varepsilon_d^{vp}} =$$ ω*ω_d*(-ad3+(s3+1/3*(-s1-s2-s3))/(s1+s2+s3));

$$\frac{\partial \alpha_{d(4)}}{\partial \varepsilon_d^{vp}} =$$ ω*ω_d*(-ad4+(sqrt(2)*s4)/(s1+s2+s3));

$$\frac{\partial \alpha_{d(5)}}{\partial \varepsilon_d^{vp}} =$$ ω*ω_d*(-ad5+(sqrt(2)*s5)/(s1+s2+s3));

$$\frac{\partial \alpha_{d(6)}}{\partial \varepsilon_d^{vp}} =$$ ω*ω_d*(-ad6+(sqrt(2)*s6)/(s1+s2+s3));

$$\frac{\partial f}{\partial x} =$$ (λi-κ)/(1+e_0)*(-1/(1+x));

$$\frac{\partial x}{\partial \varepsilon_v^{vp}} =$$ -ξ*x;

$$\frac{\partial x}{\partial \varepsilon_d^{vp}} =$$ -ξ*ξ_d*x;